University of Stavanger

Faculty of Science and Technology

MASTER'S THESIS

Study program/ Specialization: Offshore Technology Marine and Subsea Technology	Spring semester, 2012 Open
Writer: Stanislav V. Duplenskiy	…… (Writer's signature)
Faculty supervisor: Professor Ove Tobias Gudmestad External supervisor(s): Professor Anatoly Borisovich Zolotukhin (Gubkin University) Professor Yuriy Alekseevich Kharchenko (LLC "Gazprom dobych shelf")	
Titel of thesis: Protection of Subsea Pipelines against Ice Ridge Gouging in Conditions of Substantial Surface Ice	
Credits (ECTS): 30	
Key words: Offshore, Arctic, Pipelines, Ice ridge, Scouring, Gouge depth, Design load, Trench depth, ANSYS	Pages: 108 +enclosure: 30 + 2 video files, presentation Stavanger, 14.06.2012 Date/year

Frontpage for master thesis
Faculty of Science and Technology
Decision made by the Dean October 30th 2009

PROTECTION OF SUBSEA PIPELINES AGAINST ICE RIDGE GOUGING IN CONDITIONS OF SUBSTANTIAL SURFACE ICE

Duplenskiy, Stanislav Valerievich, *master student.*

Faculty of Science and Technology, University of Stavanger
Faculty of Oil and gas field development, Gubkin University of Oil and Gas, Moscow

ABSTRACT

The development of Arctic offshore hydrocarbon fields involves transportation systems for oil and gas, which are represented either by tankers shipping or by pipeline systems. The later have sustained behavior with respect to hydrocarbons delivery and relatively non-sophisticated operational requirements. However, some important challenges regarding Arctic conditions have to be carried out before the pipeline is constructed.

Attention is given to the conditions of a specific hydrocarbon field of the Sakhalin offshore and a design of the 28 km offshore pipeline. Hydraulic assessment determines the size and number of pipelines as also temperature and pressure profiles, while mechanical estimations provide the wall thickness. As a result the main pipeline design aspects regarding dimensions and stresses occur are obtained, which is required for the next stage of the thesis.

In the second part the issue of the pipeline interaction with first year ice ridges is described. A study of probable sizes of ice ridges, their peculiarities and morphology is performed in order to evaluate the design ridge geometry, physical properties and to understand how a ridge interacts with the soil. Consequently, there introduced two models for estimation of the maximum gouge depth, caused by the ice ridge scouring the seabed.

At the same time the research shows that even below the gouge the forces transmitted through the soil could be adverse, such that the proper protection of a pipeline is required. A beam model of a pipeline exposed to bending and tension in terms of combined transverse and lateral loadings is proposed and analyzed. Based on the limit state design criteria the required trench features and mainly soil conditions for the safety reasons of the pipeline are proposed. Simultaneously the pipeline failure probability is assessed. As a result it was proven that the pipeline might be buried just below the probable scour depth if the certain conditions of the "sandwich" backfilling with a weak soil layer on the bottom are met.

After gaining an understanding of the physical processes related to gouging, numerical modeling is established in the last section. A finite-element analysis in ANSYS 13.0 software is carried out. The results obtained provide both: justification of the proposed theoretical models, and more precise assessment of some parameters when necessary, namely the soil behavior subscour, which is almost impossible to describe theoretically.

Conclusions summarize the acquired findings, provide reasonable recommendations for the offshore pipelines design in the Arctic regions and give the scope for future works and studies.

Master thesis
Key words:
Offshore, Arctic, Pipelines, Ice ridge, Scouring, Gouge depth, Design load, Trench depth, ANSYS

ACKNOWLEDGMENTS

I would like to gratefully appreciate my supervisor Professor Ove Tobias Gudmestad for his support and good comments during this study. His much knowledge in the areas of Marine technology, Marine operations and Offshore engineering was highly accessible for me and the atmosphere of study was at extremely friendly but classically high level.

I should heartily appreciate my scientific advisor from Gubkin University, Professor Anatoly Zolotukhin, whose teaching I admire all the time. Thanks to him I had an opportunity to study in Norway and to gain an international education. He supported and encouraged my first steps in Offshore engineering.

I sincerely appreciate wise advises and support of Dr. Pavel Liferov, whose experience in relevant field study is formidable and whose works inspirited me to carry out the study of the considered phenomenon.

I am thankful very much to Associated Professor in Gubkin University, Vladimir Balitskiy. Without him the study process following both Universities' requirements would be impossible.

I would also like to thank a lot Professor Sveinung Løset for the perfect course of Arctic Offshore Engineering during my stay in Svalbard. His lectures opened my eyes on Arctic conditions and his relation to students made me to be interested in given material much, being involved in ice peculiarities studying completely.

I wish to give a special thank to Professor Yuriy Kharchenko for his guiding comments, helpful in writing this master thesis.

TABLE OF CONTENT

ACKNOWLEDGMENTS ii
LIST OF FIGURES vii
LIST OF TABLES ..... **Ошибка! Закладка не определена.**
NUMENCLATURE x
CHAPTER 1. INTRODUCTION 1
1.1. BACKGROUND 1
1.2. PROBLEM STATEMENT 1
1.3. PURPOSE AND SCOPE 2
1.4. THESIS ORGANIZATION 2
CHAPTER 2. DESIGN BASIS 1
2.1. GENERAL 1
2.2. DESIGN STANDARDS 1
2.3. FIELD DATA 1
2.3.1. Gas composition 1
2.3.2. Production schedule 2
2.4. PIPELINE DATA. 3
2.4.1. Material data 4
2.4.2. Design factors 5
2.4.3. Material thermal conductivity properties 6
2.5. ENVIRONMENTAL DATA 6
2.5.1. Wind conditions 6
2.5.2. Waves 7
2.5.3. Currents 7
2.5.4. Seawater properties. 7
2.5.5. Seabed properties. 7
2.5.6. Ice conditions. 8
2.6. REFERENCES 11
CHAPTER 3. PIPELINE DESIGN 13
3.1. DESIGN PROCESS 13
3.2. DIAMETER SELECTION 15
3.2.1. Fluid properties. 16
3.2.2. Hydraulic analysis 18
3.2.3. Discussion 20

3.3. PRESSURE AND TEMPERATURE PROFILES....21
3.4. MATERIAL SELECTION....22
3.4.1. Steel grades....23
3.4.2. Fabrication methods....23
3.4.3. Discussion....24
3.5. WALL THICKNESS SELECTION....25
3.5.1. Limit state based design criteria....25
3.5.2. Wall thickness parameters....25
3.5.3. Load control condition....28
3.5.4. Discussion....28
3.6. ON-BOTTOM STABILITY DESIGN....28
3.6.1. General....28
3.6.2. Absolute lateral static stability method....29
3.6.3. Discussion....31
3.7. SUMMARY....33
3.8. REFERENCES....34
CHAPTER 4. THEORETICAL MODELING OF ICE RIDGE SCOURING....35
4.1. ICE RIDGES STUDY....35
4.1.1. Ice ridge shapes....35
4.1.2. Ridge morphology....38
4.2. ICE SCOURING....39
4.2.1. General....39
4.2.2. Soil behavior....43
4.2.3. Force scouring model....44
4.2.4. Energy scouring model....51
4.2.5. Keel destruction....57
4.2.6. Comparison of scouring models....58
4.3. GOUGE PARAMETERS' STATISTICAL DISTRIBUTION....59
4.3.1. Gouge depth....59
4.3.2. Gouge width....60
4.3.3. Scour length....60
4.3.4. Direct contact with pipe probability....61
4.4. SUMMARY....62
4.5. REFERENCES....63

CHAPTER 5. ON SUBGOUGE SOIL DEFORMATIONS AND THE PIPELINE RESPONSE 65
5.1. GENERAL 65
5.2. ARCTIC OFFSHORE STANDARDS 65
5.2.1. ISO 19906 66
5.2.2. ISO 13623 66
5.2.3. API-RP-2N 66
5.2.4. DNV-OS-F101 66
5.2.5. CAN/CSA-S471-92 66
5.2.6. RMRS 2-020301-001 66
5.3 SUBSCOUR SOIL BEHAVIOR 67
5.3.1. Subscour deformations 67
5.3.2. Soil properties' behavior subscour 70
5.4. IMPLICATIONS ON THE PIPELINE 72
5.4.1. General 72
5.4.2. Ridge contact with the pipeline 73
5.4.3. Soil-pipe interaction model 75
5.4.3.1. SLS stress 81
5.4.3.2. ULS strain 84
5.4.3.3. ULS collapse 86
5.4.4. Pipeline displacement 86
5.4.5. Pipeline trenching 88
5.4.6. Discussion 90
5.5. SUMMARY 91
5.6. REFERENCES 92
CHAPTER 6. FINITE ELEMENT ANALYSIS OF THE RIDGE-SOIL-PIPELINE INTERACTION 95
6.1. GENERAL 95
6.2. ANALYSIS SYSTEM SELECTION 96
6.3. ENGINEERING DATA SET-UP 97
6.4. SEABED SCOURING SIMULATION 98
6.4.1. Geometry 98
6.4.2. Mesh 99
6.4.3. Loads and boundary conditions 99
6.4.4. Analysis settings 100
6.4.5. Results evaluation 101

6.5. SUMMARY 102
6.6. REFERENCES 103
CHAPTER 7. CONCLUSIONS AND FURTHER STUDIES 104
7.1. CONCLUSIONS 104
7.2. FURTHER STUDIES 105
APPENDIX A. FLUID PROPERTIES 106
APPENDIX B. PIPELINE SIZING CALCULATIONS 109
APPENDIX C. PIPELINE ON-BOTTOM-STABILITY CALCULATIONS 115
APPENDIX D. SCOUR DEPTH CALCULATIONS 118
APPENDIX E. SCOURING IMPACT ON THE PIPELINE CALCULATIONS 128
APPENDIX F. ANSYS FILES 135

LIST OF FIGURES

Figure 2.1. Example of high and low production profiles 2
Figure 2.2. Production profile. 3
Figure 2.3. Stress-strain curves for different steel grades 5
Figure 3.1. Design stages and commitment to cost and technical issues 14
Figure 3.2. Chart diagram for inner diameter selection.....15
Figure 3.3. Typical production profile of an oilfield 16
Figure 3.4. Temperature profile along the pipeline route.....21
Figure 3.5. Pressure profile along the pipeline route.....22
Figure 3.6. The use of pipeline in terms of fabrication methods 24
Figure 3.7. Wall thickness for different steel grades.....27
Figure 3.8. Significant flow velocity amplitude u_s at the seabed level 30
Figure 3.9. Mean zero-up crossing period at the seabed level 30
Figure 3.10 Required submerged pipeline weight at 25 m water depth.....32
Figure 3.11. Required pipeline weight vs. water depth.....32
Figure 4.1. Geometrical parameters for typical first-year ice ridge 36
Figure 4.2. Triangular keel formation 36
Figure 4.3. Multiple peak keel formation 37
Figure 4.4. Comparison of keel shape 37
Figure 4.5. Distribution of ice solid phase volume content of the “mean statistical” ridge 38
Figure 4.6. Ice ridge scour illustration.....40
Figure 4.7. 1st design scheme for the scouring process modeling 41
Figure 4.8. 2d design scheme for the scouring process modeling.....42
Figure 4.9. 3d design scheme for the scouring process modeling.....42
Figure 4.10. Behavior of soil subjected to the scouring by the ridge keel. 43
Figure 4.11. Force system on the ice ridge.....44
Figure 4.12. Ice ridge keel draft values distribution 50
Figure 4.13. Gouge depth vs. keel breadth 51
Figure 4.14. Gouge depth vs. ice thickness 51
Figure 4.15. Profile of disposed soil around the ridge.....53
Figure 4.16. Ridge elevation and gouge depth vs. scour length for different soil conditions. 55
Figure 4.17. Arbitrary results of gouging in sands versus clays 56
Figure 4.18. Seabed profiles 56
Figure 4.19. Distribution of the gouge depths 60

Figure 4.20. Gouge width distribution 60
Figure 4.21. Gouge length distribution 61
Figure 5.1. Subscour horizontal sand deformation field according to equation (5.2; 5.3) 68
Figure 5.2. Subscour horizontal deformation fields comparison.....69
Figure 5.3. Vertical subgouge soil deformations, according to equation (5.4) 69
Figure 5.4. Soil shear strength versus depth below the gouge, according to equation (5.8) 71
Figure 5.5.Ice-soil-pipeline interaction scenarios.....72
Figure 5.6. Sub gouge soil deformations and pipeline response representation.....73
Figure 5.7. Direct contact with pipe model. 73
Figure 5.8. Force on the pipeline in condition of direct contact with the considered ridge 74
Figure 5.9. Beam on the Winkler foundation model for the pipeline response analysis. 75
Figure 5.10. Proposed beam model of the soil-pipeline interaction. 76
Figure 5.11. Non-linear behavior of the soil- pipeline interaction representation 76
Figure 5.12. Adhesion factors plotted as a function of undrained shear strength 77
Figure 5.13. Horizontal bearing capacity factors for granular and cohesive soils 78
Figure 5.14. Vertical uplift factors for sand and clay 79
Figure 5.15. Critical pipe-soil relative deformations vs. depth below the gouge. 80
Figure 5.16. Pipeline bending force and moment areas 82
Figure 5.17. Pipeline equivalent stress versus soil shear strength and scour width. 84
Figure 5.18. Pipeline compressive strain curves for different scour width. 85
Figure 5.19. Pipeline tensile strain curves for different scour width. 85
Figure 5.20. Pipeline bending and unit moment areas 87
Figure 5.21. 3D sketch of the results from proposed theoretical approach to the modeling of ice ridge scouring and its effect on the embedded pipeline 88
Figure 5.22 Trench parameters for the backfilling with clay layer 89
Figure 5.23 Trench parameters for backfilling with sand 90
Figure 6.1. Flow chart of the FEA process.....95
Figure 6.2. Engineering data of materials set-up.....97
Figure 6.3. Geometry of the seabed scouring simulation model 99
Figure 6.4. Mesh for the seabed scouring simulation model.....99
Figure 6.5. Boundary conditions' and contacts' settings 100
Figure 6.6. Horizontal sand deformations 101
Figure 6.7. Vertical sand deformations 101
Figure 6.8. Velocity field of the soil movement. 102

LIST OF TABLES

Table 2.1. Fluid composition. 2
Table 2.2. Production schedule of the gas field. 3
Table 2.3. Flowline parameters. 4
Table 2.4. Pipeline data 4
Table 2.5. Pipeline material data 5
Table 2.6. Stress-strain relationship 5
Table 2.7. Design factors 6
Table 2.8. Thermal conductivities for typical pipeline materials 6
Table 2.9. Wind velocities (m/s) 10 m above the sea level 6
Table 2.10. Air density and drag coefficients 6
Table 2.11. Design wave parameters 7
Table 2.12. Current data 7
Table 2.13. Seawater data 7
Table 2.14. Seabed data 8
Table 2.15. Ice data 9
Table 3.1.Effect of steel grades on wall thickness. 27
Table 4.1. Ridge features 48
Table 4.2. Forces action 49
Table 4.3. Gouge properties. 49
Table 4.4. Scouring in sand 55
Table 4.5. Scouring in clay 55
Table 4.6. Comparison of results of different models for scouring in sand 58
Table 4.7. Comparison of results of different models for scouring in clay 58
Table 5.1. Forces on the pipeline from the ice ridge for different scour depths 74
Table 5.2. Parameters of soil impact on the pipeline at the gouge base. 79
Table 5.3. Stresses in the pipeline in terms of scouring 83
Table 5.4. Pipeline bending and unit moments' expressions 87

Symbols

Latin characters

A_s – Wave particles acceleration;
B – Keel breadth/scour width;
b – Cover depth;
C_{da} , C_{dw}– Drag coefficients;
C_p– Isobaric heat capacity;
C_{sa}– Skin friction coefficient;
c – Cohesion;
D – Pipeline outer diameter;
D_b – Pipeline burial depth;
D_i – Joule-Thompson coefficient;
d – Pipeline internal diameter;
d – Scour depth;
$\bar{d}$ – Average observed gouge depth;
E – Elasticity modulus;
E_k – Ridge kinetic energy;
E_i – Ice field potential energy;
E_p – Ridge potential energy;
F_a – Active friction force;
F_b – Buoyancy;
F_c – Coulomb's passive friction force;
F_d – drag force;
F_I – Mass force;
F_i – Driving force from surrounding ice floe;
F_{li} – Level ice reaction;
F_L – Lift force;
F_{pipe} – Force on the pipe due to direct contact;
F_W – On-bottom stability factor;
f – Soil lateral force on the pipeline;
f_0 – Pipeline ovality;
$f_{y(u),temp}$ – Temperature de-rating;
g – Gravity acceleration;
H_s – Significant wave height;
h_i – Level ice thickness;
h' – Height of frontal mound;
h – Ice ridge consolidated layer thickness;
h_k – Keel height;
h_s – Sail height;
I – Moment of inertia;
K – Pipeline roughness;
K_0 – Soil pressure coefficient at rest;
K_p – Passive earth pressure coefficient;
k_a – Average heat transfer coefficient;
k_i – Ice plate stiffness;
KC – Keulegan-Carpenter number;
I – Pipeline moment of inertia;
L – Pipeline length;
l – Scour length;
$\bar{l}$ – Average observed scour length;
$\bar{M}_g$ – Gas molar mass;
M – Bending moment;
$\bar{M}$ – Bending moment area from the unit load;
M_R, M_L – Right and left fixed end moments;
N – Seabed reaction;
n – Scour-pipeline intersection frequency;
n_v – Ridge density per 1 km;
Pr – Prandtl number;
P – Earth pressure;
P_1 – Inlet pipeline pressure;
P_2 – Outlet pipeline pressure;
P_a – Average pipeline pressure;
P_{gouge} – Probability of gouge existence;
P_{damage} – Probability of pipeline damage;
P_{pc} – Pseudo-critical pressure;
P_r – Reduced pressure;
p_b – Pressure containment resistance;
p_{el} – Elastic collapse pressure;
p_i – Internal pressure of the pipe;
p_n – Limit pressure on the ridge;
p_{pl} – Plastic collapse pressure;
p_s – Pipeline collapse pressure;
p_u – Horizontal lateral ultimate soil resistance;
q – flow rate;
q_u – Vertical lateral ultimate soil resistance;
Re – Reynolds number;
S – Elasticity rigidity;
s_u – Soil undrained shear strength;
T– Pipeline operational axial force;
T' – Axial force in the pipeline;
T_1 – Inlet pipeline temperature;
T_a – Average pipeline temperature;
T_b – Ridge block size;
T_e – Environmental temperature;
T_p – Peak period;

T_{pc} – Pceudo-critical temperature;
T_r – Reduced temperature;
t – Characteristic pipeline wall thickness;
t_b – Wall thickness (bursting criteria);
t_c – Corrosion coating thickness;
t_{cor} – Wall thickness corrosion allowance;
t_{fab} – Wall thickness fabrication tolerance;
t_{nom} – Nominal pipeline wall thickness;
t_s – Standard wall thickness;
t_u – Ultimate axial soil resistance;
T_b – Ice blocks size;
T' – Axial tension force on the pipe;
t – Pipeline wall thickness;
u_a – Wind speed;
u_d – Current speed over pipeline diameter;
u_c – Surface current speed;
u_p – Pipeline displacement;
u_r – Current reference speed;
u_s – Wave near-bottom particle velocity;
u_s – Soil horizontal deformations;
v_i – Ice ridge speed;
v_s – Soil vertical deformations;
W – Ice ridge weight;
W_s – Sectional modulus;
w_b – Keel width at the sea bottom;
w_k – Keel width at the sealevel;
w_s – Submerged pipeline weight;
y_u, z_u – Pipeline-soil critical relative deformations;
Z – Gas compressibility factor;
z – Depth below the gouge centerline.

Greek characters

α – Temperature expansion coefficient;
α_k – Keel angle;
α_s – Sail angle;
α_u – Material strength factor;
β – Seabed slope angle;
γ – Wave peakedness;
γ_e – Resistance strain factor;
γ_F – Environmental load factor;
γ_m – Material resistance factor;
γ_{sc} – Safety class resistance factor;
Δ – Gas specific gravity;
δ– Ice ridge elevation;
η – Macro porosity of ridge keel;
η_s – Macro porosity of ridge sail;
θ – Phase angle;
θ_c – Current attack angle;
θ_w – Wave attack angle;
ε_{lc} – Limiting compressive strain value;
ε_p – Pipeline strain;
ε_t – Ultimate tensile strain;
λ – Hydraulic friction coefficient;
μ – Friction coefficient;
μ_g – gas dynamic viscosity;
ϑ– Poisson's ratio;
ρ_0 – Gas density at standard conditions;
ρ_a – Air density;
ρ_i – Ice density;
ρ_{ia} – Ice ridge density above the sea level;
ρ_{iw} – Density of ridge's submerged part;
ρ_s – Soil density;
ρ_w – Water density;
σ_{eq} – Equivalent von Mises stress;
σ_h – Hoop stress;
σ_l – Longitudinal stress;
σ_y – Specified minimum yield strength;
σ_t – Specified minimum tensile strength;
φ – Internal friction angle;
ϕ_w – Wall friction angle;
ω – Angle of surcharged soil slope;
∇– Ice ridge submerged volume.

Abbreviations

ALS – Accidental Limit State;
CRA – Corrosion Resistant Alloy;
DNV – Det Norske Veritas;
HFW – High Frequency Welding;
LSD – Limit State Design;
LRFD – Load and Resistance Factor Design;
SAW – Submerged Arc Welding;
SAWH – Submerged Arc Welding Helical;
SAWL – Submerged Arc Welding Longitudinal;
SLS – Serviceability Limit State;
SMLS – Seamless Pipeline;
SMTS – Specified Minimum Tensile Strength;
SMYS – Specified Minimum Yield Strength;
ULS – Ultimate Limit State.

CHAPTER 1. INTRODUCTION

1.1. BACKGROUND

In recent years there is a tendency of shifting offshore field development up to the North, where the substantial amount of hydrocarbon resources has been found. However, the income of reserve base from these areas is in its slow path. Low winter temperatures and ice presence making the work related to offshore engineering much more complicated. This requires the application of new technologies, proper project design and a lot of investment involved. Except the challenging maintenance of platforms and ship-shaped structures, a relevant issue of hydrocarbon transportation by pipelines in the arctic conditions appears.

Surveys of seabed of shallow seas bordering the Arctic oceans disclosed large ploughed areas gouged by the sea ice features. Ice ridges drifting with the ice driven by wind and current can cut deep gouges into the seabed approaching the shallow water regions. Scouring the seabed ice ridges might contact the pipeline, transmitting the load from natural forces, likely to rupture the line. Moreover, the large soil deformations below the ridge bottom might damage the pipeline, though the ridge itself doesn't reach it.

Initially this problem has been recognized in the Beaufort Sea and off the East Coast of Canada where the strong icebergs and multi-year ice features interactions with the seabed were being frequently observed. Significant attention to the issue has been paid during the development of Sakhalin-1 and Sakhalin-2 projects, which showed that the conservative estimate of the Beaufort Sea experience is unreliable and could not be applicable in different seabed, metocean and ice conditions.

With that the development of Arctic offshore projects continues: the subsequent development of the areas of the Sea of Okhotsk, the Barents, the Kara and the eastern Arctic Seas, different in their environments, include pipeline facilities, which have to be protected during entire period of their operation against anticipated phenomenon.

1.2. PROBLEM STATEMENT

As mentioned the seabed scouring dictates the pipeline design to a large extent. However the existing design codes, including those related to arctic conditions, do not give strong recommendations for the pipeline protection and refer to the probabilistic study of ice ridges intersecting the designing pipeline route. In case when there is no such data it appears problematically to carry out the conceptual pipeline project design. Besides, the probabilistic analysis doesn't account for the soil peculiarities, which are important in assessing the scouring hazard below the gouge itself.

Thus the effective pipeline protection measures could be developed only when the physics and the processes, lying behind the considered scouring event, are fully understood, such that the technique for scouring analysis and its implications on a pipeline would provide reasonable results on the pipeline response contributing to the overall design logic.

The pipeline protection is mainly associated with trenching and determination of the safe embedment depth into the soil thickness. Though the problem is well-understood now, the present researches do not provide reliable and comprehensive technique for burial depth assessment.

1.3. PURPOSE AND SCOPE

This research focuses on the pipeline from the specific gas field offshore the Sakhalin Island with conditions relevant for Sakhalin-3 Kirinskiy block. It is anticipated to study the main pipeline design features and show how the scouring affects the design. The work involves the combination of tasks related to geotechnics, ice mechanics and pipeline engineering, making the study more sophisticated.

It is proposed to use theoretical approach to the problem to solve, since its importance is high in terms of forecasting considered events, which could not be observed naturally, despite the shortcoming of the theoretical models could give a possible but acceptable error.

Scope of the thesis:

- Study of standards and papers with respect to the considered issue;
- Select and analyze the design basis data required for subsequent research;
- Carry out the main standard pipeline design aspects and develop main technical solutions required in subsequent study;
- Analyze the effect of gouging in different soils by introducing the new theoretical approach;
- Study how the soil deformations are propagating below the gouge base in terms of different seabed conditions;
- Analyze the pipeline behavior by introducing the soil-pipeline interaction model;
- Decide for pipeline protection measures;
- Perform finite-element analysis in ANSYS software.
- Discuss and evaluate results.

1.4. THESIS ORGANIZATION

Chapter 2 (Design Basis) provides the design basis required in this study, including design codes applied, field data, pipeline material properties and design concept, and environmental data with metocean and ice conditions to be anticipated further.

Chapter 3 (Pipeline Design) comprises some of the main aspects in the design process to perform the operability and integrity of the pipeline. It accounts for the pipeline hydraulic analysis with the subsequent sizing, selection of wall-thickness and plotting of pressure and temperature profiles. As a result the pre-stressed condition in terms of temperature, pressure and material strength are established for the pipeline response to the action caused by the ridge.

Chapter 4 (Mathematical Modeling of Ice Ridge Scouring) contains the study of ice ridges shapes, morphology and their relevance offshore the Sakhalin Island, discussing for the design ice ridge. Two theoretical models are introduced and implemented for analysis of scoring depth in this chapter. The effect of gouging in different soil and environmental conditions is performed. Results obtained are analyzed in terms of statistical likelihood of occurrence.

Chapter 5 (On Subgouge Soil Deformations and the Pipeline Response) gives an overview of standards, covering somehow the scouring phenomenon. The chapter starts studying the soil behavior from the classical geotechnical point of view and develops it further into the implications on the pipeline. For this end the study performs the pipeline response to the subgouge soil behavior and forceful protective measures, assuring the pipeline integrity and operability in accordance with standards' requirements.

Chapter 6 (Finite-Element Analysis of Ridge-Soil-Pipeline Interaction) addresses the combined approach in the analysis of soil behavior in terms of introduced numerical model, studying the scouring itself and subscour soil deformations. The chapter provides the theoretical results comparison with the numerical outcome and adjusts them for the practical reason.

CHAPTER 2. DESIGN BASIS

2.1. GENERAL

The pipeline is designed for a gas field allocated in the Sea of Okhotsk, 28 km east to Sakhalin Island. Full subsea development scheme in a water depth of 90 m is proposed in this thesis. Clustered production wellheads are equipped with production x-mas trees, protected by a subsea template. It is anticipated that the produced gas goes to a subsea manifold, gathering and distributing it into a pipeline, which delivers gas to the onshore process facilities, where it is treated and sent to a compressor station, connecting the flowline with the existing gas transportation system "Sakhalin-Khabarovsk-Vladivostok".

Only the subsea part of the pipeline design is considered and merely the shore approach is analyzed in terms of protection from ridge gouging.

2.2. DESIGN STANDARDS

Pipeline design methodology, considerations and calculations are based on standards commonly used worldwide. The following standards have been applied in this thesis:

- *DNV-OS-F101 (2007)* – Submarine Pipeline Systems;
- *DNV-RP-E309 (1988)* – On-bottom Stability Design of Submarine Pipelines;
- *STO Gazprom 2-3.5-051-2006* – Regulations of Gas Trunk Pipelines Design (in Russian);
- *API 5L (2007)* – Specification for Line Pipe;
- *ISO 19906 (2010)* – Arctic Offshore Structures;
- *ISO 13623 (2000)* – Petroleum and natural gas industries – Pipeline transportation systems;
- *RMRS 2-020301-001* – Russian Maritime Register of Shipping – Rules of classification and construction of subsea pipelines.

2.3. FIELD DATA

2.3.1. Gas composition

The gas composition is required in order to obtain gas properties, necessary for the pipeline design. The composition of the fluid, produced from the reservoir and directed to the pipeline is considered to be a constant throughout the entire field life. It is represented in table 2.1:

Table 2.1. Fluid composition.

Gas component		*Molar fraction, %*	*Molar mass, g/mol*
Methane	CH_4	88,95	16,04
Ethane	C_2H_6	3,74	30,07
Propane	C_3H_8	1,70	44,10
i-Butane	C_4H_{10}	1,10	58,12
n-Butane	C_4H_{10}	1,50	58,12
i-Pentane	C_5H_{12}	0,71	72,15
n-Penatne	C_5H_{12}	0,65	72,15
Hexanes	C_6H_{14}	0,55	86,18
Heptanes	C_7H_{16}	0,47	96,00
Carbon dioxide	CO_2	0,23	44,01
Nitrogen + others	N_2 +	0,40	28,01
Water	H_2O	0,57	18,02

2.3.2. Production schedule

The development schedule selection philosophy is set by the operating company [1]. A high production profile is governed by high investments associated with majority of wells and equipment. This type provides a better NPV and gets money back very fast, however the control of reservoir is poorer. The example of such a profile is illustrated in figure 2.1 (a).

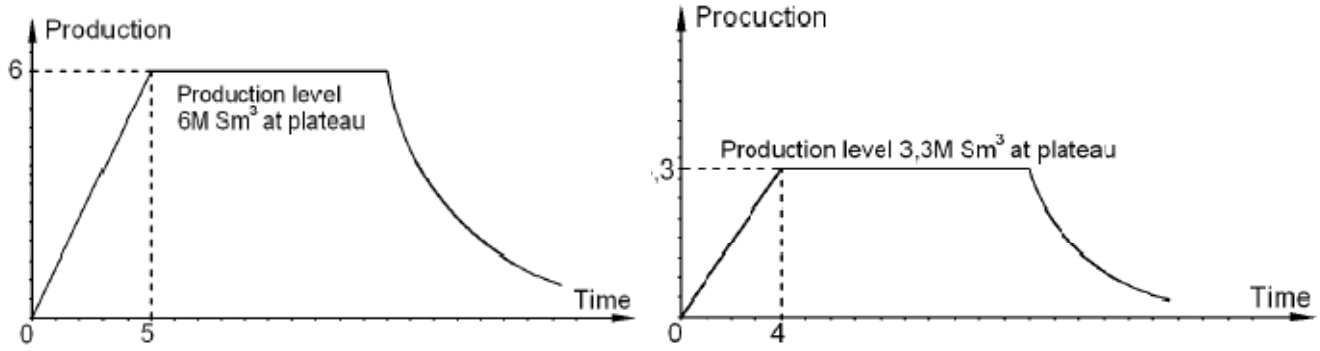

a) b)

Figure 2.1. Example of high (a) and low (b) production profiles [1].

A low production profile (figure 2.1. (b)) is characterized by lower investments and good reservoir control, but it takes a long time to get the money back. This time is even longer in the context of offshore field development due to the period it takes to start the production.

Both systems have pros and cons but both investments reduction and good NPV performance are desirable. The proposed solution therefore lays between high and low profiles and is represented by a 30 year production scheme under consideration that the reserves are estimated to be 90 billion scm of gas. This is indicated in table 2.2 and figure 2.2:

Table 2.2. Production schedule of the gas field.

Year	Annual production, bscm/year	Cumulative production, bscm	Active wells	Year	Annual production, bscm/year	Cumulative production, bscm	Active wells
1	0,68	0,68	2	***16***	3,38	57,9	5
2	2,11	2,79	4	***17***	3,31	61,21	5
3	3,6	6,39	6	***18***	3,29	64,5	5
4	4,22	10,61	6	***19***	3,26	67,76	5
5	4,22	14,83	6	***20***	3,22	70,98	5
6	4,22	19,05	6	***21***	3,16	74,14	5
7	4,22	23,27	6	***22***	3,06	77,2	5
8	4,22	27,49	6	***23***	2,13	79,33	4
9	4,16	31,65	6	***24***	2	81,33	4
10	4,13	35,78	6	***25***	1,92	83,25	4
11	4,06	39,84	6	***26***	1,78	85,03	3
12	4,01	43,85	6	***27***	1,4	86,43	3
13	3,67	47,52	5	***28***	1,24	87,67	3
14	3,59	51,11	5	***29***	1,18	88,85	3
15	3,41	54,52	5	***30***	1,15	90	3

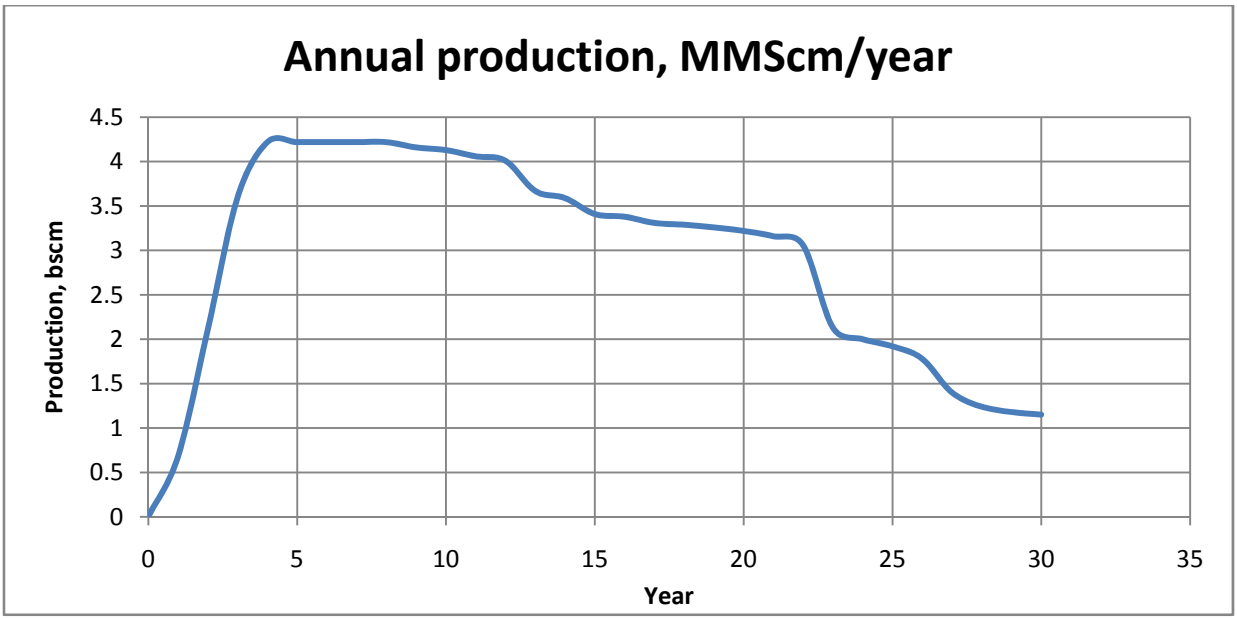

Figure 2.2. Production profile.

2.4. PIPELINE DATA.

In this research it is proposed that the pipeline system is represented by 2 trunk flowlines of smaller diameter instead of 1 large diameter pipeline. Although such a decision could be unacceptable for lines more remote from the shore in terms of excessive pressure drop and cost saving, in this case the short subsea part of the pipeline allows flexibility in diameter selection. As a consequent advantage, the total reliability of the system at steady state flow as well as in transient regime is enhanced due to technological versatility of flow assurance improvement. In addition this double pipeline system provides:

- The possibility of inspection and cleaning tool (pig) launch in the loop if there is no opportunity for vessel coming towards the field location and launching the pig at the flowline starting point (for instance in a condition of substantial ice or deteriorated weather);
- Reduced risk for hydrate plugging as the double pipeline system diminishes the flow rate per each pipe, decreasing the pressure drop and allows therefore maximum pressure reduce beyond the bound of hydrate formation;
- Reduced probability of process unplanned shut-down due to alternative of fluid pumping in one of 2 pipelines and unstable flow regime prevention.

The anticipated system allows the design of a pipeline with respect to the plateau production. The flow rate and other data for hydraulic and thermal analysis are established in tables 2.3 and 2.4 respectively.

Table 2.3. Flowline parameters.

Parameter	***Unit***	***Value***
Flow rate, q	*MMscm/day*	11,6
Inlet pressure, P_1	*MPa*	16,7
Minimum outlet pressure, P_2	*MPa*	8,0
Inlet temperature, T_1	*°C*	70

Table 2.4. Pipeline data [2]

Nominal diameter	***12 3/4”***	***14”***	***16”***	***18”***	***20”***
Outer diameter, D, mm	323,9	355,6	406,4	457,0	508,0
External corrosion coating	6 mm asphalt enamel (density 1400 kg/m^3)				
Insulation coating	Absent				
Wall thickness tolerance, t_{fab}, mm	1				
Corrosion allowance, t_{cor}, mm	3				
Pipe roughness, K, mm	0,030				
Ovality f_0	0,005 (5%)				

Several pipeline dimensions were studied for hydraulic condition suitability analysis. Corrosion protection is carried out by 6 mm of asphalt enamel (bitumen) coating, providing a good behavior for long term corrosion protection and adequate material properties for relevant pipeline operating temperatures, which is a normal practice for present pipeline projects [3,4].

2.4.1. Material data

A pipeline material data is essential for the pipeline design and design analysis. The pipeline is assumed to be manufactured from carbon-manganese steel (C-Mn) as the most commonly used competitive material. The information about the steel grades considered for comparison according to API [2] is given in table 2.5. The pros and cons of using higher material grade are discussed in section 3.5.1.

The stress-strain relationship apparently appears to be one of the most important pipeline characteristics while analyzing the (soil) action on the pipe and its response. The relationship is based on the Ramberg-Osgood material response characterization and shown in figure 2.3 below for each steel grade, complemented by table 2.6, showing two characteristic points on the stress-strain curves: SMYS – where steel starts to yield at the constant stress applied; SMTS – the maximum stress, that material can withstand.

Table 2.5. Pipeline material data [2]

Parameter	*Unit*	*Values*		
Material grade		**X60**	**X65**	**X70**
Density	kg/m^3	7850	7850	7850
SMYS	*MPa*	414	448	483
SMTS	*MPa*	517	531	565
Elasticity modulus	*MPa*	$2{,}07 \cdot 10^5$	$2{,}07 \cdot 10^5$	$2{,}07 \cdot 10^5$
Poisson ratio	-	0,3	0,3	0,3
Thermal expansion coefficient	*1/°C*	$1{,}17 \cdot 10^{-5}$		

Table 2.6. Stress-strain relationship

Strength	*Stress, MPa*			*Strain*
	X60	*X65*	*X70*	
SMYS	414	448	483	0,005
SMTS	517	531	565	0,200

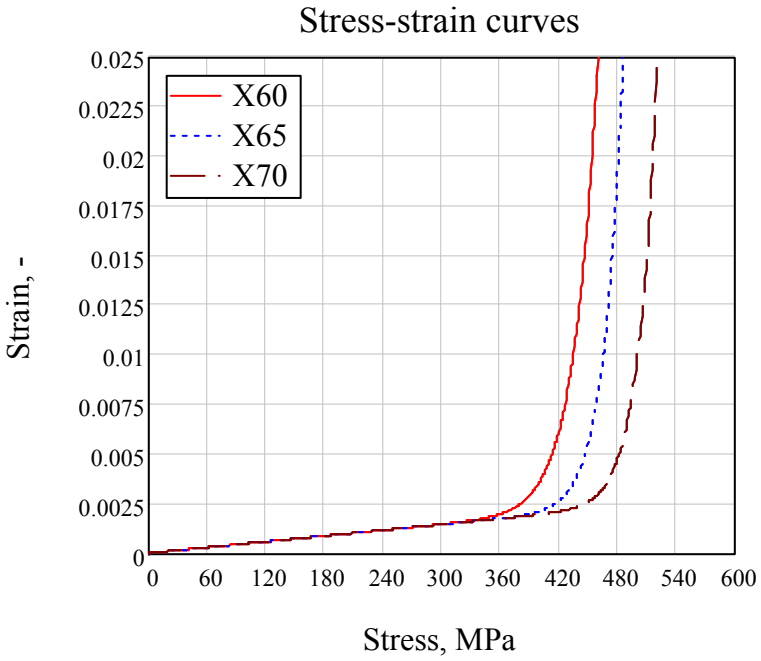

Figure 2.3. Stress-strain curves for different steel grades

2.4.2. Design factors

Design factors (table 2.7) are chosen on the basis of DNV requirements [5] for the pipeline design. The material resistance factor governs the ultimate limit state design, since fatigue design is not involved in the study scope. Due to possible human activity and some risk of human injury and significant pollution for temporary conditions safety class for pressure containment is set to medium. Stress de-rating in terms of operating temperature is given by figure 2 of DNV [5].

The design factors for gouging implications on the pipeline design beforehand were taken with higher values – scouring process is not well understood yet, but the consequences of the wrong design are severe. Basing the theoretical study and calculations on the pipeline limit states the overstated factors might cover relevant omissions, assumptions and approximations somehow.

Table 2.7. Design factors [5]

Factor	*Class*	*Value*
Material resistance factor, γ_m	SLS/ULS/ALS	1,15
Safety class resistance factor (pressure containment), γ_{sc}	Medium	1,138
Safety class resistance factor (scouring implications), γ_{sc}	High	1,308
Material strength factor, α_u	Normal	0,96
Temperature de-rating, $f_{y(u),\ temp}$	70 °C temperature	10 MPa
Resistant strain factor, γ_e	High	3,3
Environmental load factor, γ_F	ULS	1,3

2.4.3. Material thermal conductivity properties

Thermal conductivity coefficients, required for pipeline thermal analysis are expressed in table 2.8 [6]:

Table 2.8. Thermal conductivities for typical pipeline materials [6]

Material	*Thermal conductivity, λ, W/mK*
Pipeline steel	47
Seabed soil	2,0
Concrete coating	1,5
Asphalt enamel	0,16
Water	0,6

2.5. ENVIRONMENTAL DATA

2.5.1. Wind conditions

The wind velocities and directions are critical for the environmental action on the upper part of the ridge. Wind conditions are characterized by a seasonal alternation of direction from the mainland and the ocean [7]. In winter northern, northwestern or western directions prevail. Southern and eastern winds become prevalent when the warm season sets in. The wind velocities occurring with n-year frequency are shown in table 2.9.

Table 2.9. Wind velocities (m/s) 10 m above sea level [7]

Average time	*Frequency (years)*				
	2	*10*	*25*	*50*	*100*
1 hour	25	32	34	38	41
1 minute	33	42	46	50	54
3 seconds	36	46	50	55	59

In this thesis the 10-year wind with 1 minute duration having speed of 42 m/s was suggested. Lower probability of wind occurrence in a combination with maximum observed ridge dimensions and 100-year current is fairly unlikely. Other data on wind is shown in table 2.10.

Table 2.10. Air density and drag coefficients [4, 16]

Parameter	*Unit*	*Value*
Drag coefficient, C_{da}	-	*0,9*
Skin friction coefficient, C_{sa}	-	10^{-3}
Air density, ρ_a	kg/m^3	*1,3*

2.5.2. Waves

Although waves in the case of substantial ice do not affect the ice movement due to attenuation [8], they are important for the pipeline on-bottom stability assessment during open sea conditions. Truskov [10] has made a finite element analysis of the wave conditions in the Sea of Okhotsk using the data from the Piltun-Astokhskoye field platform. Water attack angles either for the waves or for the current are assumed as 90° to the pipeline axis. The design is performed with respect to wave with parameters established in table 2.11.

Table 2.11. Design wave parameters [10]

Parameter	***Unit***	***Value***	
Return period	-	10 years	100 years
Significant wave height, H_s	m	7,2	9,8
Peak period, T_p	s	12,5	14,6
Peakedness, γ	-	3,3	
Wave attack angle, θ_w	degrees	55	

Two waves were chosen according to DNV [11] governing the design wave dependence on whether the current or the wave on-bottom stability influence is dominating.

2.5.3. Currents

The water circulation pattern of northeastern Sakhalin shelf is a complex system of vortices and intense flows with a predominant tidal component. The current velocity range is a desirable parameter determining the ice drift and the subsea water motion, essential for this study. It was reported [7] that 100-year current lays below 0,2 m/s; Truskov [10] gives more pessimistic values based on finite-element analysis, emphasizing the slowest speeds of 0,2-0,3 m/s. The highest are 2-4 times higher. The values selected are given in table 2.12.

Table 2.12. Current data

Parameter	***Unit***	***Value***	
Return period	-	10 years	100 years
Surface current speed, u_c	m/s	1,4	2,0
Current speed, u_r 3 m above the seabed	m/s	0,46	0,64
Current attack angle, θ_c	degrees	50	

2.5.4. Seawater properties.

Seawater density, temperature and drag coefficient are shown in table 2.13. The minimum possible water temperature was proposed in terms of relevance for thermal analysis.

Table 2.13. Seawater data

Parameter	***Unit***	***Value***
Minimum temperature, T_e°	C	*-1,8*
Density, ρ_w	kg/m^3	*1030*
Drag coefficient, C_{dw}	-	*0,9*

2.5.5. Seabed properties.

The pipeline seabed area is characterized by the following:

- The homogeneous seabed structure with the upper layers formed by fine sand;
- Even seabed angle from the shoreline to the 5 km offshore extent at the 85 m water depth, further seawards the seabed remains flat;
- The gas field area and the corridor of the pipeline route are zones of active fishing with trawling equipment;

Data on soil is depicted in table 2.14

Table 2.14. Seabed data

Parameter	***Unit***	***Value***		
		Sand	***"Stiff" clay***	***"Soft" clay***
Wall friction angle, ϕ_w	degrees	*25,4*	*20*	*0*
Internal friction angle, φ	degrees	*30*	*23*	*0*
Cohesion, c	kPa	*0*	*10*	*3,5*
Friction coefficient (pipeline – soil), μ_p	-	*0,7*	*0,5*	*0,3*
Friction coefficient (ice – soil), μ	-	*0,5*	*0,4*	*0,3*
Soil density, ρ_s	kg/m^3	*1500*	*1600*	*1800*
Elasticity modulus, E_s	MPa	*200*	*140*	*10*
Poisson ratio, v_s	-	*0,3*	*0,3*	*0,3*
Seabed slope	degrees	*1*		

Despite the seabed of the Sakhalin shelf is generally represented by the sand [10], the weaker layers are analyzed being the potential backfilling materials for the pipeline protection purposes.

2.5.6. Ice conditions.

The ice conditions in the northeastern part of the Sakhalin shelf are mainly represented by characterization of the following ice features:

- Level ice;
- Rafted ice;
- Ridges;
- Stamukhas;
- Ice zones;

Level ice

The surrounding ice cover is normally described in terms of the level ice thickness. The level ice itself of course is not of big concern for the subsea pipeline, however acting as a driving force it is important for ridge impact related to the seafloor gouging. Hence, the selection of level ice parameters with some confidence is critical while designing the pipeline against the considered phenomenon.

The 100-year design values of level ice thickness and ice drifting speed with corresponding 1% probability of exceedance were anticipated in table 2.15, as Vershinin et al. reported [14].

Rafted ice

Rafted ice thickness would contribute much in design of the majority of offshore structures, however its implication on the scouring process is negligible and considered to be absent.

Ridges

Only first-year ridges have been observed in the region of the Sea of Okhotsk. 18 ridges measurements performed by SakhalinNIPImorneft [13] allowed estimate hummocked ice parameters.

As the ridges corresponding to 10- 100- and 10000-year values are not normally distinguished, the design ridge set is based on the consideration of maximum observed sail height [7]. However the probability analysis of the ridge and the scour features and their implications on the pipeline is present in subsequent study and is based on:

- The distribution of ridge keel drafts;
- The distribution of ridge keels breadths (gouges widths);
- The distribution of gouge length.

The ridge dimensional parameters together with some anticipated physical values are reflected in table 2.15.

Stamukhas

Identically to the rafted ice parameters, stamukhas are not referred to in this study.

Table 2.15. Ice data

Parameter	*Unit*	*Value*
Maximum level ice thickness (100-year value), h_i	*m*	*1,2*
Ice speed (100-year value), v_i	*m/s*	*1,1*
Ridge sail height, h_s	*m*	*6,0*
Consolidated layer thickness, h	*m*	*2,8*
Keel angle, α_k	*degrees*	*30*
Sail angle, α_s	*degrees*	*20*
Single keel breadth, *B*	*m*	*30*
Ice density, ρ_i	*kg/m^3*	*916*
Ridge average block size, T_b	*m*	*0,4*
Sail porosity, η_s	*-*	*0,07*
Elasticity modulus, E_i	*MPa*	*8000*
Poisson ration, v_i	*-*	*0,34*
Ice ridge rubble internal friction angle, □$_i$	*degrees*	*20*
Keel rubble cohesion, C_i	*kPa*	*15*
Average observed gouge depth, $\bar{d}$ [14]	*m*	*0,13*
Average ridge density per 1 km, n_v [14]	*1/km*	*0,5*
Average observed scour length, $\bar{l}$ [14]	*m*	*100,7*

Ice zones

Three ice zones could be distinguished off the Sakhalin Island:

- *Landfast ice* – narrow band of continuous stable first-year ice along the Sakhalin Island, adjacent to the coastline. Up to the depth of several meters seawards the landfast is represented by the level ice, but slightly further the area is typically rough and covered with hummocks of ridges or grounded stamukhas. In winter the extreme extension of the Sakhalin fast ice could reach 16 m water depth [15], such that in some regions the area of 2-4 km is well-protected against heavy ice features penetration into the soil;
- *Flaw lead* – the coastal flaw leads, frequently seen off the northeast coast of Sakhalin [15], are intermediate thin ice areas between the edge of the landfast ice

and offshore pack. Consisting of thinner ice, the flaw leads zones reduce the probability of ice ridges scouring deeper gouges [15]. With that this zone creates good conditions for various vessel operations, such as subsea pipeline repair.

- *Pack ice* – the most part of the northeastern Sakhalin shelf is covered by the offshore pack of substantial ice, drifting mainly southwards [15]. The pack ice is rough and hummocked, though big-sized level ice floes could be found. It is pack ice zone together with relatively shallow waters, which provides the most hazardous gouge depths

2.6. REFERENCES

[1] O. T. Gudmestad (2011): *Arctic Offshore Engineering lecture notes*. UNIS, Longyerbyen.

[2] API Specification 5L (2000): *Specification for Line Pipeline.* 42^{d} edition, Washington D. C., USA.

[3] FMC Technologies (2010): *Development of Main Design Solutions of Kirinskoye Gas Condensate Field Subsea Production Complex (in Russian).* LLC "Gazprom Dobycha Shelf" internal document, Moscow, Russia.

[4] INTECSEA (2011): *Shtokman pipeline FEED design basis memorandum.* LLC "Gazprob Dobycha Shelf" internal document, Moscow, Russia.

[5] DNV (2007): *Submarine pipeline systems*. Offshore Standard DNV-OS-F101, Det Norske Veritas, Høvik.

[6] Braestrup, M.W., Andersen, J.B., Andersen, L.W., Bryndum, M.B., Christensen, C.J. and Nielsen, N.R. (2005) *Design and Installation of Marine Pipelines.* Blackwell Publishing and ASME, Fairfield, New Jersey, USA.

[7] O.T. Gudmestad, A.B. Zolotukhin, A.I. Ermakov, R.A. Jakobsen, I.T. Michtchenko, V.S. Vovk, S. Løset, K.N. Shkhinek (1999): *Basics of offshore petroleum engineering and development of marine facilities*. Moscow, "Neft i gas" publishing house, 350 p.

[8] S. Løset (2011): *Arctic Offshore Engineering lecture notes*. UNIS, Longyerbyen.

[9] S. Løset, K. Shkhinek, O. T. Gudmestad, P. Strass, E. Michalenko, R. Frederking, T. Karna (1999): *Comparison of the physical environment of some Arctic seas.* Cold regions science and technology 29 (1999), pp. 201-214;

[10] P. A. Truskov (1999): *Metocean, Ice and Seismic Conditions Offshore Northeastern Sakhalin Island.* Offshore Technology Conference, Houstonm Texas, 3-6 May 1999, paper number OTC 10816.

[11] DNV (1988): *On-bottom Stability Design of Submarine Pipelines.* Recommended Practice RP-E305, Det Norske Veritas, Høvik.

[12] http://www.stanford.edu/~tyzhu/Documents/Some%20Useful%20Numbers.pdf

[12] G. N. Surkov, P. A. Truskov (1995): *Study of Ice Pressure Ridges and Stamukh Offshore of Sakhalin.* The Tenth Int. Symp. On "Pkhotsk sea and sea ice", Mombetsu, Hokkaido, Japan, pp 86-88.

[13] Gazprom (2006): *Technological Design Standards of Trunk Pipelines (in Russian).* Organization Standard, STO Gazprom 2-3,5-051-2006, Moscow, Russia.

[14] S.A. Vershinin, P.A. Truskov, P.A. Liferov (2007): *Ice features action on seabed.* IPK "Russkaya kniga", Moscow, Russia, 196 p. (in Russian).

[15] T. Walle (2004): *Ice gouging offshore Sakhalin Island*. Master thesis, Department of Material Science and Technology, Stavanger University College, Stavanger, 105 p.

[16] ISO/FDIS 19906 (2010): *Petroleum and natural gas industries – Arctic offshore structures.* International standard, International Standardization Organization, Geneva.

[17] ISO 13623 (2000): *Petroleum and natural gas industries – Pipeline transportation systems.* International standard, International Standardization Organization, Geneva.

[18] API Recommended practice 2N (1995): *Recommended Practice for Planning, Design and Constructing Structures and Pipelines for Arctic Conditions.* 2^{d} edition, Washington D. C., USA.

[19] CAN/CSA S471-92 (1992): *General requirements, design criteria, the environment and loads.* Canadian Standards Association, National Standard of Canada, 87 p.

[20] RMRS 2-020301-001 (2008): *Rules of classification and construction of subsea pipelines*. Russian Maritime Register of Shipping, Saint-Petersburg, Russia.

CHAPTER 3. PIPELINE DESIGN

3.1. DESIGN PROCESS

In order to provide reliable subsea pipeline systems the detailed design should be performed in accordance with international standards. The first task is to assemble information about the design requirements in order to have a notion about operational features and to leave nothing to be assumed. The design should be based on [1]:

- The chemical composition of the fluid to be transported via the pipeline;
- The maximum and minimum pressure at the upstream end;
- The maximum and minimum pressure at the downstream end;
- Temperature of the fluid;
- Bathymetric and topographic information, especially the locations and heights of the end points;
- The available source of geotechnical information about the seabed properties;
- Oceanographic information about the sea surrounding the pipeline;
- Any known constraints on the route specifics (politics, environment, other uses of seabed)

Once this information has been collected, the pipeline design is able to be carried out. Normally it consists of several stages; the objective and scope of either is determined by the operator mainly and depends on the size of the project. The major general stages with respect to the pipeline design are [2]:

1) Conceptual engineering:
   - To establish technical feasibility and constraints on the system design and construction;
   - To remove non viable alternatives;
   - To perform basic cost analysis and scheduling;
   - To identify interface with other systems planned or existing.

This stage of the pipeline design allows being flexible in technologies and decision making, while work expenditures are minimum (figure 3.1). It eliminates potential difficulties and areas where more effort may be required in the data acquisition and design areas. However the best specialists should be here in order to provide the best alternative fitting all technical requirements on future design stages.

2) Preliminary engineering:
   - To verify pipeline sizing;
   - To select the pipeline material;
   - To apply code requirements on pipeline installation, commissioning and maintenance;
   - Prepare authority applications

Here system specific knowledge grows, either cost incurred does; but the ease to change decreases much.

3) Detailed engineering

The stage of detailed engineering includes the development of pipeline design to a point where the technical input for all procurement and construction tendering can be defined in

sufficient detail, diminishing an opportunity for global changes in design. The primary objects can be summarized as follows:

- Route selection and optimization;
- To carry out hydraulic and thermal analysis in order to determine the pipeline diameter, temperature and pressure profiles and whether thermal insulation or cooling are required;
- To select wall thickness and materials for all types of coatings;
- Confirm code requirements on strength, vortex-induced-vibrations, on-bottom stability, global buckling and installation;
- Development of the design and drawings in sufficient detail for the subsea scope. This may include pipelines, tie-ins, crossings, span corrections, risers, shore approaches, subsea structures;
- Preparation of alignment sheets based on the most recent survey data;
- Preparation of specifications, typically covering materials, cost applications, construction activities (pipelay, survey, welding, riser installations, subsea structures installation) and commissioning (flooding, pigging, hydrotest, cleaning, drying);
- To design cathodic protection system.

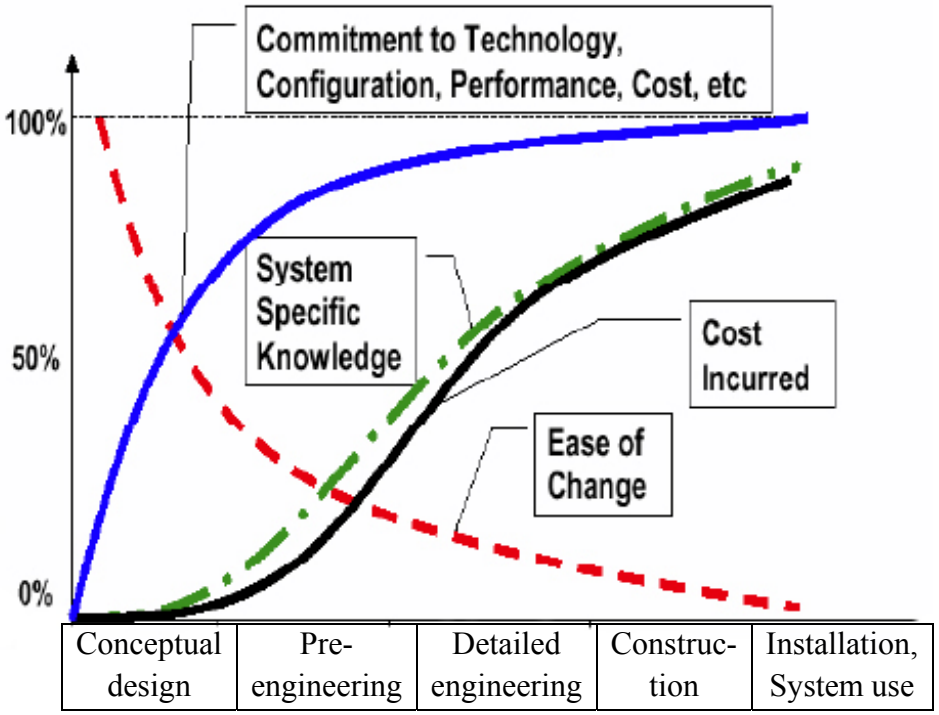

Figure 3.1. Design stages and commitment to cost and technical issues [3]

Since the main point of this thesis is the study of interaction mechanisms between ice ridges and pipelines not all of these stages will be accounted and performed in the research. Nevertheless it is necessary to carry out some design in order to tie the work to the specific conditions and to show that the anticipated challenge is relevant for actual objects.

As it was shown in previous chapter, ice ridges at the location of the Sea of Okhotsk can interact with the sea bottom on water depths less than 30 m. The main attention therefore will be given to the shore approaching pipeline part. This part is presumed to be trenched following

several considerations: 1) floating ice ridge could wrap the pipe in the case of direct contact; 2) wave breaking zone is taking place where the pipeline is affected by the huge hydrodynamic forces from waves. Thus the design process will be simplified and include:

- Diameter selection;
- Material selection;
- Wall thickness determination;
- On-bottom stability check;

3.2. DIAMETER SELECTION

The majority of technical literature doesn't give a technique on calculation of internal diameter for gas pipelines, starting the design description with wall thickness selection and stresses in the pipe. However the actual analysis could be carried out on the basis of knowledge in hydraulics and code requirements.

The chart diagram for inner diameter sizing is indicated in figure 3.2.

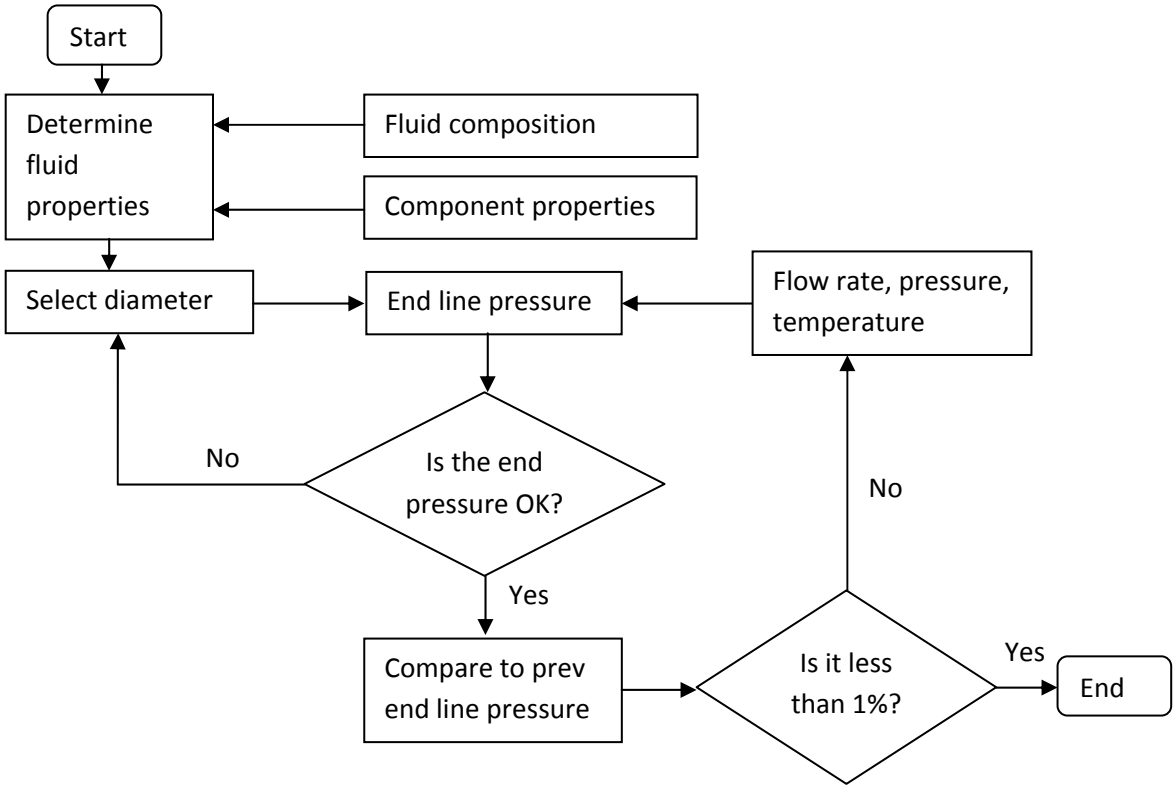

Figure 3.2. Chart diagram for inner diameter selection

It is clear that the pipeline inner diameter should be selected on the basis of:

- Fluid properties;
- Annual flow rate;
- Availability of the system;
- Required pressure at pipeline end;

Obviously the flow rate is variable during the field exploitation period and depends on the production profile which has to be decided according to the economical and technical aspects. The typical production profile (figure 3.3) is represented by three different phases in the lifetime of a field before it is abandoned:

1. Production build-up;
2. Plateau production;
3. Tail production

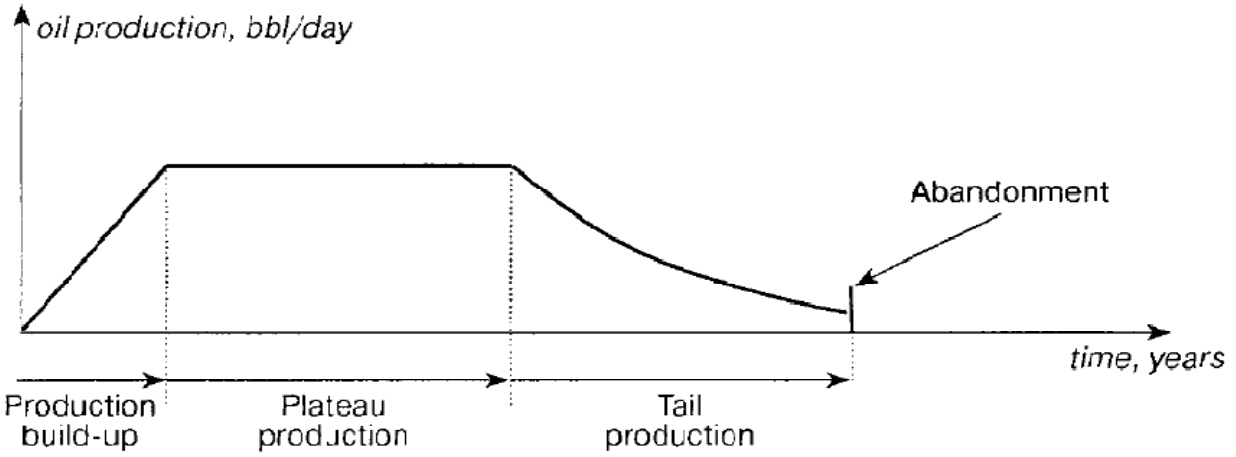

Figure 3.3. Typical production profile of an oilfield [4]

The sizing should be carried out with respect to the plateau production. If it is very high the larger pipelines are required.

It is also important to distinguish chemical composition of hydrocarbons from different fields. It affects density, viscosity, compressibility, thermal conductivity and other physical properties. This information is essential in order to calibrate the pipeline size based on required pressure at delivery, as well as it is desirable for corrosion and thermal insulation coatings.

3.2.1. Fluid properties.

Normally gas is a multi-component mixture, primary consisting of hydrocarbons. In addition to that, water, nitrogen, carbon dioxide and hydrogen sulfide are often present. The content of each affects thermophysical properties of natural gas, which are important values in hydraulic analysis. Defining these properties one could emphasize gas molar mass, density, compressibility factor, dynamic viscosity, isobaric heat capacity and Joule-Thompson coefficient.

Gas molar mass

Since natural gas is a mixture of components, the average molar mass of gas can be calculated from the mole fractions x_i of the components and their molar masses M_i

$$\bar{M}_g = \sum_{i=1}^{n} M_i x_i \tag{3.1}$$

Gas density

In general, density varies by changing pressure and temperature conditions of a fluid. For liquids this effect is negligibly small – opposite to gas which is sensitive to the thermobaric conditions. Density of gas determined under the standard pressure $P_0=0,1013\ MPa$ and temperature $T_0=293,15\ K$ might be calculated from the following equation:

$$\rho_0 = 10^3 \cdot \frac{\bar{M}_g P_0}{R_\mu T_0 Z_0} \tag{3.2}$$

Here $R_\mu = 8{,}31$ is the gas constant; Z_0 - gas compressibility factor at standard conditions.

Gas specific gravity

Gas specific gravity defines the ratio of the gas and the air densities at the same temperature and pressure:

$$\Delta = \frac{\rho_0}{\rho_a} = \frac{M}{29} \tag{3.3}$$

Where ρ_a - air density in standard conditions.

Gas compressibility factor

This coefficient accounts for the real gas behavior. Its value generally increases with pressure and decreases with temperature. At higher pressure molecules are colliding more often, which allows repulsive forces between molecules to have significant effect, making the molar volume of real gas greater than the molar volume of corresponding ideal gas. When pressure is lower, it is easier for molecules to move, making coefficient smaller than 1. Compressibility factor is represented by the function of reduced pressure P_r and temperature T_r. According to Gazprom standard [5]:

$$Z = 1 + A_1 P_r + A_2 P_r^2 \tag{3.4}$$

Where

$$A_1 = -0{,}39 + \frac{2{,}03}{T_r} - \frac{3{,}16}{T_r^2} + \frac{1{,}09}{T_r^3}$$

$$A_2 = 0{,}0423 - \frac{0{,}1812}{T_r} + \frac{0{,}2124}{T_r^2}$$

$$P_r = \frac{P}{P_{pc}}$$

$$T_r = \frac{T}{T_{pc}}$$

Here P and T are absolute nominal pressure and temperature in the pipeline; T_{pc} and P_{pc} are known as gas pseudo-critical temperature and pressure. They could be expressed through the critical parameters of each gas component with T_{ci} being the critical temperature above which it is not possible to liquefy a gas and P_{ci} - the minimum pressure required to liquefy a gas component at its critical temperature:

$$T_{pc} = \sum_{i=1}^{n} x_i T_{ci} \tag{3.5}$$

$$P_{pc} = \sum_{i=1}^{n} x_i P_{ci} \tag{3.6}$$

Critical parameters for gas components could be taken from Russian GOST [6].

Dynamic viscosity

The dynamic viscosity is a measure of the resistance to the flow exerted by gas. It is an important parameter in the pressure loss for gas flow in the pipeline. High viscous pressure drop in a pipeline segment may impact on production deliverability. There are many empirical relations to calculate gas viscosity based on the temperature and pressure. In distinction from the

viscosity of oil, the gas viscosity increases with increasing temperature. This distinguished feature is accounted in the following expression [5]:

$$\mu_g = \mu_0(1 + B_1 P_r + B_2 P_r^2 + B_3 P_r^3) \quad (3.7)$$

$$\mu_0 = (1{,}81 + 5{,}95 T_r) \cdot 10^{-6}$$

$$B_1 = -0{,}67 + \frac{2{,}36}{T_r} - \frac{1{,}93}{T_r^2}$$

$$B_2 = 0{,}8 - \frac{2{,}89}{T_r} + \frac{2{,}65}{T_r^2}$$

$$B_3 = -0{,}1 + \frac{0{,}354}{T_r} - \frac{0{,}314}{T_r^2}$$

Joule-Thompson coefficient.

This coefficient is critical for the hydraulic and thermal analysis. It considers temperature change due to pressure drop in the process of adiabatic choking. The temperature in terms of this effect could drop even below the environmental temperature, causing a hazard of hydrate formation or gas liquefaction reaching dew point temperature. The value of this coefficient is depicted by [5]:

$$D_i = H_0 + H_1 P_r + H_2 P_r^2 + H_3 P_r^3 \quad (3.8)$$

$$H_0 = 24{,}96 - 20{,}3 \cdot T_r + 4{,}57 \cdot T_r^2$$

$$H_1 = 5{,}66 - \frac{19{,}92}{T_r} + \frac{16{,}89}{T_r^2}$$

$$H_2 = -4{,}11 + \frac{14{,}68}{T_r} - \frac{13{,}39}{T_r^2}$$

$$H_3 = 0{,}568 - \frac{2{,}0}{T_r} + \frac{1{,}79}{T_r^2}$$

Isobaric heat capacity

The equation for heat capacity calculation is outlined as [5]:

$$C_p = \frac{R_\mu}{\overline{M}_g} \cdot (E_0 + E_1 P_r + E_2 P_r^2 + E_3 P_r^3) \quad (3.9)$$

$$E_0 = 4{,}437 - 1{,}015 \cdot T_r + 0{,}591 \cdot T_r^2$$

$$E_1 = 3{,}29 - \frac{11{,}37}{T_r} + \frac{10{,}9}{T_r^2}$$

$$E_2 = 3{,}23 - \frac{16{,}27}{T_r} + \frac{25{,}48}{T_r^2} - \frac{11{,}81}{T_r^3}$$

$$E_3 = -0{,}214 + \frac{0{,}908}{T_r} - \frac{0{,}967}{T_r^2}$$

3.2.2. Hydraulic analysis

The mixture of hydrocarbon components can exist as a single-phase or a multi-phase mixture depending on temperature, pressure and fluid composition. Despite in the well stream there is some water and condensate (≈1,5%), it is anticipated that they will not disturb the flow, making it unstable. With that this induces special implications on the system availability, since the special operating measures allowed export in the unstable flow regions are not considered

robust or practical. In this regard the additional use of the proposed double pipeline system appears in the possibility of flow circulation even if the wellhead production is partially closed.

Thus the single-phase flow hydraulic theory could be applied with a certain level of confidence. This theory is well understood and analytical models may be used. The basis for the pressure drop and the temperature profile calculation is the conservation of mass, momentum and energy of the flow.

It is well known that gas is compressible so as it flows, pressure drops, the gas expands increasing flow velocity causing the increase of drag. Opposite to velocity term which is very important the elevation effect is small due to relatively low gas density.

In the standard of Gazprom [5] the expression depicting the gas flow is given by the flow rate [MMsm^3/day]:

$$q = 3{,}32 \cdot 10^{-6} \cdot d^{2{,}5} \sqrt{\frac{P_1^2 - P_2^2}{\lambda \Delta Z_a T_a L}} \tag{3.10}$$

Where P_1 is the pressure inside the pipe at the beginning of trunk pipeline, MPa; P_2 – minimum delivery pressure, MPa; L – pipeline length, km; T_a – average gas temperature, K; λ – hydraulic friction coefficient; Δ - gas-air density ratio; Z_a - average compressibility factor; d – inner diameter in mm.

Rearranging this equation with respect to the minimum inner diameter:

$$d = \sqrt[5]{q^2 \cdot 9{,}07 \cdot 10^{10} \cdot \frac{\lambda \Delta Z_a T_a L}{P_1^2 - P_2^2}} \tag{3.10a}$$

Hydraulic friction coefficient depends on Reynolds number and relative roughness. It could be determined by the Moody diagrams or by empirical relationship. Gases in pipes always flow in quadratic friction mode (turbulent flow). Therefore, opposite to friction for oil flows, there is only one formula for friction coefficient in gas pipelines:

$$\lambda = 0{,}067 \cdot \left(\frac{158}{Re} + \frac{2K}{d}\right)^{0{,}2} \tag{3.11}$$

K – pipe roughness; Re – Reynolds number in given dimensions [5]:

$$Re = 17{,}75 \cdot 10^3 \frac{q\Delta}{\mu_g d} \tag{3.12}$$

Here μ_g- dynamic viscosity, Pa·s.

From 3.3.1 it is well seen that the set of parameters (compressibility factor and viscosity) depends on the average temperature and pressure. The average pressure is expressed as follows [5]:

$$P_a = \frac{2}{3}\left(P_1 + \frac{P_2^2}{P_1 + P_2}\right) \tag{3.13}$$

Whereas the average temperature [5]:

$$T_a = T_e + \frac{(T_1 - T_e)}{aL}(1 - e^{-aL}) - D_i \frac{P_1^2 - P_2^2}{2aLP_a}\left(1 - \frac{1}{aL}(1 - e^{-aL})\right) \tag{3.14}$$

This equation accounts either for the heat loss to the environment (second term) or the Joule-Thompson effect of temperature diminishing due to the sustainable pressure drop (third term). T_e – temperature of surrounding environment, K; T_1 – initial temperature, K. Parameter a is given by [5]:

$$a = 225{,}5\frac{k_a D}{q\Delta C_p \cdot 10^6} \tag{3.15}$$

It involves isobaric heat capacity C_p and average heat transfer coefficient k_a, W/m^{2}K. D – is the outside pipeline diameter, mm; q – gas flow rate, MMm^3/day. Under assumption that the gas temperature is uniform inside the pipe, and thermo insulation is absent the heat transfer coefficient could be calculated for the subsea pipeline from equation:

$$\frac{1}{k_a} = \frac{t}{\lambda_t} + \frac{t_c}{\lambda_c} + \frac{1}{\alpha} \tag{3.16}$$

Where t – pipeline wall thickness, t_c – corrosion coating thickness, λ_t, λ_c – wall thermoconductivity for pipeline steel and for coating respectively; α - heat transfer from the pipe surface to water (to soil for trenched section). One can be obtained from Gazprom code of practice [5]. For heat transfer to water:

$$\alpha_w = 0{,}26\left(\frac{u_r D \cdot 10^{-3}}{\nu_w}\right)^{0{,}6} Pr_w^{0{,}37}\frac{\lambda_w}{D \cdot 10^{-3}} \tag{3.17}$$

Where Pr_w – Prandtl number for water:

$$Pr_w = \frac{\nu_w \rho_w C_{pw}}{\lambda_w} \tag{3.18}$$

u_r – the current speed at the seabed level, m/s; ν_w - kinematic viscosity of water, m^2/s; C_{pw} - isobaric heat capacity for water; λ_w - thermoconductivity for water.

For heat transfer to soil [5]:

$$\alpha_s = \frac{2\lambda_s \cdot 10^3}{D \cdot ln\left[\frac{2D_b}{D \cdot 10^{-3}} + \sqrt{\left(\frac{2D_b}{D \cdot 10^{-3}}\right)^2 - 1}\right]} \tag{3.19}$$

Where λ_s - soil thermoconductivity coefficient; D_b - burial depth.

3.2.3. Discussion

It is well seen that equations written above are interdependent, which means that a number of iteration is required. At the first step following assumptions and approximations were made:

- Average temperature is a logarithmic average of value T_1 and T_e:

$$T_a = \frac{T_1 - T_e}{ln\frac{T_1}{T_e}} \tag{3.20}$$

- Hydraulic friction coefficient is set to 0,02;
- The average pressure in first approximation is set as between initial P_1 and minimum required P_2;
- Before on-bottom stability is done, pipeline is assumed to be uncoated by concrete. If there will be a need in concrete iteration repeats;
- Average temperature is calculated for the pipeline as it is rests on the seabed without trenching anywhere.

The calculations on pipeline diameter selection are given in Appendix B in the sequence of flow chart 3.2. Minimum allowable pipeline inner diameter for given conditions is 370,0 mm, which corresponds to 406,4 mm (16”) standard outer diameter taking into account wall thickness selection.

3.3. PRESSURE AND TEMPERATURE PROFILES

Establishing pressure and temperature profile is critical to evaluate the flow conditions in the pipeline. Opposite to the pressure profile, which is easy to perform using expression (3.10), the temperature distribution requires additional values of thermophysical gas properties (such as Joule-Thompson coefficient and isobaric heat capacity) and environmental data (surrounding temperature and heat transfer).

Thermal parameters are especially important for the gas flow, where it is necessary to keep temperature above the hydrate formation and dew point values. Moreover these parameters are influencing the pressure drop, and, consequently, the final decision upon the flowline diameter.

Temperature profile could be described by the equation [5] for gas flow regarding temperature T at every point x, km:

$$T = T_e + (T_1 - T_e)e^{-ax} - D_i \frac{P_1^2 - P_2^2}{2aLP_a}(1 - e^{-ax}) \tag{3.21}$$

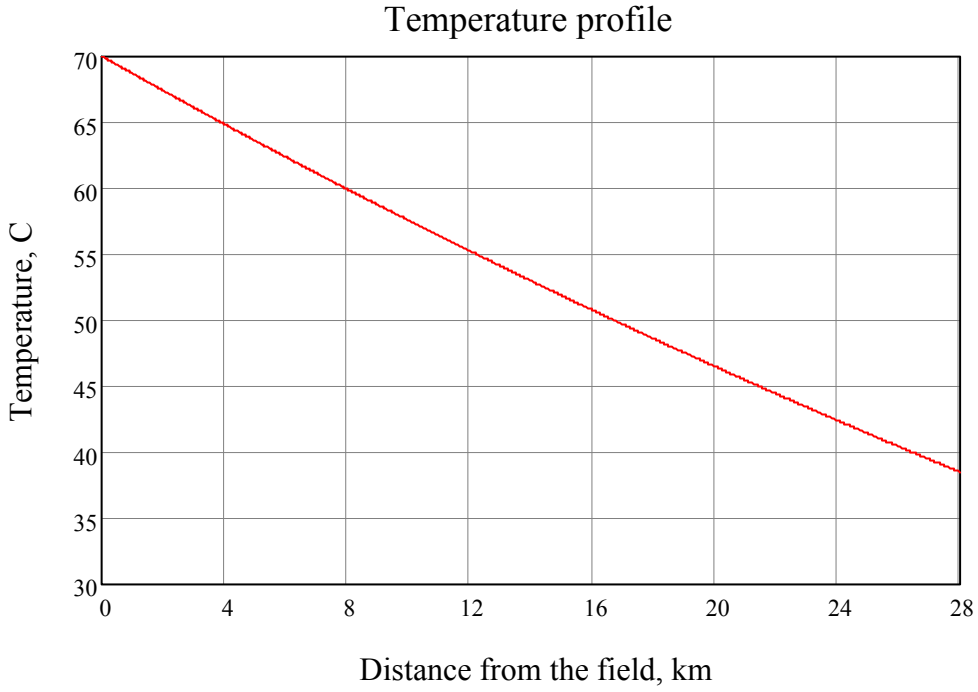

Figure 3.4. Temperature profile along the pipeline route.

Temperature drop has an exponential behavior. Although in this case it drops smooth, bigger distance from the shore will increase both: Joule-Thompson and heat transfer to the environment effects, which could reduce the temperature even below the value of surrounding water. From established profile it could be concluded that there is no considerable need in thermal insulation for given conditions.

Pressure distribution P is derived from the equation 2.1:

$$P = \sqrt{P_1^2 - \frac{9{,}07 \cdot 10^{10} \cdot q^2 \lambda \Delta Z_a T_a x}{d^5}} \tag{3.10b}$$

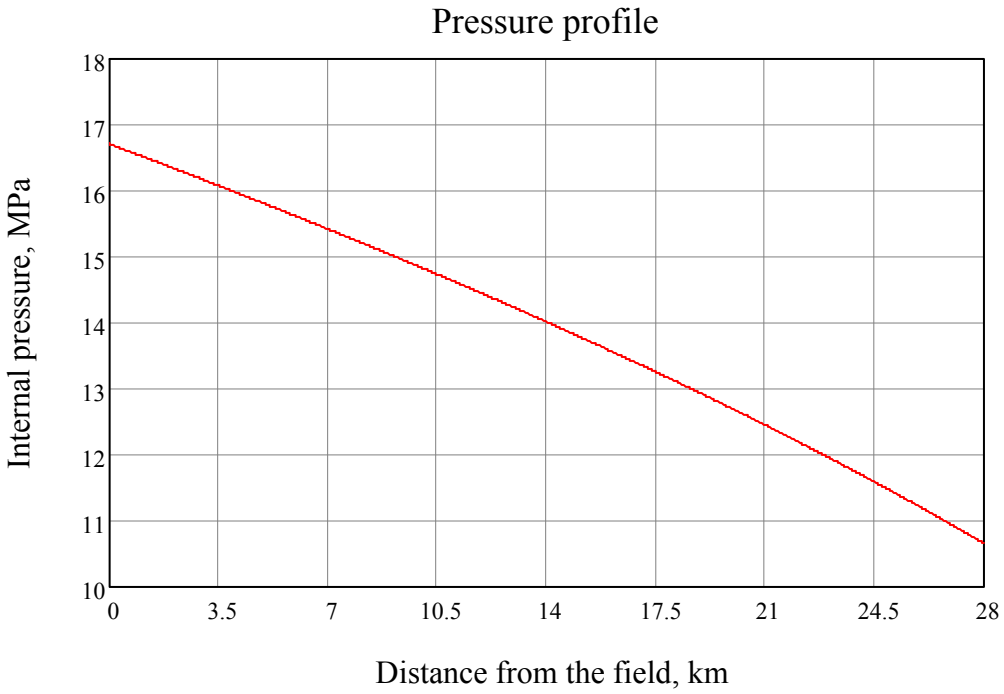

Figure 3.5. Pressure profile along the pipeline route.

As it is seen from the graph pressure profile for gas line is not even and has some parabolic tendency, caused by gas decompression with sustainable properties variations. It is necessary to note that for relatively short pipeline section pressure drop is huge. Obviously this is governed by the small diameter selected above, which could be unacceptable decision for the longer pipeline.

3.4. MATERIAL SELECTION

Apart from exerting loads acting during operation and installation subsea pipelines have to withstand the harmful effect of transported fluids and external environment. Largely this should be provided by the design of the pipeline material. According to DNV [7] materials applied in oil and gas subsea pipelines are described by the following considerations:

- Mechanical properties;
- Hardness;
- Fracture toughness;
- Fatigue resistance;
- Weldability;
- Corrosion resistance

The pipeline is exposed to transverse and longitudinal forces, bending and elongating the pipe. This behavior is characterized by hardness able to absorb overstresses by deformations. This is one of the main mechanical properties of materials, determining the general design. The pipeline material should also have sufficient toughness which describes the ability to resist impact from immediate loads. Such when it is a hazard of falling objects, trawl impact, etc. this parameter could be very important. Fatigue resistance involves the material tolerance to cycling loads, causing slow deterioration in the pipeline steel. Weldability is critical to assure that the welded pipelines and seams provide equal mechanical properties alongside the overall length.

It is necessary to note that there is no best steel fitting all requirements. There is always a dependency between properties mentioned above. And generally it happens that in order to increase the quality of any desirable feature one should trade-off the quality of another.

Either property is applicable to every concept of the pipe material. However it is C-Mn steel which seems to be the most competitive for fabricating subsea pipelines. The steel is a primary element in construction of pipelines, although various alloying ingredients, such as carbon (0,10% - 0,15%), manganese (0,80% - 1,60%), silicon (up to 0,40%), phosphorus (up to 0,20%), sulfur (up to 0,10%), nickel and chromium are present. The selection of composition and content of the different alloys determine the steel grade and thereafter strength, hardness and other mechanical properties.

The main disadvantage of carbon steel pipes is a weak corrosion resistance. It can be improved by including corrosion resistant materials (martensitic, duplex, austenitic stainless steels) making the material to be a CRA (corrosion resistant alloy). Normally these means are feasible for internal corrosion protection, external one may be achieved by cathodic protection and external coatings.

3.4.1. Steel grades.

Steel grade selection in addition to discussed properties should consider the following factors:

- Cost;
- Weight requirement;

Common steel grades are designed with respect to American Petroleum Institute standard [8] providing steel strengths up to X80. In this thesis X60, X65 and X70 are taken as the design basis for material selection.

According to the economical considerations, expenditures for steels fabrication increases for the higher grades, however the increase of grade permits a reduction of pipeline wall thickness. This may reduce the overall cost of a unit weight of a pipeline.

Pipeline material affects installation process much. It is more difficult to weld higher steel grades, which results in lower lay rate. From the other hand in deep water areas where the vessel equipment is required to withstand maximum lay tension the use of high steel grades may be more suitable, as the reduction of pipeline weight by the terms better steel quality reduces the lay tension.

The combination of all factors has to be accounted in steel grade selection. Thus X70 steel grade was chosen in Oman-India Gas Pipeline [2]. This recommendation was dictated by the intersection of technical feasibility of possible wall thicknesses range for X70 steel and the collapse criteria relevant with water depths up to 3500 m.

3.4.2. Fabrication methods.

C-Mn steel pipelines fabrication is subdivided into several types of manufacturing processes, affecting the possibility of wall thickness, allowable diameter selection, speed of fabrication and cost considerations. There exist seamless, submerged arc welded and high frequency welded pipelines (figure 3.6)

Seamless (SMLS) – fabrication of seamless pipelines is carried out without welding by a hot forming process. No welds and good track record in service are advantages for seamless pipelines [9]. On the other hand, wall thickness varies along the pipe length from +15% to -2,5%

resulting in out-of-roundness and –straightness. The other drawback is that manufacturing of large diameter seamless pipes appears to be expensive, limiting the outer diameter for 16 inches.

Submerged arc welding – longitudinal seam (SAWL) – SAWL pipes fabrication is made either by UOE or JCOE processes. These are perfect pipes for large diameter and high pressure flowlines in terms of good out-of-roundness (+/- 1%) and wall thickness tolerance (+10%; -12%) [9].

Submerged arc welding – helical seam (SAWH) – SAWH pipelines are used for large diameter oil and gas transportation. Steel strips or bands are rolled in cylindrical form and welded. Strip or band angle, width and curvature determine the diameter. Wall thickness tolerance is close to SAWL pipelines, however ovality is often higher, and long welds are subjected to corrosion, which is more aggressive at bottom areas. This is main disadvantage as well as limited wall thickness sets bounded use in some conditions, such as high pressure (outside and inside), and high functional loads.

High frequency welded (HFW) – after making a longitudinal weld by high frequency current without the use of filler metal, pipes are formed by strips in continuous rolling process. Cold expansion, hot stretching or sizing can be applied in order to reach desirable diameter and wall thickness. These pipelines are competitive to above mentioned beyond 26 inches in diameter and 25 mm of wall thickness [1] as the tolerance (+/- 5%) and ovality are smaller, and cost implications are less.

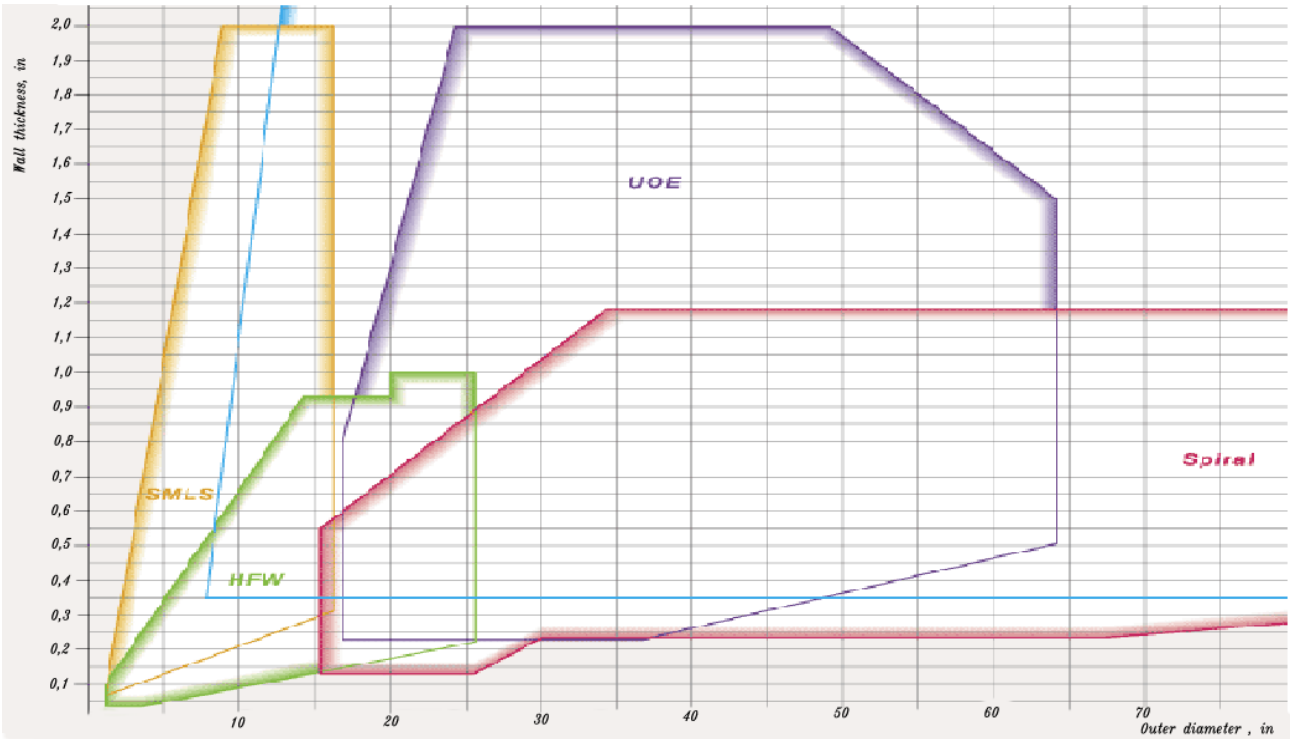

Figure 3.6. The use of pipeline in terms of fabrication methods [1].

3.4.3. Discussion

Accounting all factors on material selection X65 steel provides less material consumption compare to X60 steel and better results in weldability and pipelaying than X70, which could be

important in conditions of not stable weather out of Sakhalin Island. According to calculations on inner diameter selection UOE SAWL fabrication method is recommended in terms of technological availability of the certain diameter pipeline manufacturing.

3.5. WALL THICKNESS SELECTION

3.5.1. Limit state based design criteria

Limit state design criteria has been being used recent time in application to pipelines more widely and has started to be reflected in DNV standards [10]. The design procedure in this case is governed by the Load and Resistance Factor Design (LRFD) format establishes the distribution of load and strength functions and verifies that the designed load in any scenario L_{Sd} doesn't exceed the designed resistance R_{Rd}. [7]:

$$f\left(\frac{L_{Sd}}{R_{Rd}}\right)_i \leq 1 \tag{3.22}$$

DNV divides four limit states:

- *Ultimate limit state* – involves structural integrity and strength; as such the pipeline is designed to have a very low probability reaching this limit state since the consequences are severe. In this research for considered pipeline section only burst describes ULS design as collapse and buckling are unlikely to happen;
- *Serviceability limit state* – includes the disruption in use of the pipeline as intended (excessive ovality, large displacements or vibrations);
- *Fatigue limit state* – design against fatigue damage resulting from cycling loads from different sources and accumulated throughout its life. Sources include currents, waves or slugging. All of them are not anticipated in terms of pipeline for single-phase gas flow, buried in the seabed;
- *Accidental limit state* – involves damage due to unusual, unplanned loading conditions. The acceptance criteria for ALS in this case is related for overall allowable probability for severe consequences. It is allowed to perform the design against such type of loads by direct calculation of the effect imposed on the pipeline.

The pipeline damage due to ice ridge gouging may be considered as being from accidental load if the probability of such event occurrence is less than 10^{-2}. There have been done several researches about probabilistic distribution of ice ridges dimensions and gouge depths range [11, 12, 13] however the assessment of probability of the certain ridge to damage the pipeline should involve field data and statistics, which appears difficult to carry out. Moreover only bursting failure mode for pipeline wall selection is considered in this research (no collapse due to shallow water, buckling, and laying criteria); thus according to DNV recommendations the ULS design can be applied since the bound probability between ULS and ALS criteria (10^{-2}) is reduced for 1-2 orders of magnitude.

3.5.2. Wall thickness parameters

Before pipeline is constructed the wall thickness design is considered to be one of the most essential design issues. This influences the pipeline resistance to loads of different environment, such as internal and external pressure, longitudinal stress and bending. According to DNV [7] the design of a wall thickness is determined by:

- Bursting (pressure containment);

- Local buckling (collapse) due to external pressure;
- Propagation buckling due to external pressure;

The latest is not considered as the external pressure value in terms of shallow water depth is not sufficient to buckle the pipe, able to withstand given (and substantial) internal pressure. However section 5.4.3 discusses the pipeline collapse due to soil overpressure induced by the ridge movement, when the pipeline is embedded below the probable scour depth.

Corrosion allowance also dictates the increase of the wall thickness. Compensation of several millimeters of the pipeline steel provides its protection after years of maintenance when the wall will be partially deteriorated. Accounting components for bursting, corrosion allowance and fabrication tolerance the nominal wall thickness is:

$$t_{nom} = t_b + t_{cor} + t_{fab} \tag{3.23}$$

The nominal value t_{nom} should be taken from standard fabrication wall thicknesses t_s. However the research describes the pipeline put into operation; therefore all subsequent calculations referred to wall thickness will be established with respect to characteristic wall thickness $t = t_s - t_{cor} - t_{fab}$.

Pressure containment design is based on hoop stress due to the pressure differential between internal and external environments. In this regard the general requirement for the pipeline [2]:

$$\sigma_h < \eta_k \cdot \sigma_y \cdot k_t \tag{3.24}$$

Where η_k is the design factor – by all major codes is specified as 0,72; σ_y – *SMYS* – Specified Minimum Yield Strength; k_t - material temperature de-rating factor. DNV [7] uses modified formula for the bursting criteria:

$$p_i - p_e \leq \frac{p_b(t_b)}{\gamma_m \gamma_{sc}} \tag{3.25}$$

Where the first term is a load; γ_m - material resistance factor (table 2.7 in the design basis); γ_{sc} – safety class resistance factor (table 2.7); p_b - pressure containment resistance:

$$p_b(t_b) = \frac{2t_b}{D - t_b} f_{cb} \frac{2}{\sqrt{3}} \tag{3.26}$$

Where

$$f_{cb} = Min\left[f_y; \frac{f_u}{1{,}15}\right] \tag{3.27}$$

Here f_y and f_u are characteristic yield and tensile strength of the material. They could be computed from:

$$f_y = \left(\sigma_y - f_{y,temp}\right) \cdot \alpha_u \tag{3.28}$$

$$f_u = \left(\sigma_u - f_{u,temp}\right) \cdot \alpha_u \tag{3.29}$$

Where σ_u - SMTS – Specified Minimum Tensile Strength (table 2.5); $f_{y,temp}$, $f_{u,temp}$ - de-rating values of the yield strength and the tensile strength respectively due to temperature (table 2.7); α_u - material strength factor (2.7), determines the material strength fluctuation along the entire pipeline. Hence, minimum allowable wall thickness is:

$$t_b \geq \frac{D(p_i - p_e) \cdot \gamma_m \gamma_{sc}}{\frac{4f_{cb}}{\sqrt{3}} + (p_i - p_e) \cdot \gamma_m \gamma_{sc}} \tag{3.30}$$

Except pressure containment the pipeline is expected to be exposed to [14]:

- Longitudinal stresses due to temperature change and pressure containment;
- Bending loads, caused by ice ridge action.

Hence the pure bursting design criteria could be valid only for the flowline part deeper than the water depth where gouging is possible and where the pipeline is unrestrained. But this section can exert loads originated from free spans and trawl actions, such that the wall thickness may be enhanced as well in subsequent calculations.

So far it is difficult to assess the combination of the pipeline protection against ice ridge action by the means of burying in the certain depth and the wall thickness increase. In this concern it is anticipated that the wall thickness governs the bursting resistance reduced by 30%, 40%, 50%. The analysis of these three cases gives a superficial conclusion about technical availability of the system. Results of wall thicknesses and hoop stresses (for the characteristic wall thickness during pipeline operation – corrosion allowance and fabrication tolerance are excluded) for different steel grades are presented in the following table 3.1 and figure 3.7:

Table 3.1.Effect of steel grades on wall thickness.

Parameter	***0% reduction (bursting criteria)***			***30% hoop stress reduction***			***40% hoop stress reduction***			***50% hoop stress reduction***		
	X60	***X65***	***X70***	***X60***	***X65***	***X70***	***X60***	***X65***	***X70***	***X60***	***X65***	***X70***
Wall thickness, t_b, mm	9,2	8,5	7,9	13,0	12,0	11,2	15,1	14,0	13,0	18,0	16,6	15,5
Nominal WT, t_{nom}, mm	13,2	12,5	11,9	17,0	16,0	15,2	19,1	18,0	17,0	22,0	20,6	19,5
Standard WT, t_s mm	14,3	12,7	11,9	17,5	17,5	15,9	20,6	19,1	17,5	23,8	22,2	20,6
Characteristic WT, t, mm	10,3	8,7	7,9	13,5	13,5	11,9	16,6	15,1	13,5	19,8	18,2	16,6
Hoop stress, σ_h, MPa	298,8	355,2	392,0	226,2	226,2	257,6	182,5	201,4	226,2	151,7	165,7	182,5

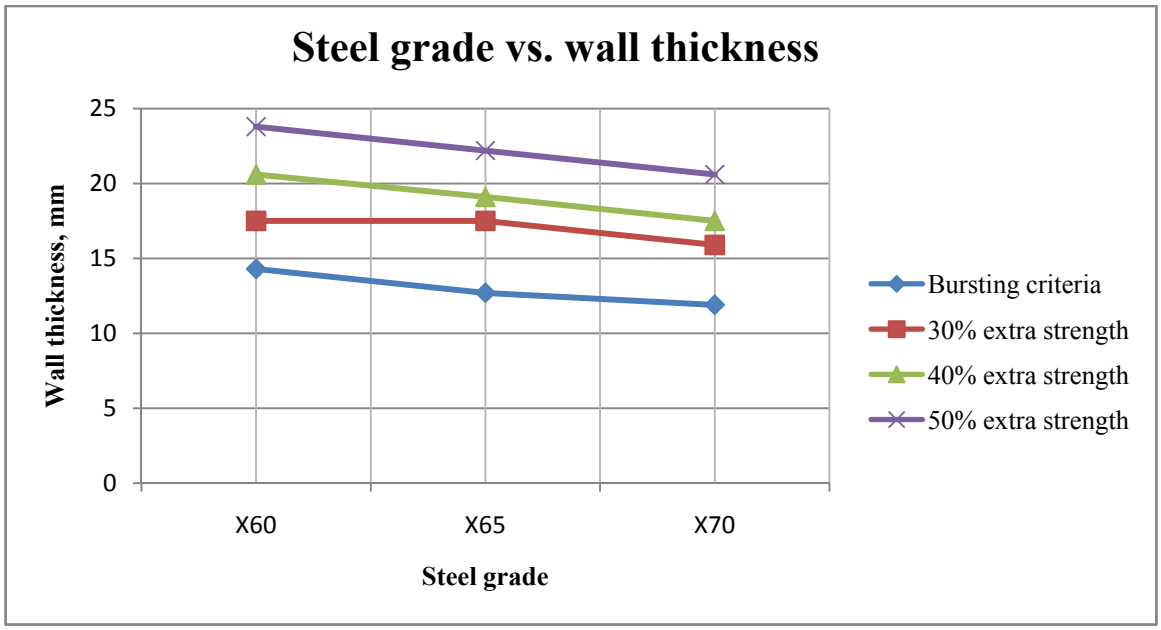

Figure 3.7. Wall thickness for different steel grades.

3.5.3. Load control condition

In terms of the thesis' study, the pipeline designed to withstand internal pressure will be controlled on its resistance against combined loading. It is governed by the design against yielding due to a combination of internal pressure, bending moment and axial force. Generally it is governed by the von Mises equivalent stress which is described in Chapter 5. However DNV [7] recommends checking of the following condition at all cross-sections:

$$\left\{\gamma_m\gamma_{sc}\frac{|M_{sd}|}{\alpha_c \cdot M_p(t)} + \left\{\frac{\gamma_m\gamma_{sc}S_{sd}(p_i)}{\alpha_c S_p(t)}\right\}^2\right\}^2 + \left(\alpha_p\frac{p_i - p_e}{\alpha_c p_b(t)\frac{2}{\sqrt{3}}}\right)^2 \leq 1 \quad (3.31)$$

Where M_{sd} - design moment (eq. 4.5 [7]); S_{sd} - design effective axial force (eq. 4.7 [7]); M_p and S_p - plastic capacities for a pipe.

$$S_p = f_y\pi(D-t)t \quad (3.32)$$

$$M_p = f_y(D-t)^2t \quad (3.33)$$

α_c is a flow stress parameter and α_p account for effect of D/t ratio:

$$\alpha_c = (1-\beta) + \beta\frac{f_u}{f_y}$$

$$\alpha_p = \begin{cases} 1-\beta, & \frac{p_i}{p_b} < 0.7 \\ 1-3\beta\left(1-\frac{p_i}{p_b}\right), & \frac{p_i}{p_b} > 0.7 \end{cases}$$

$$\beta = \begin{cases} 0{,}5 & for\ D/t < 15 \\ \left(\frac{60 - D/t}{90}\right) & for\ 15 < D/t < 60 \\ 0 & for\ D/t > 60 \end{cases}$$

3.5.4. Discussion

The thicker is the pipeline wall and the stronger is the material, the less soil cover pipeline should have in order to withstand considered load. Despite the overrun of the steel is critical for the pipeline design and undesirable, trenching in a big depth demands significant expenditures in comparison with enhanced wall thickness since the action from the ice ridge could be substantial even through a thick layer of soil. Furthermore, the steel grade should be uniform along the entire length of the pipeline and due to seabed obstructions seabed features and construction limitations; the route in specific places requires bending of the pipe [1]. It is also known that the higher is the steel grade the stiffer is the pipeline. Thus being interested in lowering trenching cost and considering pipeline design in terms of route selection X65 steel with wall thickness providing additional 50% strength capacity to hoop stress was selected.

3.6. ON-BOTTOM STABILITY DESIGN

3.6.1. General

Once pipeline diameter, wall thickness and material are established, subsea pipelines should be designed to be stable on the seabed when exposed to waves and currents. This governs vertical and lateral stability check according to DNV-RP-E305 [15]. Recommended practice of

1988 was chosen rather than the recent standard DNV-OS-F109 [16] in terms of data for the current location availability. Another reason is that RP-E305 gives straightforward understanding of processes related to on-bottom stability design.

Vertical stability requires the pipeline to be designed against floatation or sinking while lateral stability restricts horizontal movement of the pipe. In latest codes (starting from 1988) lateral stability design allows small displacements of the pipe. In this regard there exist three design methods:

- Dynamic lateral stability method;
- Generalized lateral stability method;
- Absolute lateral static stability method;

However in this section only simplified absolute static pipeline stability based on static equilibrium of forces is checked in order to ensure the pipeline resistance against motion to be sufficient to withstand hydrodynamic loads.

Insufficient stability leads to enhanced pipe wall thickness or concrete coating application. For gas flowlines this means changing in gas hydraulics due to temperature and pressure profiles shifting.

3.6.2. Absolute lateral static stability method

To satisfy absolute static stability following criteria should met [15]:

$$w_s \geq \left[\frac{(F_D + F_I) + \mu_p F_L}{\mu_p}\right] \cdot F_w \tag{3.34}$$

Where F_D and F_I are peak horizontal drag and inertia forces; F_L - vertical (lift) load; w_s - submerged weight of a pipeline unit length; μ - seabed friction; F_w – calibration factor (figure 5.12 in DNV [15]). The pipeline unit weight is:

$$w_s = \rho_s \pi d t g + \rho_c \pi D t_c g - \rho_w \frac{\pi (D + 2t_c)^2}{4} g \tag{3.35}$$

Where the first term denotes steel weight, the second is the corrosion coating weight and the third governs buoyancy. Hydrodynamic loads are calculated from:

$$F_L = \frac{1}{2}\rho_w D C_L (u_s \cos\theta + u_d)^2 \tag{3.36}$$

$$F_D = \frac{1}{2}\rho_w D C_D |u_s \cos\theta + u_d| (u_s \cos\theta + u_d) \tag{3.37}$$

$$F_I = \frac{\pi D^2}{4}\rho_w C_M A_s \sin\theta \tag{3.38}$$

Here C_L, C_D, C_M – lift, drag and mass force coefficients (0,9; 0,7; 3,29 respectively) u_s – significant near-bottom wave velocity amplitude perpendicular to a pipeline; u_d - steady current velocity perpendicular to pipeline at its level; A_s - significant acceleration perpendicular to a pipeline; θ - phase angle of the hydrodynamic force in the wave cycle.

It is necessary to mention that near-bottom water particle (due to waves) and current velocities, affecting forces that pipe exerts reduce with water depth.

The wave-induced particle velocity can be estimated from figure 2.1. of DNV [15]. The significant wave height H_s and peak period T_p are given in section 2.5.2; d_w is the water depth where the stability is calculated. Water depth value is approximated to be 25 m – minimum where the pipeline is not trenched.

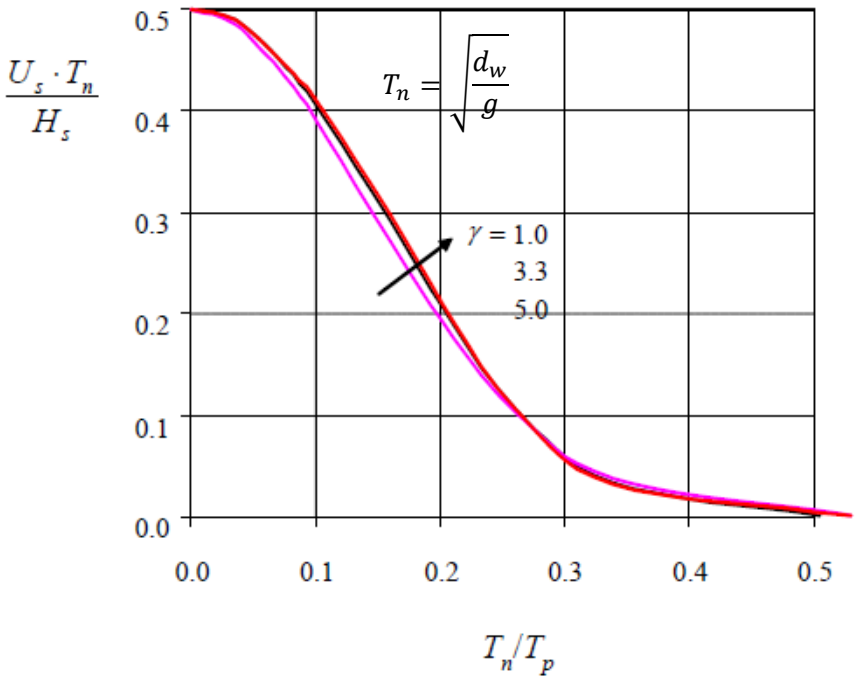

Figure 3.8. Significant flow velocity amplitude u_s at the seabed level [15]

Wave period changes with depth as well. Figure 3.9 determines zero-up crossing period range for actual conditions.

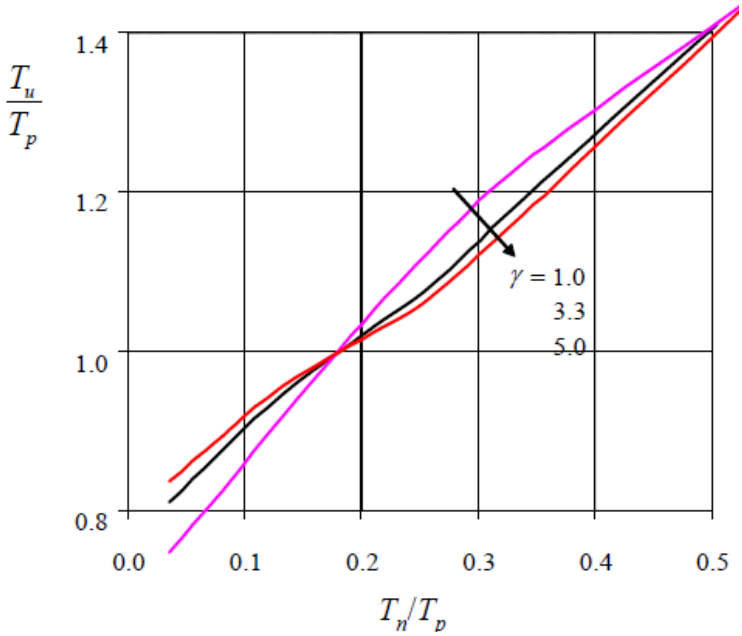

Figure 3.9. Mean zero-up crossing period T_u at the seabed level [15]

These parameters give possibility to calculate acceleration of water particles and Keulegan-Carpenter number required for calibration factor F_w assessment:

$$A_s = 2\pi \frac{u_s}{T_u} \tag{3.39}$$

$$KC = \frac{u_s T_u}{D} \tag{3.40}$$

Assume current decrease with depth down to $z_r = 3\ m$ above the seabed. This means not uniform current velocities distribution in the vertical direction. At the seabed level the bottom boundary layer restricts current flow even more such that the water motion is absent. Therefore velocity profile evenly drops starting from 3 m. The method for calculation current velocity at the pipeline level is given in section A.4 of DNV [15] for combined wave and current flow and implies the reduction of current speed:

$$\frac{u_d}{u_r} = \frac{1}{\ln\left(\frac{z_r}{z_0} + 1\right)}\left\{\left[1 + \frac{z_0}{D + 2t_c}\right]\ln\left[\frac{D + 2t_c}{z_0} + 1\right] - 1\right\} \tag{3.41}$$

Where z_0 is the bottom roughness parameter taken from table A.1 of DNV [15]. This method is valid provided the following are satisfied:

$$z_r > 0{,}2A_0\left(\frac{A_0}{K_b}\right)^{-0{,}25} \tag{3.42}$$

$$\frac{A_0}{K_b} \geq 30 \tag{3.43}$$

$$\frac{u_s}{u_r} \geq 1 \tag{3.44}$$

Where

$$A_0 = \frac{u_s T_p}{2\pi}$$

$$K_b = 30 z_0$$

Obtained wave particle velocities should be multiplied by the sine of attack angle assumed in tables 2.11 and 2.12.

3.6.3. Discussion

The Sea of Okhotsk wave conditions imply extremely severe peak periods and significant wave heights making wave-induced forces dominating on loads from current especially when the water depth is shallow. Under this statement according to DNV regulations the stability design of the considered pipeline is carried out for 100-year wave and 10-year current. Two hydrodynamic forces are acting on the pipeline caused by water particles acceleration - inertia force; and velocity (including current) – drag force. It is well known that acceleration and speed functions do not coincide in phase; hence the phase angle corresponding maximum value of required weight was iterated.

It was concluded that uncoated pipe tends to float in the sea, as its submerged weight is only 505 N/m, whereas only the value of lift force, acting on 25 m water depth, is 810 N/m. With that the lateral stability in 25 m water depth could be provided if the weight is 2500 N/m. Figure 3.10 illustrates the results of calculations.

Subsequent analysis has shown that heavy concrete coating doesn't give satisfactory results. The weight increased as expected, however forces have been enhanced due to their dependency on the pipeline outside diameter. Thus the usage of heavy mattresses is proposed in order to provide vertical and lateral stability of the pipe.

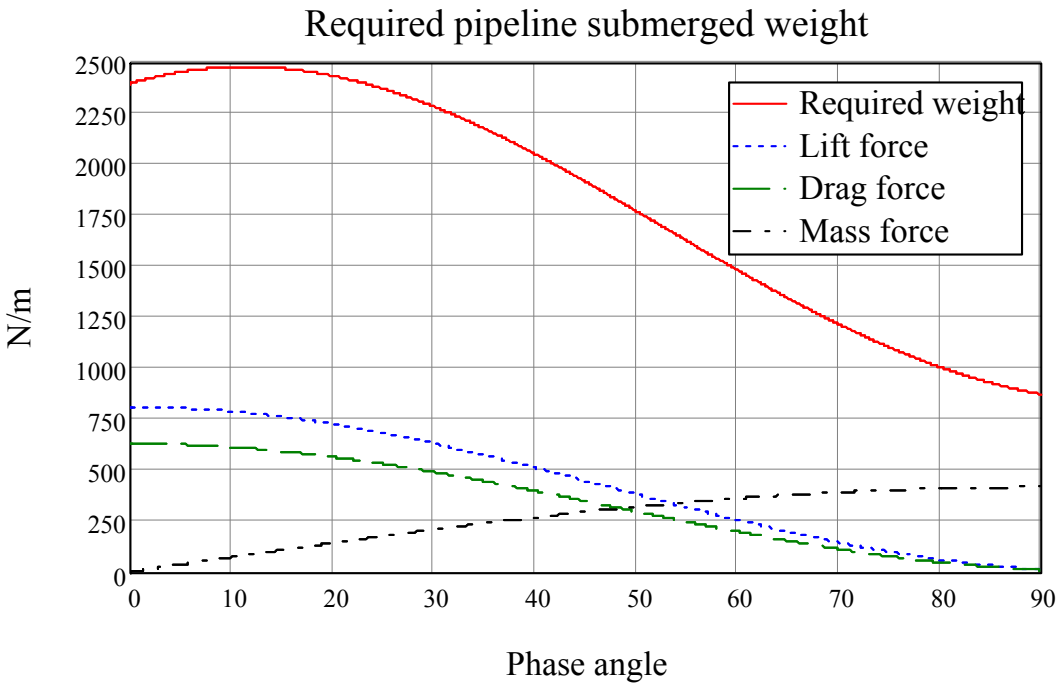

Figure 3.10 Required submerged pipeline weight at 25 m water depth.

Furthermore, the water depth increase implies the less drag, mass and lift forces action, and as a sequence, the required weight reduction. Hence, it is critical to find the depth, where the pipeline is stable uncoated, in order to decrease the expenditures on mattresses procurement and installation. Figure 3.11 plots required pipeline weight versus water depth, starting from 25 m. Its intersection with actual submerged pipeline weight curve sets the requirements for additional weighting on pipe: from 25 m to 66 m water depths.

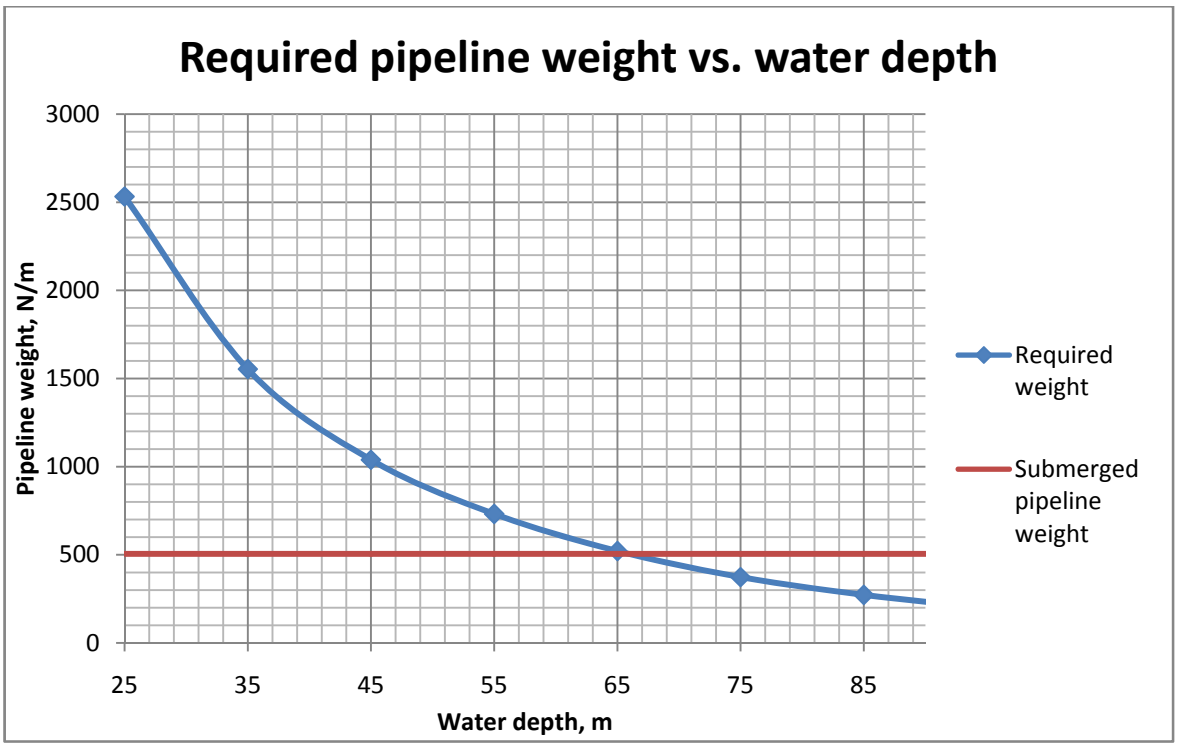

Figure 3.11. Required pipeline weight vs. water depth.

3.7. SUMMARY

The subsea pipeline concept and design is a comprehensive and challenging task in any oil and gas field development. In arctic conditions this task is even more complex. However prior to analysis of the main considered issue for arctic offshore pipelines, the overall design logic related to standard cases should be visible, which is performed in this chapter.

With due considerations of standards associated with offshore pipelines the sizing of the pipeline provided the external pipe diameter value of *406,4 mm.* Such solution provides robustness in the pipeline hydraulics, which satisfies the minimum required delivery pressure in a wide range of wall thicknesses. The flexibility in decision upon the later allowed the control of stresses appearing in terms of internal and external pressures.

Temperature profile estimated in section 3.4 gives a reasonable conclusion that the thermal insulation is irrelevant for given conditions. This is mainly associated with the short distance of the designed pipeline. Thus, despite there is some water in the pipeline and the pressure is high along the entire pipeline length, the temperature will never allow the hydrates formation in the steady state gas flow as also the heavy hydrocarbons liquefaction is impossible.

From the other hand high temperature values affect the longitudinal stresses, which might complicate the protection against combined loading on pipeline, including one from the ice ridge action. Hence, it was proposed to increase the wall thickness in order to give the pipeline an additional strength.

Although it is anticipated that 50% additional strength capacity (to bursting in terms of hoop stress), provided by enhanced wall thickness, covers adverse stresses from trawl actions, free spans and those appear during the pipelay; the study should account for the analysis of either impact. However their nature is well-understood now and consequently falls outside the scope of present research. The adjusted analysis of wall thickness in terms of ice ridge impact is performed in Chapter 5.

Requirements set above allow the pipeline to be manufactured from steel X65 by the well-proven UOE SAWL method. Selecting X65 instead of lower steel grades allows the cost savings in terms of steel overrun. At the same time it provides better weldability figures, then higher grades, critical for pipelaying in severe conditions.

Pipeline on-bottom stability is conditioned by the three explicit areas: 1) near-shore pipeline section (water depths *0 – 25 m*), embedded into the soil, where the stability against floating up is governed by the soil density (*1500 kg/m^3*) grater then the pipeline's one (*1300 kg/m^3*); 2) the pipeline section, subjected to substantial action of hydrodynamic loads (water depths *25 – 66 m*) – is stable, when covered with concrete mattresses; 3) the pipeline section from *66 m* to *90 m* water depth - stable, free rested on the seabed without additional swamp weight. Such decision economizes expenditures of the pipeline construction and determines the protection of the near-shore section against the seabed scouring, though the question how deep the pipeline must be trenched is to be answered below.

3.8. REFERENCES

[1] D. Karunakaran (2011): *Pipelines and Risers lecture notes*. UIS, Stavanger.

[2] Y. Bai, Q. Bai (2005): *Subsea Pipelines and Risers.* Elsevier, Oxford, UK.

[3] O. T. Gudmestad (2011): *Arctic Offshore Engineering lecture notes*. UNIS, Longyerbyen.

[4] O. T. Gudmestad, S. Løset, A. I. Alhimenko, K. N. Shkhinek, A. Tørum, A. Jensen (2007): *Engineering Aspects Related to Arctic Offshore Developments.* Lan, St. Petersburg, Russia, 255 pages.

[5] Gazprom (2006): *Technological Design Standards of Trunk Pipelines (in Russian).* Organization Standard, STO Gazprom 2-3,5-051-2006, Moscow, Russia.

[6] GOST (1997): *Natural Gas. Methods of Calculation of Physical Properties. Definition of Physical Properties of natural gas, its components and processing products (in Russian).* Russian National Standard, GOST 30319.1-96*, Moscow, Russia.

[7] DNV (2007): *Submarine pipeline systems*. Offshore Standard DNV-OS-F101, Det Norske Veritas, Høvik.

[8] API Specification 5L (2000): *Specification for Line Pipeline.* 42^{d} edition, Washington D. C., USA.

[9] A. Palmer, R. King (2008): *Subsea Pipeline Engineering.* 2^{d} edition, PennWell, Tulsa,, Oklahoma, USA.

[10] S. Løset, K. Shkhinek, O. T. Gudmestad, P. Strass, E. Michalenko, R. Frederking, T. Karna (1999): *Comparison of the physical environment of some Arctic seas.* Cold regions science and technology 29 (1999), pp. 201-214;

[11] O.T. Gudmestad, A.B. Zolotukhin, A.I. Ermakov, R.A. Jakobsen, I.T. Michtchenko, V.S. Vovk, S. Løset, K.N. Shkhinek (1999): *Basics of offshore petroleum engineering and development of marine facilities*. Moscow, "Neft i gas" publishing house, 350 p.

[12] P. A. Truskov (1999): *Metocean, Ice and Seismic Conditions Offshore Northeastern Sakhalin Island.* Offshore Technology Conference, Houstonm Texas, 3-6 May 1999, paper number OTC 10816.

[13] G. N. Surkov, P. A. Truskov (1995): *Study of Ice Pressure Ridges and Stamukh Offshore of Sakhalin.* The Tenth Int. Symp. On "Pkhotsk sea and sea ice", Mombetsu, Hokkaido, Japan, pp 86-88.

[14] P. P. Borodavkin (2006): *Marine Structures. Part 1. Design.* Nedra, Moscow, Russia, 555 pages.

[15] DNV (1988): *On-bottom Stability Design of Submarine Pipelines.* Recommended Practice RP-E305, Det Norske Veritas, Høvik.

[16] DNV (2007): *On-bottom Stability Design of Submarine Pipelines.* Recommended Practice DNV-RP-F109, Det Norske Veritas, Høvik.

CHAPTER 4. THEORETICAL MODELING OF ICE RIDGE SCOURING

The pipeline steel, dimensions and hydraulic parameters'' distribution for a typical hydrocarbon field on the shelf off the Sakhalin Island have been designed. But the pipeline design itself is substantially contributed by subsequent study, where the ridge souring effect is analyzed.

Previous to study of the pipeline response to gouging it is necessary to examine the ice ridge properties, which would delineate the distinguished features of scouring process, such as scour width, depth and soil behavior below the gouge base.

4.1. ICE RIDGES STUDY

4.1.1. Ice ridge shapes

Sea ice can be forced into a ridge by pressure or shear processes. The presence of ridge formation in ice-covered waters is always taking place. They could be developed in the border zone between the fast ice and the drifting ice sheet where the ice cover is subjected to compression. High ridging intensity is also to be found in straits with strong currents. Ridges might be categorized into first-year and multi-year ridges, which differ by their properties significantly. In this study the main attentions is given to first-year ice ridge due to its relevancy in the Sea of Okhotsk.

First-year ice ridges are sophisticated ice features with a wide variability of sizes and shapes [1]. A lot of studies have been made in order to measure their properties providing general information about the geometrical peculiarities. As a rule a ridge has a large amount of chaotic conglomeration of broken ice (partially frozen) below the waterline – a keel, and a sail, formed by smaller ice rubble accumulation above the sea level. Part of the ridge close to waterline is commonly consolidated and has a thickness a little more than the level ice.

ISO 19906 [2] recommends a typical cross-section of a ridge, shown in figure 4.1, where h_c – is the thickness of consolidated layer; h_s – sail height; h – level ice thickness; h_k – keel height (from the sea level to its bottom); w_k, w_b – keel width at the sea level and at the bottom, respectively.

Information about the correlations between the mentioned parameters has important implications for the loads the ridge could exert either on the seabed or on the pipeline.

However the reality is that the shape can vary much from this general one. Timco and Burden [1] have carried out a statistical research of 112 ridges sample, and reported that there is only few ridges obeying the illustrated proportions. In many cases there were large deviations and asymmetries in ridges' geometry, demonstrating their complexity. Despite non-symmetrical sails and keels, and displacements of keel and sail centerlines normally take place during this study, a reasonable representation of the general characteristics was made and analyzed.

The correlations between the indicated parameters were developed as follows [1]:

$$h_k = 3{,}95 \cdot h_s \tag{4.1}$$

$$w_k = 3{,}91 \cdot h_k \tag{4.2}$$

From geometry:

$$w_b = w_k - 2h_k \cot \alpha_k \tag{4.3}$$

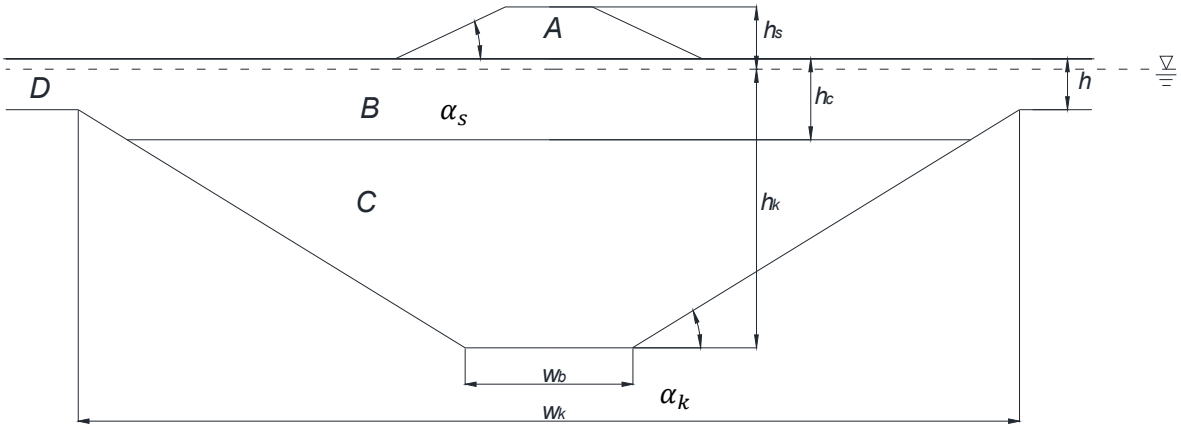

Figure 4.1. Geometrical parameters for typical first-year ice ridge [2]. A – sail; B – consolidated layer; C – keel; D – level ice.

It was also shown that the sail angle α_s has an average value of 20°, while the angle of the keel shape α_k is approximated by 26° [1,2,15]. The keel angle estimated in Timco's work provides a triangular shape of the ridge. The more recent research of Obert and Brown [3] has demonstrated a variety of keel shapes studying ridges in the north of Canada. Except triangular and trapezoidal keel shapes there exist multiple peak and w-shaped keels. The formation mechanism exercises reasonable implications on keel shapes, as described below.

Triangular keels are formed when 2 ice sheets create rubble above and below the ice level. The distinguished feature of such a ridge formation is that the consolidated layer might be solid initially opposite to porous rubble as in a rubble field formation. Triangular keel classification [3] includes ridges with limited small width at the bottom, so as the w_k/w_b ratio is large.

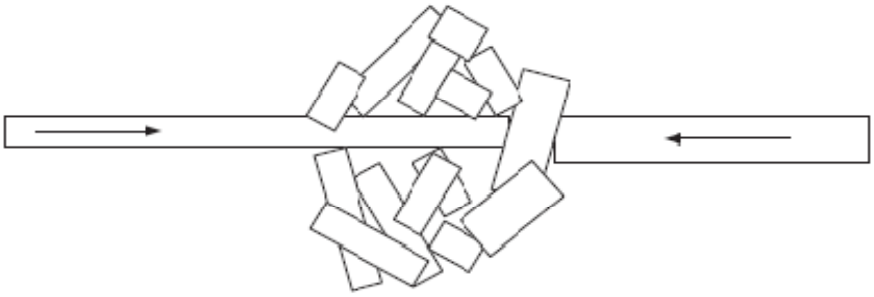

Figure 4.2. Triangular keel formation [3]

Trapezoidal keels have steeper keel angles such that the bottom is wide and flat. It is necessary to note, that the keel angle of trapezoidal ridges normally coincides with the value of the triangular keel angle, which means that such shape is resulting from the lateral growth of a triangular keel, generally causing a wide but shallow bottom.

Multiple peak keels have a set of peaks developed from rubble fields by two ways: 1) three or more triangular keels are merged together; 2) rubble, created by ice sheets different in

thickness, develops more random peaks as indicated in figure 4.3. Both types result in a large keel width in comparison with other keels.

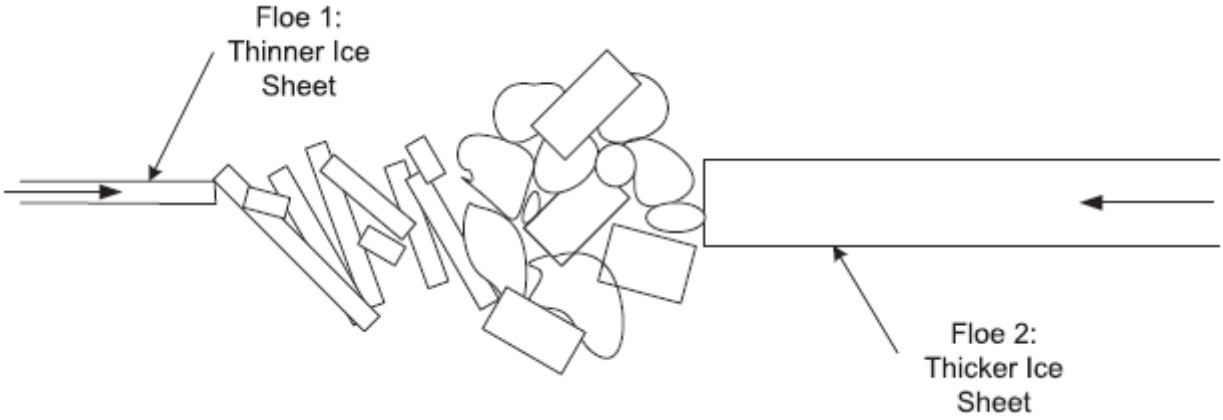

Figure 4.3. Multiple peak keel formation [3]

W-shaped keels are particular cases of multiple peak keels with pronounced two peaks of similar depth, originated by independent keels pressured together.

Obert and Brown [3] have concluded that triangular, trapezoidal and w-shaped keels are similar in size magnitude and differ only in the slope and width to depth ratio (figure 4.4).

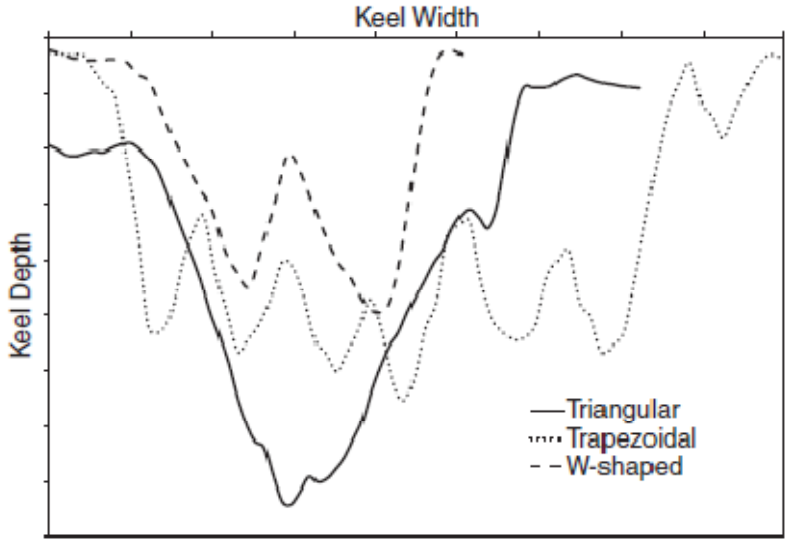

Figure 4.4. Comparison of keel shapes [3]

The angle of either keel doesn't change much, whereas the heights of trapezoidal and w-shaped keels are different. According to figure 4.4 triangular keels are likely to cause significant gouging in greater water depths, therefore correlations proposed by Timco and Burden [1] are reasonable for the ridge shape determination. In this research the angle of the keel slope is assumed as *30°* (table 2.15). Such inclination gives triangular shape of the ridge with relatively short keel width at the bottom, which seems to be more realistic from the point of ridge formation.

Another important dimensional parameter is the breadth of the ridge *B*. It appears difficult find a good estimator for the outstanding breadth value, since it varies much from ridge to ridge. In this regard the average *B* was selected in table 2.15.

4.1.2. Ridge morphology

Although ice ridge has a sail and a keel, formed by blocks of rubble ice, highly consolidated at the sea level, the morphology of each component is not nearly homogeneous. Furthermore the internal structure of a ridge changes continuously throughout the season. This is primary associated with two important processes: from one hand it is growth of consolidated part of the ridge due to water between ice blocks freezing up; from another – deterioration of unconsolidated rubble due to heat transfer from surrounding water.

One of the works dedicated to ridge morphology, has been carried out by Kharitonov [4], is directly connected to Sakhalin shelf ridges and stamukhas studies based on the thermodrilling method. The results demonstrated in figure 4.5 have shown where the solid phase dominates and exceeds the average volume content of an ice in the ridge. It is well seen that the consolidated layer is represented by the dome-shaped branch; the closer to the keel bottom, the less solid-state content is observed. Such changeable morphology implies the decrease of porosity with depth. Certainly it contributes to the keel strength and scouring itself as the soil resistant force could be large enough to cause fractures and destruction in bottom-close keel, where ice blocks are not well consolidated.

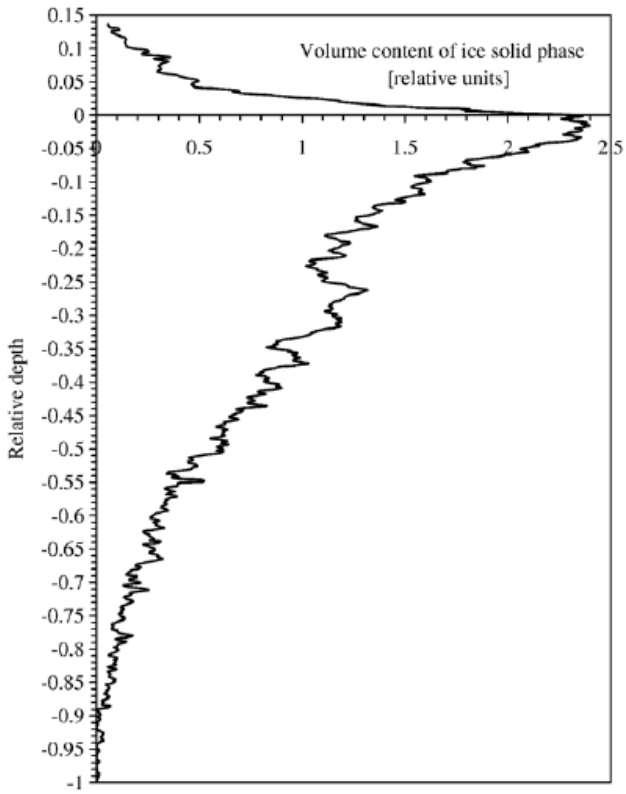

Figure 4.5. Distribution of ice solid phase volume content of the "mean statistical" ridge [4]

Kharitonov reports [4] that the average sail macro porosity of ridges in the Sea of Okhotsk falls within 6 – 8 %, which is 3-4 times less than keel macro porosity (22 – 24%).

Another research [5] has shown the keel macro porosity dependency on the block thickness T_b:

$$\eta = 0{,}11 \cdot \ln(T_b) + 0{,}37 \tag{4.4}$$

The ridge blocks dimensional parameters have been studied by Bonnemaire et al. [6]. Researchers detached three groups: around 0,3; 0,6 or 0,9 m thick with the average value of

0,57 m. Blocks width and length were reported to be of 1,6 m and 2,5 m respectively, the mean inclination angle - 40° to the horizontal plane with its tendency to decrease with the smaller size. Observed by Bonnemaire average block thickness value governs macro porosity of 31% (eq. 4.4), which slightly deviates from data observed by Kharitonov [4], however Surkov [7] also reported that linear porosity (based on drilling methods, namely used in Kharitonov's research) could be 15-25% less than volumetric one. Thus equation 4.4 is accepted in this research as the best estimator for ice ridge porosity.

The macro porosity, used in subsequent calculations, should be distinguished from total porosity represented by brine pockets inside ice blocks. Brine inclusions strongly affect the ridge strength and demand additional study. Under assumption that brine volume is small and all pores are occupied either by water or by air, the density of porous keel part of the ridge therefore will be outlined as:

$$\rho_{iw} = \eta\rho_w + (1-\eta)\rho_i \tag{4.5}$$

The upper sail part, located above the sea level has a density:

$$\rho_{ia} = \eta_s\rho_a + (1-\eta_s)\rho_i \approx (1-\eta_s)\rho_i \tag{4.6}$$

Where η_s - sail porosity, given in table 2.15.

4.2. ICE SCOURING

4.2.1. General

Ice scouring process is caused by the ridges, driven by wind, current and surface ice, in contact with seabed in water depths up to 45 m [8]. The gouges can be more than 50 m wide and 2 m deep, and although gouges from ridges are much less in depth than from icebergs, they are more frequent. The most intense gouging happens in water 15-20 m deep as shallow waters could not be reached by large masses in terms of motionless fast ice and insufficiency of driving force to push them so far against the resistance of seabed. However this range varies from one place to another. For example, ice gouging at depths greater than 40 m has been reported in Chukchi Sea [9].

Chapter 2 gives observed values of maximum sail heights with respect to the environmental data of the field location. In a combination with equation (4.1) the estimated hazardous water depth where gouging occurs is about 20-24 m which follows the findings of Vershinin et al. [10].

It was proven [11] that ice ploughing is a contemporary process, that the force required to cut a deep gouge is very large, that the ice is strong enough to cut the gouges, and that there is enough driving force from drifting ice, wind and current.

Thought of as a cutting device, an ice mass is almost always very blunt. The front face with angle of approximately 30 degrees (figure 4.1) is unlikely to be either planar or smooth. In gouged areas, the seabed is usually almost horizontal and so the cutting angle of incidence is low.

The scour breadth is usually many times greater than the depth. With that the ice pushes a seabed soil ahead of it. Soil slides and rolls transversely, and forms a berm on each of the sides, which is also important, while describing the scouring process. The ridge scouring is illustrated in figure 4.6 (AutoCAD drawing).

It is complicated to correctly interpret the gouging profile due to many factors [9], such as the time history of gouging, the soil infill due to repeated gouging, and the normal seabed sediment process due to waves and currents. Nevertheless, the most of gouges have constant cross-section for quite long distance.

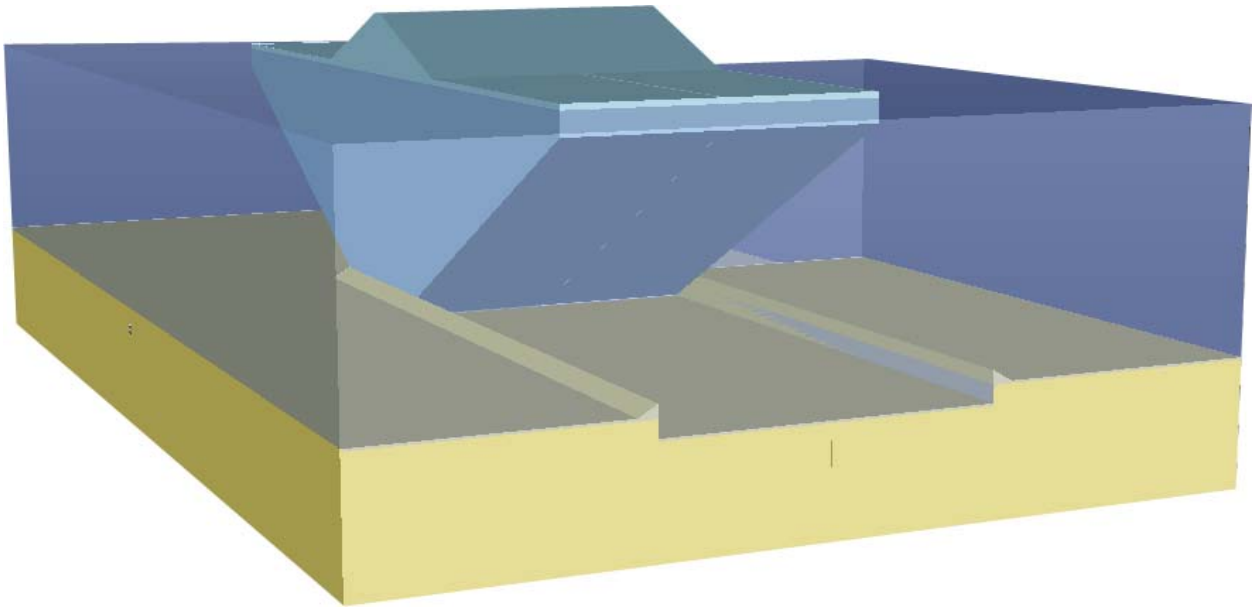

Figure 4.6. Ice ridge scour illustration.

The ice ridge scouring the seabed could damage marine pipeline. But except ploughing process itself, intensive deformations occur beneath the gouge, and a pipeline would still be damaged by being dragged with the soil. Hence it becomes clear, that the required depth for pipeline burial should be:

$$D_b = d + b \tag{4.7}$$

Where d – is the gouge depth and b – cover depth.

Anticipating the certain conditions of the ridge and environment, the gouge depth could vary from place to place. The accuracy of its value determination is high: from one hand it is cost, from another – safety of the pipeline system.

There are several models for gouge depth determination. Weeks et al. [12] suggested the probabilistic distribution with the following probability of the certain depth existence:

$$p(d) = \lambda e^{-\lambda(d-c')}; d > c' \tag{4.8}$$

Where d is the scour depth, λ is a distribution parameter and c' is a cutoff for measuring scour depth. However this method requires field data and observations for actual location which demands additional activities during seabed survey, driving in extra cost for any project development. Furthermore gouge depth, breadth, length are changing their values in time due to processes related to seabed metamorphose such as tectonics and soil erosion. Hence, the probabilistic approach may give unacceptable errors in calculations.

Another research has been carried out by Phillips et al. [13], where the maximum gouge depth was estimated at the moment of keel destruction, based on the keel cohesion values. This model implies the rubble limit state and could be applicable in sufficiently large ridge driving

forces. But the forces themselves able to originate in specific conditions have not been studied, which might give measurable errors, while analyzing the gouge depth.

In order to have a physical sense of considered study design schemes should be introduced. Liferov [8] distinguishes two general scenarios of scouring:

Case 1: the separate ridge is represented by a single ice feature floating in the sea;

Case 2: large ice field confines the ridge.

Considering the ridge as a separate feature is typical for the spring period and would be an optimistic estimate, whereas constraint ice field causes additional loads and limits ridge elevation. Hence the development of physical model in this study involves the presence of an ice field.

In this regard Vershinin et al. [10] has established several design models, determining the behavior of ice ridge when contact with soil occurs. In subsequent study the analysis of following design schemes is performed:

Scheme 1. The ice ridge has a rigid constraint with the drifting ice field and only one degree of freedom is available: high stiffness doesn't allow ridge to rotate as well as to be shifted vertically (figure 4.7). Such model corresponds to the maximum gouge depth assessment and feasible for thick ice sheet and soft soils able to be ploughed very deep without significant response. Critical vertical loads on the seabed occur due to high elasticity of the system.

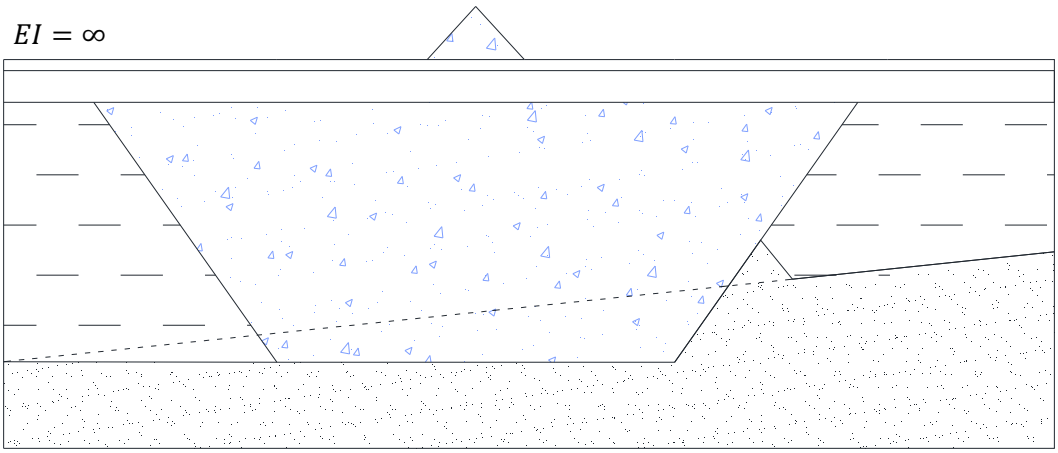

Figure 4.7. 1st design scheme for the scouring process modeling

Scheme 2 could be an extension of scheme 1. The ice ridge is enveloped by the drifting ice as in scheme 1, but the finite stiffness of ice field allows ridge upward movements. Vertical loads on soil are much less being governed by the flexural strength of the ice sheet. This scheme is more suitable for thinner level ice and stronger soils. Vershinin et al. [10] develops a particular case when the small deflection angle is allowed. It could be considered as an intermediate case between the schemes 2 and 3.

Scheme 3 is relevant for ice field with small bearing capacity. Due to bending moments, caused by ridge vertical movement and rotation, fractures and cracking in the contact threshold are possible. In such a way the constraint could be destructed. In this end the heave and pitch motions involved in schemes 2 and 3 are of relatively small values before surrounding ice flow breaks, releasing the ridge.

The subsequent development of processes indicated in figures 4.7 – 4.9 leads to a ridge grounding. Drifting ice field continues hummocking with simultaneous increase of the vertical loads on the seabed and as a result – gouging process ends.

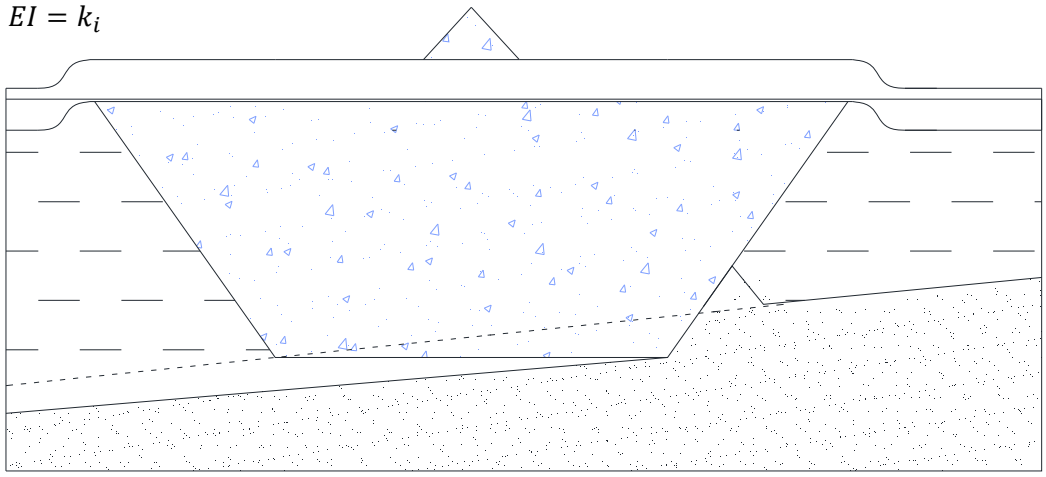

Figure 4.8. 2^d design scheme for the scouring process modeling

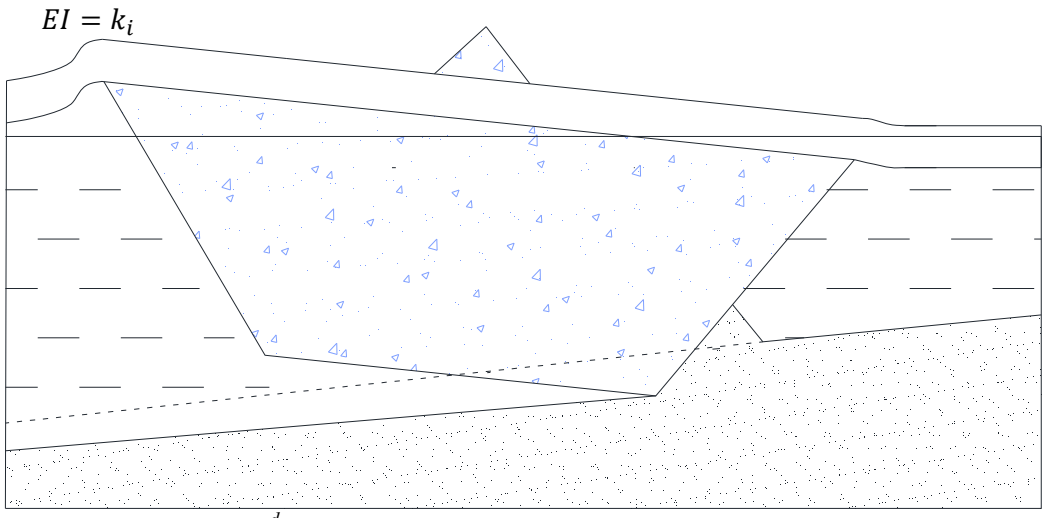

Figure 4.9. 3^d design scheme for the scouring process modeling

Although the latest model is likely to happen in relevant study, especially when heavy ridge and thin level ice are taking place, the attention is given to the first and the second design schemes, which correspond to the most unfavorable ploughing depth.

In this thesis two models associated with both schemes are introduced and developed:

1) *Force model* – analysis of static forces equilibrium. The purpose is to estimate the thickness of the soil which ridge is able to penetrate in, being loaded by a system of forces. This model implies the ridge behavior meeting the first design scheme. The principal assumption here is that initially the ridge is not exerting any load. Once environmental action appears, the ridge starts to move. With that the resistance arises restricting a movement in a certain critical scoured depth. As the analysis is performed in static equilibrium there is no ridge elevation.

2) *Energy model* – corresponds to the design scheme 2 and based on kinetic energy dissipation through the soil friction. It accounts potential energy uprising due to ridge elevation in sustainable gouging process. This model seems to be more realistic, but it may give results slightly below maximum observed.

It is necessary to note that force and energy scouring models conform to limit stress and limit momentum scenarios suggested by Loset [14]. Whereas grounding of the ridge and floe failure on the ridge-ice field boarder relates to limit force mechanism.

Before introducing force and energy interaction models' specifics, soil behavior has to be studied as it directly influences the process of scouring by ridge.

4.2.2. Soil behavior

Vershinin et al. [10] have described several experiments in different scales regarding soil attitude above the gouge bottom. According to their research soil has a consequent process of alternate responses. The first stage is described by the compaction of the soil and its transition into the limit state. Once the maximum load is applied, ridge starts to displace the soil. These deformations are represented by the movement of two wedges, proceeding in the plastic flow mode. The frontal mound is accumulated, creeping in the front face of the ridge, and develops a berm in either side. It is limited by a constant height, dependent on the keel breadth and depth [10], which is accounted in models for scour depth determination.

Dead wedge is moving in the united assembly with the keel (figure 4.10), being considered motionless with respect to it. The sliding of the soil therefore occurs in the bound of dead wedge and overriding prism.

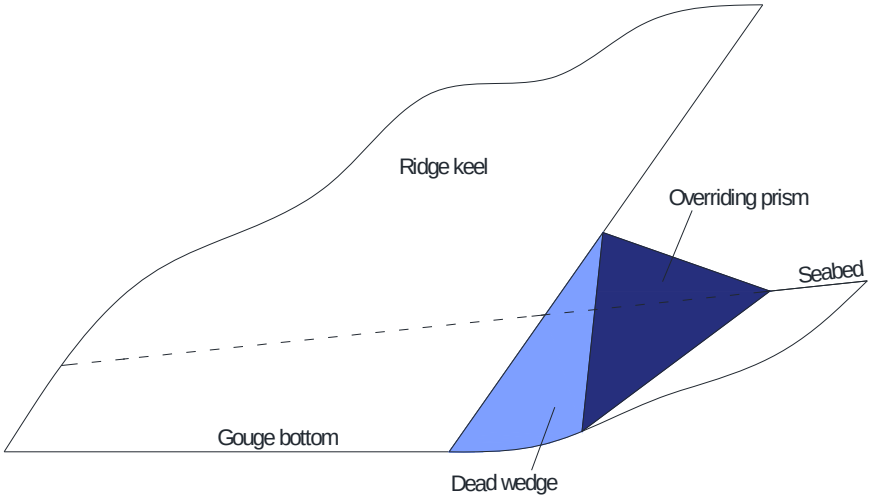

Figure 4.10. Behavior of soil subjected to the scouring by the ridge keel.

In terms of finite ridge dimensions, limiting the frontal mound height, this research accounts the soil agglomeration on the ridge sides. However it is assumed that berms do not significantly resist the ridge motion.

With that the soil type should be accounted as it plays an important role in both related processes: the scouring and the pipeline response. The scouring process analysis is performed for two soils: stronger granular sand and weaker cohesive clay (with the smaller internal friction angle). The behavior of either could be described by the Mohr-Coulomb theory, established in Chapter 5 in details. The theory governs the soil shear failure envelope as the function of soil cohesion, angle of internal friction and normal stress applied, which provides an important outcome for stronger sand: its strength is substantially larger in condition of the certain confinement. Thus it is expected, that sand resists the ice ridge motion more than clay, protecting the seabed against deeper scouring.

4.2.3. Force scouring model

The introduced model is based on the expectations that the friction forces are depended on the scour depth. The more the soil in the front face, the greater is the friction. At the maximum d the resistant forces are in balance with drag ones. Thus in presented model soil resistance is the only factor restricting the ridge to scour the seabed. In general it consists of 2 parts: a pure Coulomb friction and a passive resistance due to the buildup of soil penetration as the ridge moves.

Therewith the behavior of the ridge keel, interacting with soil, is determined by the attack angle. For sharp angles the "sledge effect" is observed [10] due to vertical uplifting force origination. Consequently ridge lifts up. However if the vertical downforce is applied (which is reasonable considering scheme 1 (figure 4.11), the ridge elevation could be eliminated. The attack angle might not coincide with the keel angle, since the ice rubble forming the keel is randomly oriented. The attack angle distribution from 0 to 90 degrees therefore could take place. However due to the large keel breadth anticipated, it is assumed that the ridge-soil contact surface follows the keel angle shape.

As it was mentioned the critical gouge depth is relevant when the following force system exists in equilibrium:

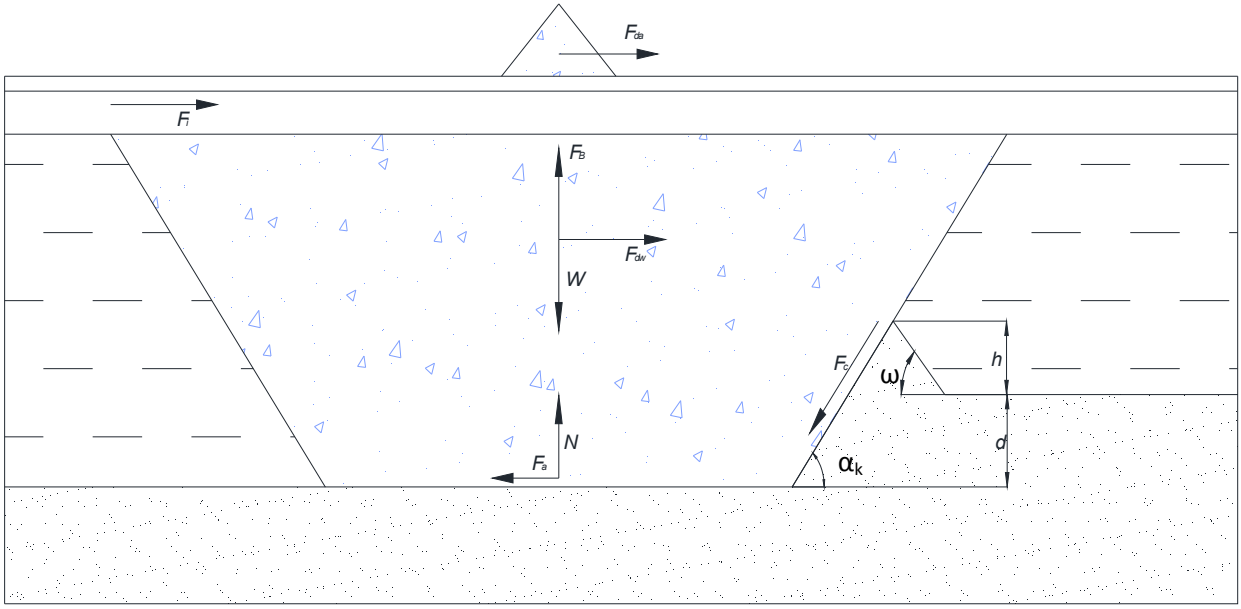

Figure 4.11. Force system on the ice ridge.

Here F_{da}, F_{dw} are drag forces from air and water respectively; F_b – buoyancy force; W – weight of the ridge; N – reaction from the seabed; F_a - friction force on the bottom of the ridge; F_c – Coulomb's passive friction force, acting in front and on both sides of the ridge; F_i – driving force from surrounding floe; ω – angle of the front surcharged soil slope; α_k – keel angle; h' – height of the frontal mound; d – scour depth.

A set of assumptions has been made in order to fulfill the model integrity:

- Ridge is assumed to be initially motionless such that all forces exert their maximum values. Otherwise drag force from current could act in opposite direction: wind accelerates the ridge and it moves faster than the current. And water resists the ice ridge movement;
- The seabed in the presented model is even and has no inclination. It was neglected in order to simplify the system without considerable error;

- Ice ridge is an absolutely rigid body with negligibly small elasticity, which doesn't consume energy for its structure reorganization;
- Ridge keel bottom has an infinite strength, so it is not being destroyed scouring the seabed;
- Substantial surface ice restricts the ridge upward motion (first design scheme is applied).

The equations of equilibrium in either direction are given by:

Horizontal direction:

$$F_{da} + F_{dw} + F_i - F_a - F_c \cos \alpha_k = 0 \tag{4.9}$$

Vertical direction:

$$F_b - W - F_c \sin\ \alpha_k + N = 0 \tag{4.10}$$

Each force component of the system is defined below.

Drag force from the wind:

Generally both wind force components push the ice: frontal (first term) and top (due to skin effect – second term) [15]. In terms of the ice ridge confined with the level ice these components are:

$$F_{da} = \frac{1}{2}\rho_a C_{da} A_{a1} u_a^2 + C_{sa}\rho_a A_{a2} u_a^2 \tag{4.11}$$

C_{da} - drag coefficient; C_{sa} - skin friction coefficient; u_a – wind velocity; ρ_a - air density. The projection areas A_{a1}, A_{a2} are given by:

$$A_{a1} = \left(h_s - \frac{\rho_w - \rho_i}{\rho_w} h_i\right) B \tag{4.12}$$

$$A_{a2} = w_k B \tag{4.13}$$

Drag force from the current:

As it is acting only transversally, its value is determined by the single component:

$$F_{dw} = \frac{1}{2} C_{dw} \rho_w A_w u_c^2 \tag{4.14}$$

C_{dw} - drag coefficient for current; ρ_w - water density; A_w - underwater projection area; u_c – current velocity. With reference to a figure 4.1 the effective area of current influence is:

$$A_w = \left(h_k - \frac{\rho_i}{\rho_w} h_i\right) B \tag{4.15}$$

Weight:

To estimate the weight of the ridge density heterogeneity and the shape peculiarities have to be taken into account. The ridge weight is represented by the sum of the weights of each geometrical part: upper triangular section of the sail, intermediate consolidated rectangular and trapezoidal lower keel part with different densities. Intending the pores to be fully occupied either by water or by air the weight is governed by:

$$W = \rho_{iw} B g \cdot \left[\frac{\rho_{ia}}{\rho_{iw}} \left(h_s - \frac{\rho_w - \rho_i}{\rho_w} h \right)^2 \cot \alpha_s + \frac{\rho_i}{\rho_{iw}} h w_k + \frac{1}{2} (w_k + w_b) \left(h_k - \frac{\rho_i}{\rho_w} h \right) \right] \quad (4.16)$$

Here ρ_{iw}, ρ_{ia} are ice densities in water and air respectively (eq. 4.5; 4.6). Substituting equations (4.1; 4.2; 4.3):

$$\begin{aligned} W = \rho_{iw} B g \cdot & \left[\frac{\rho_{ia}}{\rho_{iw}} \left(h_s - \frac{\rho_w - \rho_i}{\rho_w} h \right)^2 \cot \alpha_s + \frac{\rho_i}{\rho_{iw}} 3{,}95 \cdot h \cdot h_k \right. \\ & \left. + \frac{1}{2} (2 w_k - 2 h_k \cot \alpha_k) \left(3{,}95 h_s - \frac{\rho_i}{\rho_w} h \right) \right] \\ = \rho_{iw} B g & \\ \cdot & \left[\frac{\rho_{ia}}{\rho_{iw}} \left(h_s - \frac{\rho_w - \rho_i}{\rho_w} h \right)^2 \cot \alpha_s + \frac{\rho_i}{\rho_{iw}} 15{,}44 \cdot h \cdot h_s \right. \\ & \left. + (15{,}44 h_s - 3{,}95 h_s \cot \alpha_k) \left(3{,}95 h_s - \frac{\rho_i}{\rho_w} h \right) \right] \end{aligned} \quad (4.16a)$$

Outlined equation implies the ridge weight dependency on minimum dimensional parameters, namely the consolidated layer thickness and the sail height. Thus the minimum number of assumptions decreases the uncertainty of the system.

Buoyancy force:

On the analogy with the weight equation, buoyancy force impacts the ridge keel trapeze and the subsea consolidated layer part as follows:

$$F_b = \rho_w \nabla g = \rho_w g B \left[\frac{1}{2} (w_k + w_b) \left(h_k - \frac{\rho_i}{\rho_w} h \right) + \frac{\rho_i}{\rho_w} h w_k \right] \quad (4.17)$$

$$F_b = \rho_w g B \left[(15{,}44 h_s - 3{,}95 h_s \cot \alpha_k) \left(3{,}95 h_s - \frac{\rho_i}{\rho_w} h \right) + 15{,}44 \frac{\rho_i}{\rho_w} h \cdot h_s \right] \quad (4.17a)$$

It might happen, that buoyancy and weight values are not corresponding due to correlations error in the research of Timco and Burden [1]. In the force model these forces should be in equilibrium.

Ice force:

For the ice driving force the Vershinin et al. [10] 2D model of ice hummocking force is applied. The ice limit state before ridging governs the maximum horizontal force in condition of the limited ice strength (in *MN*):

$$F_i = 0{,}43 \cdot 4{,}059 \cdot B^{0{,}622} \cdot h_i^{0{,}628} \quad (4.18)$$

Passive friction force:

To calculate the soil resistance force the passive earth pressure theory is applied. The earth pressure acts normally to the slant surface of the ridge keel and causes additional friction, depending on the wall friction angle. Ridge tends to lift up, but the rigid ice field induces a reaction on the seabed, equal to the vertical component of passive friction force, which is according to the theory:

$$F_c = \mu P cos(\phi_w) \tag{4.19}$$

Where P is the earth pressure and ϕ_w - wall friction angle; μ - friction coefficient between ice and soil. Both components acting on front face and on side faces are considered.

Front resistance:

The soil pressure force in front of the ridge:

$$P_f = \frac{1}{2} K_p \rho_s g (h' + d)^2 B + 2c\sqrt{K_p} \tag{4.20}$$

Where c is the soil cohesion (for clay) and K_p is the passive earth pressure coefficient:

$$K_p = \frac{\cos \varphi^2}{\cos \phi_w \left[1 - \sqrt{\frac{\sin(\varphi + \phi_w) \cdot \sin(\varphi + \beta)}{\cos \phi_w \cos \beta}}\right]^2} \tag{4.21}$$

Here φ – is internal friction angle of soil; ρ_s - soil density; h' is the height of frontal mound.

The height of frontal mound is initially assumed to be a half of the gouge depth and iterated according to the equation 4.22 of Vershinin et al. research [10]:

$$h' = \sqrt{\frac{d^2 \cot \varphi}{\cot \varphi + \frac{d}{3B} \cot \varphi \cot \beta}} \tag{4.22}$$

Analyzing equation (4.20) the second term could be neglected, even for clay, since its cohesion value doesn't contribute much to the passive earth pressure force (several tens of kPa vs MPa).

It is also assumed that the angle for the soil frontal mould slope ω indicated in figure 4.11 is equal to internal friction angle φ in the virtue of similarity of soil behavior, being scattered on the ground. For the force model in terms of the even seabed the coefficient of passive earth pressure K_p can be drown as:

$$K_p = \frac{\cos \varphi^2}{\cos \phi_w \left[1 - \sqrt{\frac{\sin(\varphi + \phi_w) \cdot \sin(\varphi)}{\cos \phi_w}}\right]^2} \tag{4.23}$$

Side resistance

For side resistance estimation only the sidewise soil pressure from the scoured plane has been taken. It means that on the sides the soil berm action on the ridge is absent. The pressure from both sides is therefore [15]:

$$P_s = \frac{1}{6} K_p \rho_s g d^2 w_b (w_b + d \cdot \cot \alpha_k) \tag{4.24}$$

As the introduced ice ridge model has vertical walls on the sides, the corresponding sidewise earth pressure has only horizontal component and is not affect the equilibrium in vertical direction.

The equation for horizontal component of Coulomb's force is:

$$F_{cx} = F_c \cos \alpha_k = \mu P_f \cos \phi_w \cdot \cos \alpha_k + \mu P_s \cos \phi_w \quad (4.25)$$

For vertical one:

$$F_{cy} = F_c \sin \alpha_k \ = \mu P_f \cos \phi_w \cdot \sin \alpha_k \quad (4.26)$$

It is clear from equations (4.20; 4.24) that the passive friction force strongly depends on the area of pressure impact ($(h' + d)^2 B$ and $d^2(w_b + d \cdot \cot \alpha_k)$) , determined by the scouring depth in the 2[d] power of magnitude. The more the depth, the more the friction force and the less the possibility for certain ice ridge to gouge the soil on a greater depth. Soil characteristics cause significant impact as well, such that proper soil analysis in any project development with relevant challenge is required.

Active friction force:
This force is a function of soil reaction:

$$F_a = \mu N \quad (4.27)$$

The reaction force from the equation (4.10):

$$N = W - F_b + F_{cy} = F_{cy} \quad (4.28)$$

Substituting into (4.27 and 4.9):

$$F_{da} + F_{dw} + F_i - \mu F_{cy} - F_{cx} = 0 \quad (4.29)$$

Replacing all forces with outlined formulas, the quadratic equation with respect to the gouge depth *d* is derived and easily solved.

The developed physical model implies the pessimistic scour depth value estimation on the basis of ridge considered as an ice feature loaded with drag and resistance forces. Calculations on force interaction model are presented in Appendix D. The results are given below in tables 4.1 and 4.2:

Table 4.1. Ridge features

Parameter	***Unit***	***Value***
Ridge keel macro porosity, η	-	0,27
Average keel density, ρ_{iw}	kg/m^3	947
Average sail density, ρ_{ia}	kg/m^3	852
Wind projection area, A_{a1}	m^2	176
Wind projection area, A_{a2}	m^2	2779
Current projection area, A_w	m^2	679
Keel draught, h_k	m	23,7
Keel width at the sealevel, w_k	m	92,7
Keel width at the bottom, w_b	m	10,5

Table 4.2. Forces action

Force component	Unit	Value	
		Sand	Clay
Drag force due to wind, F_{dw}	MN	0,19	
Drag force due to current, F_{dc}	MN	1,26	
Ridge weight, W	MN	396,9	
Buoyancy, F_b	MN	401,4	
Force due to drifting ice, F_i	MN	16,23	
Passive earth pressure coefficient, K_p	-	7,84	4,12
Specific horizontal Coulomb friction F_{cx}/d^2	MN/m^2	2,94	1,33
Specific vertical Coulomb friction F_{cv}/d^2	MN/m^2	1,04	0,44

According to the table weight and buoyancy are slightly differ in values, such that the 0,5% error gives 5 MN additional vertical force, which is unacceptable. The error is caused by applied correlations in ridge geometry, and in terms of physical considerations it was eliminated. It is also well seen, that drifting ice drives the ridge with force 1 magnitude greater than drag and current action. In table 4.3 it is shown that ice confined ridge ploughs soil 3 times deeper than free-floating ridge. Hence, the surrounding level ice impact could not be neglected.

The gouge parameters themselves reflected in table 4.3 include the sensitivity to sand replaced by clay with properties governed by table 2.14. Obviously the resistance to ridge movement depends on soil conditions in accordance with equations 4.19-4.23. There are a lot of papers [8, 17] claimed that weaker soils exert greater gouging, namely ice scours in sands are not as deep as in clays. From the other hand, weak layer below the scour transmits fewer forces to the buried pipeline.

Table 4.3. Gouge properties.

Parameter	Unit	Value	
		Sand	Clay
Scour width, B	m	30	30
Frontal mound height, h'	m	1,44	1,90
Scour depth, d	m	2,26	3,42
Scour depth in condition of free-floating ridge, not confined with ice, d_f	m	0,66	1,01

One can see that the need of sand replacement by weaker clay above the gouge is unreasonable, since the excess of the scour depth becomes 1,5 times greater, and is not considered in subsequent study.

Some parameters used in scour depth estimation have uncertain nature and consequently demand additional field data and research. The keel draft, showing the water depth, at which the pipeline should be buried, is one of them. Vershinin et al. [10] have shown the keel draft complementary cumulative distribution function on the basis of observations from sonar data (1996-2004), established in figure 4.12. The obtained value of keel draft from present research of *23,7 m* thus corresponds to the order of 1000-year keel.

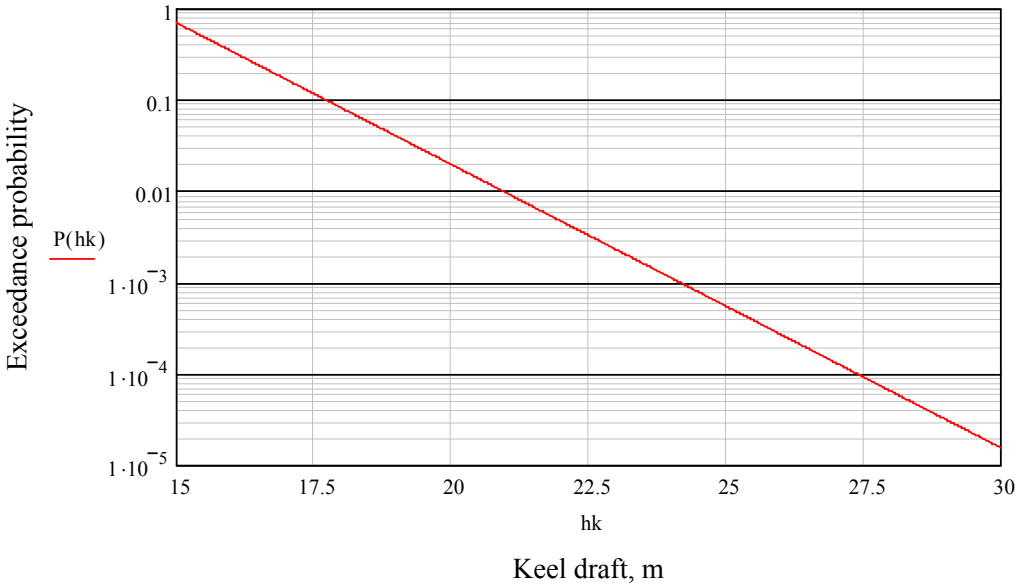

Figure 4.12. Ice ridge keel draft values distribution [10]

One of desirable dependencies necessary to be analyzed is associated with ridge representative dimensional parameter – sail height. The research has shown that the ridge cross-sectional dimensions *do not affect* the scouring. However, it might happen that the sail height correlates with keel breadth.

Although the distribution of ridge width in the Sea of Okhotsk is studied well, the standard deviation appears to be large [10]. The ridge gouge depth to keel breadth relation and its sensitivity to the soil conditions are shown in figure 4.13.

As the force from surrounding ice floe induces deeper scouring, the effect of level ice thickness should be accounted as well. It is indicated in figure 4.14. The appearance of ice immediately increases the scouring effect

Opposite to the ice induced force, the effect of ridge dimensions is bilateral: for small ridges keel breadth increase gives higher driving forces growth rather than resistant forces. This implies intensive gouging in shallow waters. From the other hand, for larger ridges, size effect disappears, limiting the scouring.

Despite the force model calculations give almost equal gouge depth in all water depths below 21,5 m, it doesn't account the mechanism of the ridge appearance in the certain location, hence the distribution of scouring with water depth is considered unreliable. Force model provides only the most unfavorable conditions for maximum physically possible gouge depth corresponding occasional stamucka's shove (slip) rather than ridge scouring.

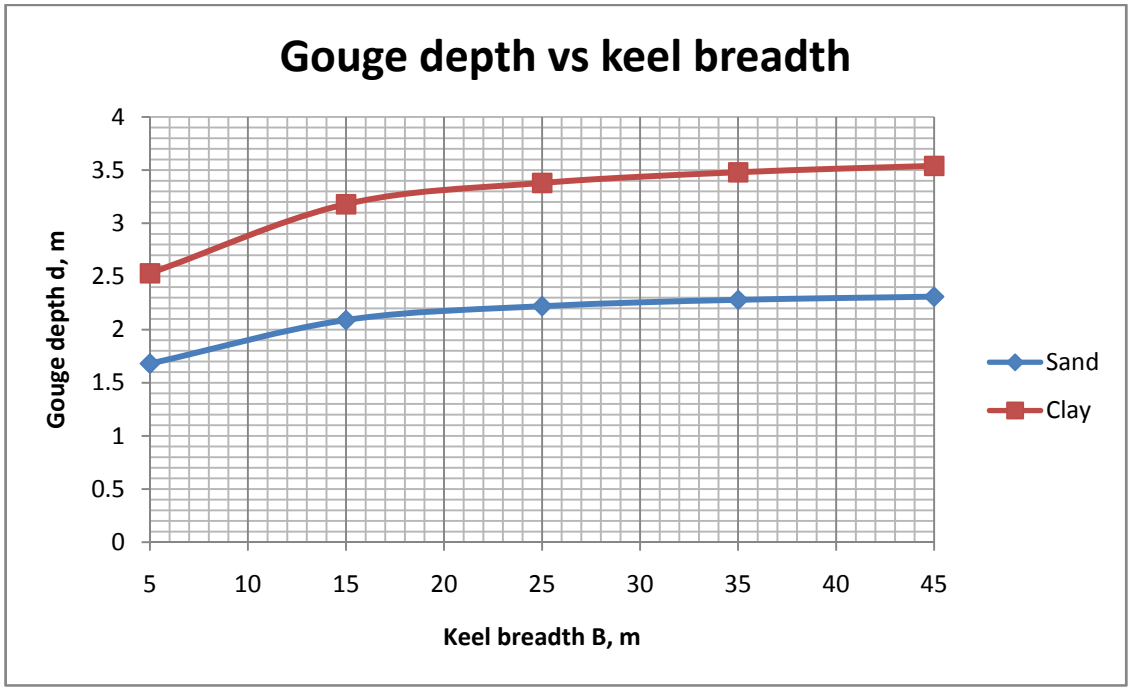

Figure 4.13. Gouge depth vs. keel breadth

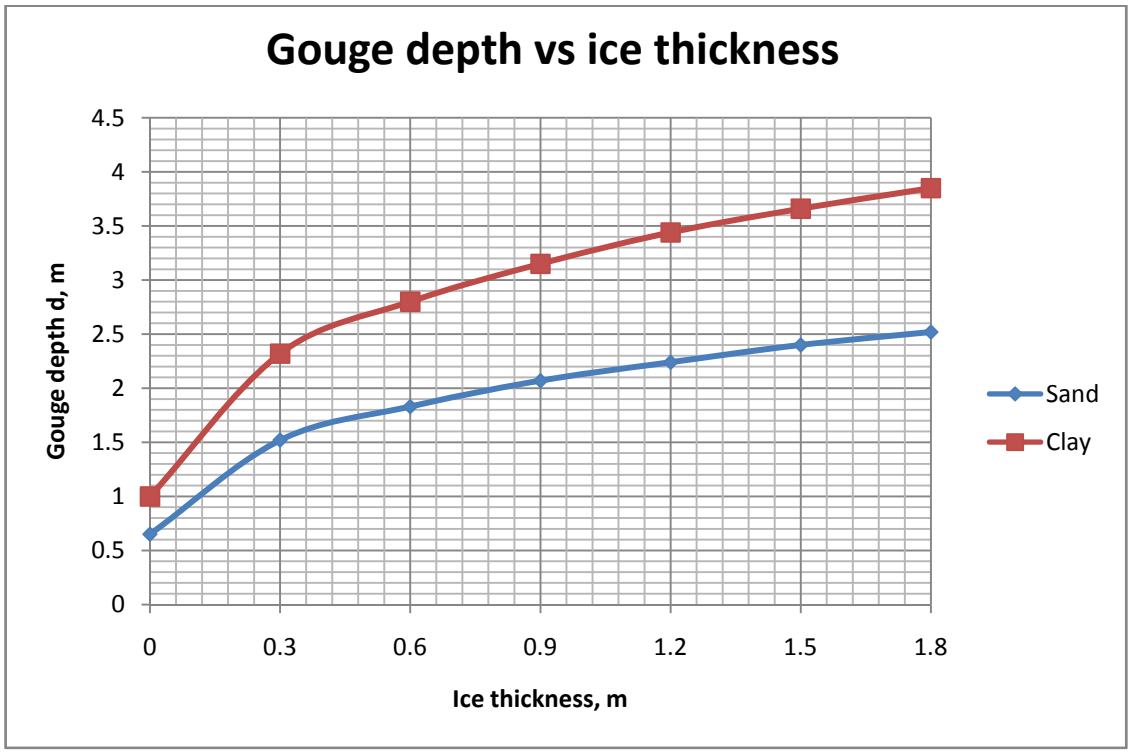

Figure 4.14. Gouge depth vs. ice thickness

4.2.4. Energy scouring model.

The energy model, opposite to the force model, accounts the dynamics of ice ridge, decelerating in the gouge process. The ridge kinetic energy starts to dissipate from the point of initial contact with soil. Thought as an ideal ice conglomerate the ridge expends energy through the work done by soil resistance forces and elevation. Forces change their values consequently as initial speed drops until the ridge is stopped.

The similar model has been proposed by Choi [15], but his research doesn't account neither the ice field, surrounding the ridge, nor the ridge morphology, nor the soil behavior.

The following assumptions have been made in suggested energy model:

- Design scheme 2 is applied, such that the work on the surface ice bending should be accounted;
- The level ice envelope is rigid enough to withstand ridge elevation without breaking;
- Initially the ice ridge is drifting with ice drifting speed v_i, which drops with scour depth increase;
- The ridge elevation is represented by a linear function of the scour length, which is reasonable according to Vershinin et al. findings [10];
- The areas of drag forces action due to wind and current are constant despite the ridge lifts up;
- Ridge keel bottom has an infinite strength, so it is not disintegrating, scouring the seabed (see 4.6.5);
- The ridge moves towards the shoreline, such that the seabed slope is the largest.

The energy balance equation can be written as:

$$E_k + W_a + W_w + W_i = W_{ar} + W_{prx} + W_{pry} + E_p + E_i \tag{4.30}$$

$$E_k + \int_0^l F_{da}\,dx + \int_0^l F_{dw}\,dx + \int_0^l F_i\,dx = \int_0^l F_a\,dx + \int_0^l F_{cx}\,dx + \int_0^{\delta(l)} F_{cy}\,dy + E_p + E_i \tag{4.30a}$$

Where E_k - initial kinetic energy of the ridge; l – scour length; $\delta(l)$ - elevation as a linear function of scour length; E_p - potential energy; E_i - potential energy of flexed ice field.

$$E_k = \frac{W v_i^2}{2g} \tag{4.31}$$

Obviously forces in equation (4.30a) might be taken from 4.2.2 with some corrections due to variable velocity and ridge elevation. Driving forces tend to increase together with relative ridge speed, being compensated by the enhanced resistance due to ridge penetration into the soil.

Drag forces:

At the beginning current and drag forces exert their minimum values on drifting ice feature, whereas they are improved when the ridge stops:

$$F_{da} = \frac{1}{2}\rho_a C_{da} A_{a1}\left(u_a - \frac{l-x}{l}v_i\right)^2 + C_{sa}\rho_a A_{a2}\left(u_a - \frac{l-x}{l}v_i\right)^2 \tag{4.32}$$

$$F_{dw} = \frac{1}{2}C_{dw}\rho_w A_w\left(u_c - \frac{l-x}{l}v_i\right)^2 \tag{4.33}$$

Buoyancy force:

Anticipating changing of the submerged ridge volume, the buoyancy reduces on the displaced weight of water due to ice lifted up on y. Under assumption that the elevation is small enough to reach the trapezoidal part of the keel, buoyancy is approximated as:

$$F_b = \rho_w g B\left[(15{,}44h_s - 3{,}95h_s\tan(\alpha_k))\left(3{,}95h_s - \frac{\rho_i}{\rho_w}h\right) + 15{,}44\frac{\rho_i}{\rho_w}h\cdot h_s - w_k y\right] \tag{4.34}$$

Ice driving force:

Initially drifting ice doesn't act on the ridge, when it slows down the maximum force is limited by the value of ice hummocking:

$$F_i = \frac{x}{l} 0{,}43 \cdot 4{,}059 \cdot B^{0{,}622} \cdot \mathrm{h}^{0{,}628} \tag{4.35}$$

Passive friction:

As it is mentioned in 4.2.2 front and side friction is caused by earth pressure force.

Front face:

From figure 4.14 the front passive pressure force accounts the seabed slope [13]:

$$P_f = \frac{1}{2} K_p \rho_s g [(h' + d)(1 + C_1 \tan\beta)]^2 B \tag{4.36}$$

Where $\tan\beta$ – the seabed slope;

$$C_1 = \frac{\cot\alpha_k}{1 - \cot\alpha_k \tan\beta} \tag{4.37}$$

The gouge depth *d* is non-permanent and could be expressed from figure 4.15 as a function of scour length *x* and elevation *y*:

$$d = x \cdot \tan\beta - y \tag{4.38}$$

Side face:

Soil sidewise pressure equation accounting seabed inclination and ridge lifting up has been outlined by Choi [15]:

$$P_s = \frac{1}{6} K_p \rho_s g \cdot \cot\beta \cdot d^3 = \frac{1}{6} K_p \rho_s g \cdot \cot\beta \cdot (x \tan\beta - y)^3 \tag{4.39}$$

Forces due to passive friction are expressed as:

$$F_c = \mu P cos(\phi_w) \tag{4.40}$$

$$F_{cx} = F_c \cos\alpha_k = \mu P_f \cos\phi_w \cdot \cos\alpha_k + \mu P_s \cos\phi_w \tag{4.41}$$

$$F_{cy} = F_c \sin\alpha_k \ = \mu P_f \cos\phi_w \cdot \sin\alpha_k \tag{4.42}$$

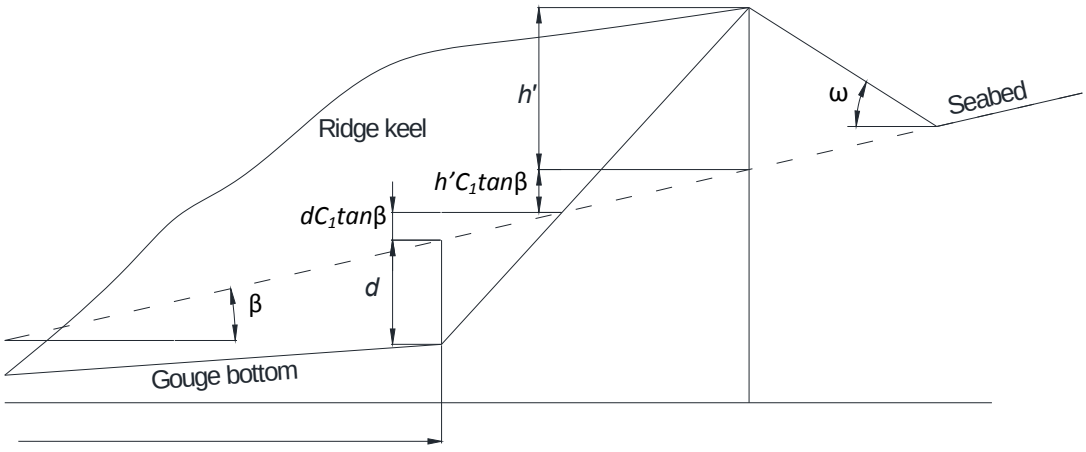

Figure 4.15. Profile of disposed soil around the ridge

Level ice reaction.

Elevating the ice ridge bends the surface ice, causing its reaction. A simple elasticity theory could be applied in order to estimate the tension force of ice field. Marchenko [18] developed the following equation with respect to force, which necessary to impose in order to deflect ice plate with stiffness k_i on value y:

$$F_{li} = k_i y \tag{4.43}$$

$$k_i = \sqrt{\frac{E_i h_i^3 \rho_w g}{24(1-\nu_i^2)}} \tag{4.44}$$

Where E_i – ice elasticity modulus; ν_i – ice Poisson ratio, which are given in table 2.15. This force is a critical component of active friction force, distinguishing its value from one obtained in force model.

Active friction.

Active friction force could be adjusted for energy model accounting the level ice reaction and buoyancy changing:

$$\begin{aligned} F_a = \mu N(y) &= \mu\big[W - F_b(y) + F_{li}(y) + F_{cy}(y)\big] \\ &= \mu\big[\rho_w g B w_k y + F_{li}(y) + F_{cy}(y)\big] \end{aligned} \tag{4.45}$$

Potential energy:

The potential energy is determined as the work made against gravity force:

$$E_p = \int_o^{\delta(l)} (W - F_b) dy = \int_o^{\delta(l)} \rho_w g B w_k y \, dy = \frac{\rho_w g B w_k \delta(l)^2}{2} \tag{4.46}$$

Ice field potential energy

Ridge elevation causes the stresses appear when surrounding ice bends. Potential energy in terms of level ice stiffness k_i is:

$$E_i = \frac{k_i \delta(l)^2}{2} \tag{4.47}$$

Solving an integral (4.30a), the equation with two unknowns is obtained – ridge vertical elevation $\delta(l)$ and scour length *l*. The relation between vertical and horizontal movement should be introduced [10]:

$$y = \delta(x) = \frac{\mu P_f(x)}{B^2 \rho_w g} \tag{4.48}$$

Substituting it into the main equation, the scour length, and then the ridge elevation might be found, designating the scour depth. The results of MathCAD calculations (Appendix D) are presented in tables below for both sand and clay conditions. Evident, that the behavior of the process follows the results, obtained from the force model – ridge easier penetrates into the weaker clay rather than into the stronger soil. This outcome might be useful for other studies, where the decision of additional pipeline protection could be the clay replacement by sand (or stronger soil).

Table 4.4. Scouring in sand

Parameter	Unit	Value	
		Ice confined	Free-floating
Scour width, *B*	m	30	30
Scour length, *l*	m	143,4	48,9
Ridge elevation, *δ(l)*	m	0,79	0,14
Scour depth, *d*	m	1,73	0,72

Table 4.5. Scouring in clay

Parameter	Unit	Value	
		Ice confined	Free-floating
Scour width, *B*	m	30	30
Scour length, *l*	m	208,7	65,3
Ridge elevation, *δ(l)*	m	0,89	0,12
Scour depth, *d*	m	2,77	1,02

The energy model allows tracking the desirable parameters from the moment of the ridge initial contact with soil and before it stops. The distribution of key parameters along the gouge depth is indicated in figure 4.16. The elevation curve shows that the ridge hardly lifts up at the beginning, which is caused by ease of penetration in terms of low soil resistance. At ≈85 m of scouring in sand the front soil pressure is large enough to provide ridge movement almost parallel to the seabed. It is indicated better in figure 4.18 where seabed profiles before and after gouging are presented.

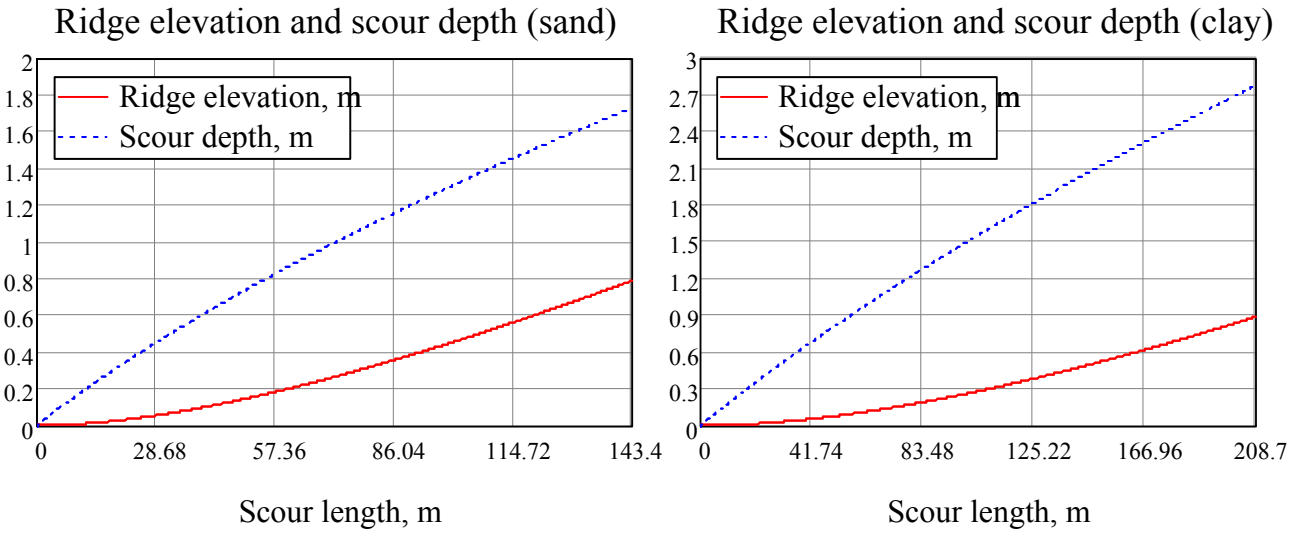

Figure 4.16. Ridge elevation and gouge depth vs. scour length for different soil conditions.

However these findings are not nearly proved by medium-scale tests on gouging described by Vershinin [10]. The result was the ridge keel sliding at the moment of initial contact with the seabed and then suddenly penetrating deep with the subsequent movement parallel to the initial seabed level. Sandy seabed showed later gouging initiation than in clay (figure 4.17). And this might govern the acceptable error, presented in this model, covered up by omission of soil shear strength and cohesion, providing a resistance of the seabed against gouging unless the sufficient amount of normal stress on it (in terms of ice ridge elevation) is reached.

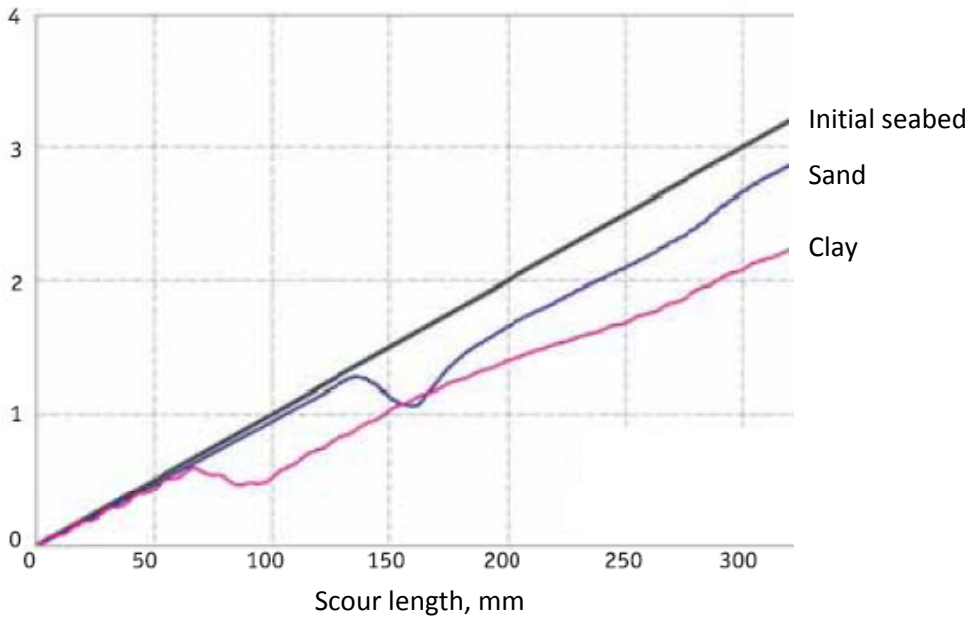

Figure 4.17. Arbitrary results of gouging in sands versus clays [10]

With that at the moment of ridge sudden penetration, the passive friction increases much, and since in the established model its value is low for insignificant gouge depth, the elimination of initial sliding along the seabed does not contribute in the substantial deviation of results.

Figure 4.18 shows that the gouge depth sustainably increases and reaches its maximum after ≈143 m of scouring (in clay -209 m) at water depth of 22 m when energy of driving forces is depleted. At the same time according to table 4.4 it is the force from the surrounding ice flow, which mainly dictates the scouring level. In this concern the gouge depth is changeable regardless ridge dimensions. Hence almost entire area to the shoreline could be ploughed nearly 2 m deep.

.

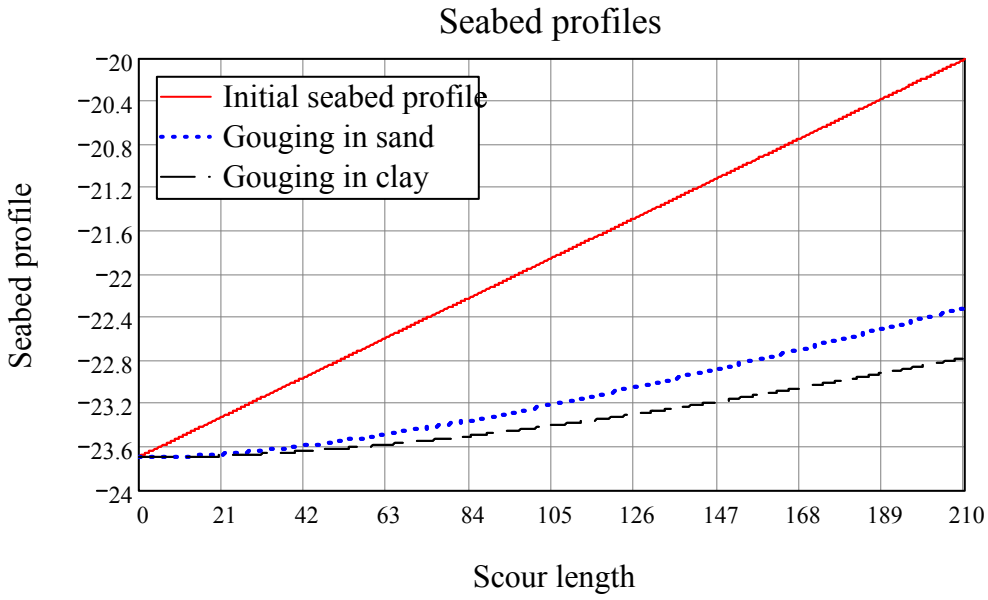

Figure 4.18. Seabed profiles

However in the Sea of Okhotsk the ice action could be limited by motionless fast ice in winter period. Although in spring, when landfast ice breaks, ridges start to scour the seabed intensively, the force from broken ice loads the ridge much less and involves the design scheme 3 in analysis. In this case the dimensions will influence the gouge and its depth will decrease with water.

The ridge has been initially taken as moving upside the largest seabed slope in terms of maximum gouge depth determination; but if the seabed is even, or its inclination angle is small the scour length could be much greater (up to 2 km [10]).

4.2.5. Keel destruction

In the consequent process of seabed ploughing ridge keel erosion could be observed [8]. As one can see from figure 4.18, scour depth continuously increases, the moving ridge therefore is exposed to enhanced seabed reaction. When it measures up the keel strength, its bottom section can sliver from the ridge. The keel decay process depends on stress and strength distribution in keel, keel width at the bottom and seabed properties.

There have been proposed several models of the keel destruction in the contact border between the ridge body and the seabed. Liferov et al. [19] have studied sequential shear of horizontal keel layers, proven by results of finite-element analysis. However for theoretical modeling the model proposed by Vershinin et al. [10] seems to be more practical. This model is associated with the deep-seated dislocation in the ridge keel, caused by front soil pressure. Opposite to horizontal cutting in Liferov et al. [19] model, the destruction goes in sliding along the sloped keel border. The keel ridge strength is determined by the limit pressure p_n it could withstand before breaking. The latest is obtained from equation (4.49) as Vershinin et al. [10] have suggested.

$$C_i \cot\varphi_i \left[\frac{1+\sin\varphi_i}{1-\sin\varphi_i \sqrt{1-\mu(p_n)^2}} \cdot e^{[(\pi-2\beta(p_n))\cdot\tan\varphi_i]} - 1 \right] - p_n = 0 \qquad (4.49)$$

Where

$$\mu(p_n) = \frac{p_n \mu}{C_i + p_n \tan\varphi_i};$$

$$\beta(p_n) = \arctan\left[\frac{p_n \tan\left(45° + \frac{\varphi_i}{2}\right)}{1+\sqrt{1-\mu(p_n)^2}} \right];$$

φ_i - internal friction angle for ice ridge (table 2.15); C_i - keel cohesion (table 2.15). The keel slope increases the ridge resistance to deep-seated dislocation [10] by the value $\overline{k_a}$, which is determined by:

$$\overline{k_a} = \frac{\tan\left(\frac{\pi}{4}+\frac{\varphi_i}{2}\right)^2 \cdot e^{2(\pi-\alpha_k)\tan\varphi_i} - 1}{\tan\left(\frac{\pi}{4}+\frac{\varphi_i}{2}\right)^2 \cdot e^{\pi\tan\varphi_i} - 1} \qquad (4.50)$$

The overall maximum load per unit keel breadth is governed by total keel strength σ_{ir} multiplied by 2/3 of the sum of gouge depth and frontal mound height:

$$\frac{F_{ir}}{B} = \frac{2}{3}\sigma_{ir}(h'+d') = \frac{2}{3}k_a p_n (h'+d') \qquad (4.51)$$

The scour depth, governing the keel destruction is found from the comparison of limit force with the front pressure force (equation (4.36)):

$$F_{ir} = P_f \tag{4.52}$$

$$\frac{2}{3} k_a p_n = \frac{1}{2} K_p \rho_s g (h' + d') \tag{4.53}$$

$$d' = \frac{4 \cdot k_a p_n}{3 \cdot K_p \rho_s g} - h'(d') \tag{4.54}$$

Under above mentioned considerations the possible scour depth for anticipated ridge decreases down to *0,54 m* and *1,06 m* for sand and clay respectively.

4.2.6. Comparison of scouring models

Tables 4.6 and 4.7 cover the results of several researches and compares estimated and/or observed scour parameters.

The force model gives an improbable gouge depth, despite it corresponds to Astafief observations [16]. It is assumed that the pipeline interaction with the ridge causing more than two meters of sandy seabed ploughing is unlikely in terms of the analysis of the gouge depth return period established below, especially in conditions of limited ridge keel strength.

The energy model outcome gives a more reasonable assessment compared to others' findings. Thus in conditions of substantial surrounding ice flow, the scour depth fits with the one gained from Vershinin et al.'s [10] model, while the free floating ridge assumption provides the same order as Choi's research [15].

Table 4.6. Comparison of results of different models for scouring in sand

Parameter			***Scour width, B***	***Scour depth, d***	***Scour length, l***	***Elevation, δ(l)***
Units			m	m	m	m
Present research	*Force model*	*IC*[1]	30	2,26	-	-
		FF[2]		0,66	-	-
	Energy model	*IC*[1]		1,73	143,4	0,79
		FF[2]		0,72	48,9	0,14
	KSC[3]			0,54	35.4	0,08
Choi research [15]		*FF*[2]	20	0,78	-	-
Vershinin et al. research [10]		*IC*[1]	22	1,84	-	-
		KSC[3]		1,44	90	0,34
Astafiev et al. [16] observations			-	2,13	-	-

Table 4.7. Comparison of results of different models for scouring in clay

Parameter			***Scour width, B***	***Scour depth, d***	***Scour length, l***	***Elevation, δ(l)***
Units			m	m	m	m
Present research	*Force model*	*IC*[1]	30	3,42	-	-
		FF[2]		1,01	-	-
	Energy model	*IC*[1]		2,77	208,7	0,89
		FF[2]		1,02	65,3	0,12
	KSC[3]			1,06	67,7	0,13

[1] – Ice confined ridge;

[2] – Free floating ridge;

[3] – Keel strength controlled condition.

If the keel strength is taken into account, the scouring in certain water depth reduces. From the other hand since the keel strength tends to increase upwards and gouging is mainly controlled by forces from the surface ice rather than by ridge dimensions, the maximum obtained scour depth could be reached in shallower waters anyway. The calculations in MathCAD presented in Appendix D governs the required keel cohesion for maximum *1,73* m scouring in sand, which is approximately *50 kPa.* According to Vershinin et al. [10] this value corresponds to high ice blocks adfreezing, which is unlikely to occur in the bottom of large keels, but highly possible in their intermediate part.

The keel draught coupled with the maximum scour depth gives a hazardous water depth of 22 m, which implies that for the given seabed slope in the shore approach area almost 1250 m of the pipeline should be trenched.

4.3. GOUGE PARAMETERS' STATISTICAL DISTRIBUTION

The gouge parameters influence the pipeline risk in a number of ways: length determintes the frequency of pipeline crossing probability. Scour width and depth affect the pipeline response and the burial depth requirement, while their distributions and design values are of big importance from the practical point of view. These parameters though require a substantial amount of statistical data and observations. In this end the analysis of obtained parameters' values suitability to the findings of other works' observation data is present below.

4.3.1. Gouge depth

The final decision on the design gouge depth is based on corresponding return period. In previous sections it was shown that it is the forces from surrounding ice, which determines how deep the ridge could scour the seabed. In this regard the 100-year values of independent ice thickness and ridge drifting speed give 10 000-year depth with the certain confidence level.

Vershinin et al. [10] summarized the results of different probabilistic researches related to the gouge depth distribution in the Sakhalin shelf (figure 4.19). The work recommends the exponential probability density function being the best (conservative) estimate:

$$P(d) = d \cdot e^{\left(-d/\bar{d}\right)} \tag{4.55}$$

Where $\bar{d}$ is the average observed gouge depth (table 2.15). The PDF function is transformed into complementary cumulative density function (CCDF) in order to estimate the exceedance probability of the certain gouge. It is established below in figure 4.19.

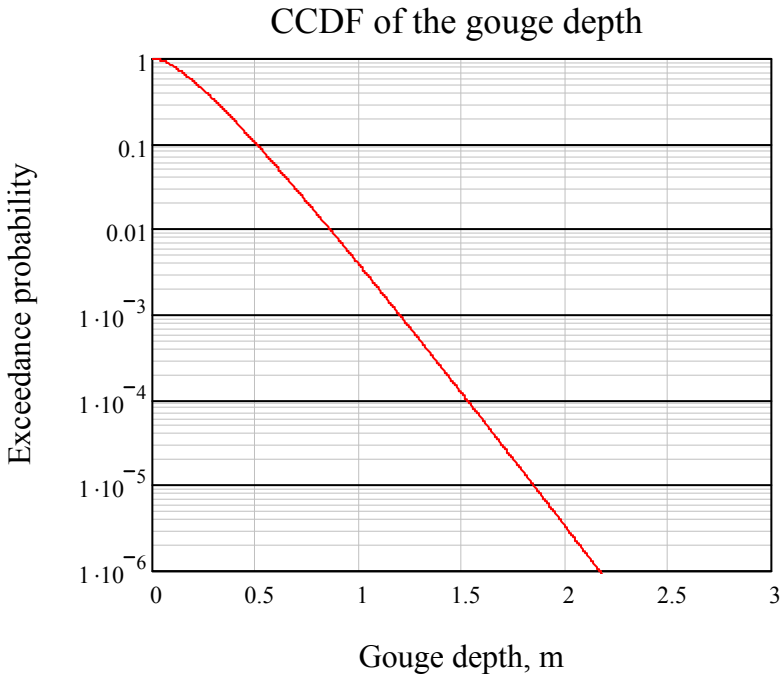

Figure 4.19. Distribution of the gouge depths [10]

4.3.2. Gouge width

The scour width as well as the gouge depth exerts direct influence on the pipeline response. Walle [21] has analyzed the Chaivo gouge database, stating that the most of Sakhalin gouge widths from both single and multi keels obeys the behavior shown in figure 4.20 below, such that the design *30 m* scour width has an order of 10^{-2} probability of occurrence, corresponding to the 100-year ridge.

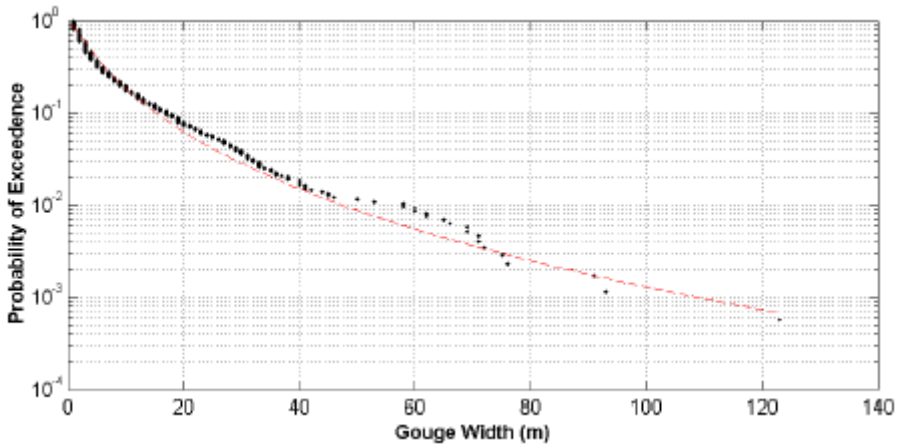

Figure 4.20. Gouge width distribution [21]

4.3.3. Scour length

The same research [21] provides the analysis of scour length on the basis of SEIC Sakhalin gouge data on the scour lengths distribution (figure 4.21). The values obtained in present study correspond to the minimum possible lengths for the certain conditions of ridge moving

shorewards. Though they fit ones described by Walle, the scour orientation uncertainty involves the doubtful exceedance probability selected.

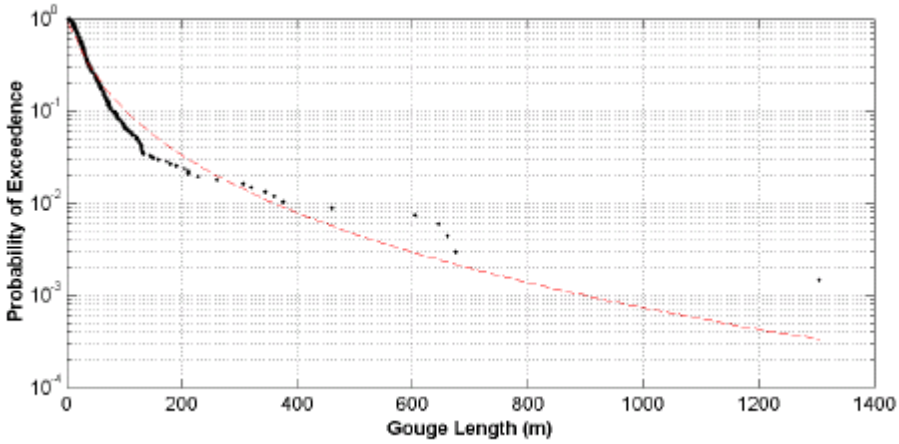

Figure 4.21. Gouge length distribution [21]

4.3.4. Direct contact with pipe probability

The probability of the pipeline damage due to its route intersection by scouring ridge during the period of its operation is one of the most desirable values in present analysis in terms of the pipeline integrity and reliability. Evident, that one is determined mainly by the scour width and depth. It is reasonable to assume that they are not interdepended, since the gouge depth is mainly governed by the environmental forces, while the width value is a feature of the ridge keel. In this regard the probability of such gouge existence than:

$$P_{gouge} = P(d) \cdot P(B) \tag{4.56}$$

And corresponds to the 10^{-7} order of magnitude. Though this value seems to be extremely conservative, it is necessary to account the scour-pipeline intersection frequency, which is termed as the average number of scours, intersecting 1 km of the pipeline annually [10]. Vershinin et. al [10] developed the following relation for its value estimation:

$$n = \frac{2}{\pi} \bar{l} \cdot n_v \tag{4.57}$$

Where $\bar{l}$ - is the average observed scour length, n_v - is the average ridge density per 1 km (table 2,15).

Considering the length of the buried pipeline section $L=1,25\ km$, with the production period of $T=30\ years$, the buried pipeline damage probability will be:

$$P_{damage} = P_{gouge} \cdot n \cdot T \cdot L \tag{4.58}$$

Corresponding 10^{-4} likelihood of damage, which is entirely acceptable by the requirements of many codes [2], though this value might change from place to place in terms of variable intersection frequency.

The probability of the direct contact between the ridge and the pipeline, buried somewhat above the possible gouging ($1.73\ m$), is determined by the damage probability of the scour of any width, which is consequently 1 percent annually and appears to be unacceptable value, though the relevant analysis is done below in Chapter 5.

4.4. SUMMARY

The chapter introduces comprehensive and universal theoretical approach to the scour depth determination, able to be applied in different environmental conditions, relevant for the certain area of pipeline allocation. Concentrating on the Sea of Okhotsk environment ,the first-year ice ridge study performs the shape and morphology determination, which allows specify the design ridge for this region, such that the recommendations for protection of the pipeline in hazardous water depths range are given. *23,7 m* estimated ridge keel draft dictates the trench length of ≈*1250 m* with the probability 10^{-3} of direct contact in deeper waters.

The question, how deep the scours could penetrate, is answered by two introduced theoretical models. The force model gave unreasonably overstated results (*2,26 m* for in-situ sand), compared to those observed, corresponding rather the stamukhas shoves than the ridge scouring itself. Although the force model is not anticipated in subsequent study, it could be useful in analysis of stamukhas interaction with the seabed, when substantial environmental loadings occur.

The energy model, accounted for the ridge dynamics, gave much better outcomes, fitted the observations and other theoretical researches. It educed an important distinguished feature of a ridge behavior: when scouring the seabed, it sustainably elevates upwards, exerting significant pressure on the sea bottom, such that the resistance to ridge's movement is greater than it was expected initially. From the model calculations the given soil and metocean conditions provided the possible scour depth of *1,73 m*. According to the keel properties, established in the work [10], the ridge is able to plough this amount of soil, having the near-bottom keel rubble strength of *50 kPa*, corresponding to the high blocks adfreezing, which is possible in conditions of the Sakhalin shelf.

The desirable gouge parameters such as depth, width and length, estimated in established model, have been compared with the statistical data for relevant location, which gave the ridge probability of direct contact with the pipeline, covered by *1,73 m* of in-situ sand. Preliminary considered as the collapse probability, the order of 10000-year contact fits all recent standards' requirements, providing a very good estimate, performed by the energy model.

Being interested in the trench depth reduction, but following the pipeline safety considerations, scouring sensitivity to the soil parameters has been carried out. The research showed that weaker soils are subjected to deeper gouges, whereas the stronger rock shipment is considered economically unjustified. Hence the results gained for gouging in original sand are transferred to the subsequent study of subscour soil behavior and its implications on the buried pipeline.

4.5. REFERENCES

[1] G.W. Timco, R.P. Burdan (1997): *An analysis of the shapes of sea ice ridges*. Cold Regions Science and Technology, 25: pp. 65-77.

[2] ISO/FDIS 19906 (2010): *Petroleum and natural gas industries – Arctic offshore structures.* International standard, International Standardization Organization, Geneva.

[3] K.M. Obert, T.G. Brown (2011): *Ice ridge keel characteristics and distribution in the Northumberland Strait.* Cold Regions Science and Technology, 66: pp. 53-64.

[4] V.V. Kharitonov (2008): *Internal structure of ice ridges and stamukhas based on thermal drilling data.* Cold Regions Science and Technology, 52: pp. 302-325.

[5] V.D. Grishenko (1988): *Morphological characteristics of ice ridges in the Arctic basin.* Proceedings of the AARI, Vol. 401, Leningrad, pp 46-55. (In Russian).

[6] B. Bonnemaire, K.V. Høyland, P. Liferov, P. Moslet (2003): *An ice ridge in the Barents Sea, Part 1: Morphology and physical parameters.* Proceedings of the POAC, NTNU, Trondheim, Norway, Vol. 2, pp. 559-568.

[7] G.A. Surkov (2001): *Scientific-methodological basis of determination of loads on offshore structures from ice ridges.* Doctor of Science dissertation. VNIIGAZ, Moscow, Russia, 383 p. (in Russian).

[8] P. Liferov (2005): *First-year ice ridge scour and some aspects of ice rubble behavior.* Doctoral thesis, Department of Civil and Transport Engineering, NTNU, Trondheim, 162 p.

[9] C. H. Nelson, L. Phillips, L. McRea, J. Barber, J. McLaughlin, M. W. Chin, L. John, *Gray Whale and Pacific Walrus Benthic Feeding Grounds and Sea Floor Interaction in the Chukchi Sea*. U.S. Geological Survey, California.

[10] S.A. Vershinin, P.A. Truskov, P.A. Liferov (2007): *Ice features action on seabed.* IPK "Russkaya kniga", Moscow, Russia, 196 p. (in Russian).

[11] A. Palmer (2000): *Are we ready to construct submarine pipelines in the Arctic*. Offshore Technology Conference, Houston, Texas, 1-4 May 2000, paper number OTC-12183.

[12] W.F. Weeks, P.W. Barnes, D.M. Rearic, E. Reimnitz (1983): *Statistical aspects of ice gouging on the Alaskan Shelf of the Beaufort Sea*. USA Cold Regions Research and Engineering Laboratory, CRREL Report 83-21.

[13] R. Phillips, J.I. Clark, S. Kenny (2005): *PRISE studies on gouge forces and subgouge deformations.* Proceedings of the POAC, Potsdam, New York, USA, Vol. 1, pp.75-84.

[14] S. Løset (2011): *Arctic Offshore Engineering lecture notes*. UNIS, Longyerbyen.

[15] K. Choi, J. Lee (2002): *Simplified Ice Ridge-Seabed Interaction Model for determination of Ice Scour Depth.* Proceedings of The Twelfth International Offshore and Polar Engineering Conference, Kitakyushu, Japan, 26-31 May 2002.

[16] V.N. Astafiev, A.M. Polomoshnov, P.A. Truskov (1991): *Stamukhi of the Northern Sakhalin Offshore.* Proceedings of the First International Offshore and Polar Engineering Conference, Edinburgh, The United Kingdom, Vol. 2, pp. 462-466.

[17] K. Been, A. Fredj, G. Comfort (2011): *Pipeline strains in soft clay backfill subject to ice gouging* . Journal of Pipeline Engineering, Vol.10, No.2, June, 2011 Pp. 87-98.

[18] A. Marchenko (2011): *Arctic Offshore Engineering lecture notes*. UNIS, Longyerbyen.

[19] P.A. Liferov, K.N. Shkhinek, S.M. Kapustyanskiy, A.G. Gilenkov, N. Serre (2006): *Scour depth determination – an approach.* Submitted to J. Cold Regions Science and Technology.

[20] http://en.wikipedia.org/wiki/Lateral_earth_pressure

[21] T. Walle (2004): *Ice gouging offshore Sakhalin Island*. Master thesis, Department of Material Science and Technology, Stavanger University College, Stavanger, 105 p.

[22] S.V. Duplenskiy (2011): *First year ice ridges interaction with marine pipelines*. Arctic Offshore Engineering project report. UNIS, Longyerbyen.

CHAPTER 5. ON SUBGOUGE SOIL DEFORMATIONS AND THE PIPELINE RESPONSE

5.1. GENERAL

In previous chapter gouging has been recognized as a potential problem for the Arctic seas. Driving forces from wind, current and drifting ice apparently turned out to be large enough to plough scours 1-2 meters deep, and the ridge keel showed the sufficient strength to maintain the sustainable gouging.

Causing significant loads (up to ≈20 MN from table 4.2) ridge keels easily could damage a pipeline, situated in soil thickness above the possible scour [1]. This scenario is examined below as accidental case with a huge probability of loads on pipeline, exceeding the allowable limit state.

At first it was thought that pipelines would be safe buried accurately below the ice ridge, able to pass over it. Then it was realized that the pipeline might be dragged with the seabed soil which is susceptible to intense deformations below gouging ice ridge. As a consequence the safe pipeline burry challenged high-priced deep trenching. In this concern for the pipeline design the most important questions remain how far downward the gouge-induced deformations penetrate and how the pipeline responses on them.

Due to high reliability of the pipeline requirement from one hand and in order to evade the excessive costs of trenching from another, the ice-soil-pipeline interaction analysis should determine the safe burial depth, allowable for given stressed-deformed state. For this end the classical practice of buried pipeline interaction with ice features analysis splits the system into two subsystems [2]: 1) “ice-soil” and 2) “soil-pipeline”. This approach allows development of mathematical models involving a set of needful assumptions:

- The presence of the pipeline doesn’t affect the subscour deformations in “ice-soil” system. Using empirical correlations, this provides the possibility of plotting the soil subsgouge deformations curve with depth;
- Soil displacements are applied to the pipeline, causing its bending. The Pipeline should be controlled against loading beyond yield strength and being into the plastic range.

This chapter operates mathematical model for the pipeline buried, ensuring the limit state design criterion, mainly associated with Von Mises equivalent stress analysis.

An alternative is to consider the integration of “ice-soil-pipeline” frame, accounting mutual components influence on each other [3, 4]. This method mainly corresponds to the numerical modeling of gouging impact on the trenched pipeline.

5.2. ARCTIC OFFSHORE STANDARDS

Before the analysis of the physical processes, undergoing below the scour, and their influence on the pipeline, the overview of the International and Russian offshore standards has to be carried out. The experience, reflected in codes would be a strong background, applied for Russian Arctic Offshore projects development in the context of ridge implications on the pipeline.

5.2.1. ISO 19906

Although *«Arctic Offshore Structures»* [5] standard in general is not for pipeline design purposes, it recommends the application of statistical data on ice-induced gouging in order to determine the frequency of gouge occurrence and its depth, width, length and direction. It is also requires the study of the soil and the ridge keel mechanical properties, as well as the ice gouge effects, including pressure exerted on the seabed soils and consequent soil displacements. The Standard mentions subgouge soil deformations and charges flowlines to be buried below the depth where unacceptable pipeline bends could occur. But the methodic on certain safe depths determination is not given and nothing is said about the variety of pipeline protection measures.

5.2.2. ISO 13623

«Petroleum and natural gas industries – Pipeline transportation systems» [6] says that the bottom scouring shall be considered when designing for the ice loads.

5.2.3. API-RP-2N

«Recommended practice for planning, design, and construction structures and pipelines for Arctic Conditions» (withdrawn) [7] also calls for the gouge parameters probability distribution studying and refers both deterministic and probabilistic related research works. In accordance with the standard, the subscour deformations, able to damage the pipeline, set the objective of its protection with the least amount of environmental disturbances and costs. But the standard doesn't avail the design aspects.

5.2.4. DNV-OS-F101

«Submarine Pipeline Systems» [8] mentions that pipeline in shore approach area might be subjected to ice ridge action.

5.2.5. CAN/CSA-S471-92

«General requirements, design criteria, the environment and loads» (withdrawn) [9] notes the scour width and depth determination necessity if gouging is probable. A special attention is paid to the need of operating pipeline periodic check with respect to its route intersection by scours.

5.2.6. RMRS 2-020301-001

«Russian Maritime Register of Shipping – Rules of classification and construction of subsea pipelines» [10] gives strong recommendations on pipeline trench depth calculation, accounting the specific of Russian ice-covered seas. Ridges number and parameters surveyed coupled with hydrological conditions, which have been being observed for (at least) the last 5 years before pipeline is constructed, govern the probability of the ridge keel to exceed the certain water depth. Thereafter the burial coefficient, providing the required burial depth could be determined. Correction factors on seabed soil properties and the pipeline safety class increase the depth somewhat. The subgouge deformations are accounted by supplemented 0,4 m of extra soil thickness. With that the Standard allows the usage of other techniques, considering wind and current regimes, sea level fluctuations due to tides, seabed properties, and statistical ice features' parameters, obtained from the representative sample.

The issue of gouging as a potential hazard for subsea pipelines has been described somehow in many codes, giving a notion about considerable need in additional researches and techniques in this field. Nonetheless, Arctic Offshore standards as listed above do not account

gouging implications on pipelines, while instructive techniques and recommendations on both scour and subscour implications are desirable aspects. In this regard the physical behavior of ridge-soil-pipeline related processes are studied below.

5.3 SUBSCOUR SOIL BEHAVIOR

5.3.1. Subscour deformations

The first evidence of subscour deformations hazard for marine pipeline came from the small-scale experiments carried out by Poorooshasb et al. [11]. The work was extended when the detailed study of gouges morphology and scouring dynamics was performed [12]. The problem assessment and discussion had been developed deeper with oil and gas companies' interest in participating in PRISE program (Pressure Ridge Ice Scour Experiment), led by C-CORE. The diversified scope of PRISE studies involved centrifugal modeling, finite-element modeling and exploration of relic gouges, such that their interpretation [13] gave substantial results of scouring influence on the pipeline.

These results demonstrated extensive horizontal subgouge movements extending to at least two gouge depths, though they were not complemented by finite-element analysis due to numerical difficulties that time [13].

One of the most recent and illustrative investigations dedicated to subscour deformations was the experiment in Delft Hydraulics Laboratory (Netherlands) [2], performed on the basis of measurements of soil porosity below the scour. Under the conditions of the keel scouring the seabed 80-150 mm deep, the movements of 10-15 mm were observed on the depth of 250 mm below the keel, while the most intensive deformations (up to 100 mm) occurred in 50 mm ridge bottom-close zone.

All tests have shown nearly same results and could be concluded as:

- There is no straightforward relationship for subgouge displacements with the gouge depth, width, soil characteristics, such that significant uncertainty remains in theoretical subscour deformations prediction [14];
- The soil displacement at the scour base are significant and could extend 2,5 of the gouge depth [13];
- Strong dependency of movements vertical distribution on keel angle: lower attack angles involve less rapid movement attenuation [15];

Under these statements it is challenging to find a mathematical expression of universal solution, describing the soil behavior below the gouge. In this regard Palmer's [13] empirical correlations based on the limited amount of centrifugal tests performed in PRISE program are used in the mathematical part of subscour deformations assessment in this thesis. The author is aware that it may give a considerable error in calculations compared to reality. However, the effect of such uncertainty might be adjusted, using finite-element modeling, performed in Chapter 6.

The maximum horizontal deformations occur at the middle of the gouge base and obey the following equation:

$$u_{s0} = 0{,}6\sqrt{Bd} \tag{5.1}$$

It is reasonable that the gouge depth d, soil properties (being used in gouge depth calculations) and ridge characteristic parameter B (breadth) are accounted, even though neither

keel attack angle, nor important soil parameters beneath the keel bottom (shear strength, internal friction angle, cohesion) were used.

The vertical decay of deformations with depth from the scour centerline z follows the exponential distribution [13]:

$$u_s(z) = u_{s0} e^{-\frac{2z}{3d}} \tag{5.2}$$

If $u(z)$ is the displacement in the gouging direction on the gouge centerline at a depth z, the displacement at the same depth, y meters off the centerline is [13]:

$$u_s(y,z) = u_s(z) \cdot \begin{cases} 1 & if\ y/B < 1/4 \\ \frac{1}{2}\left[1 + \cos\left(\frac{2|y|}{B} - \frac{1}{2}\right)\pi\right] & if\ 1/4 < y/B < 3/4 \\ 0 & if\ y/B > 3/4 \end{cases} \tag{5.3}$$

Equation (5.3) provides a stable soil displacement within half of a scour width with the maximum value for a given depth z. Subsequently the deformations fall to zero at the scour limits and do not propagate sidewise. The three-dimensional field of the sand deformations below the given gouge plotted in MathCAD is preformed in figure 5.1.

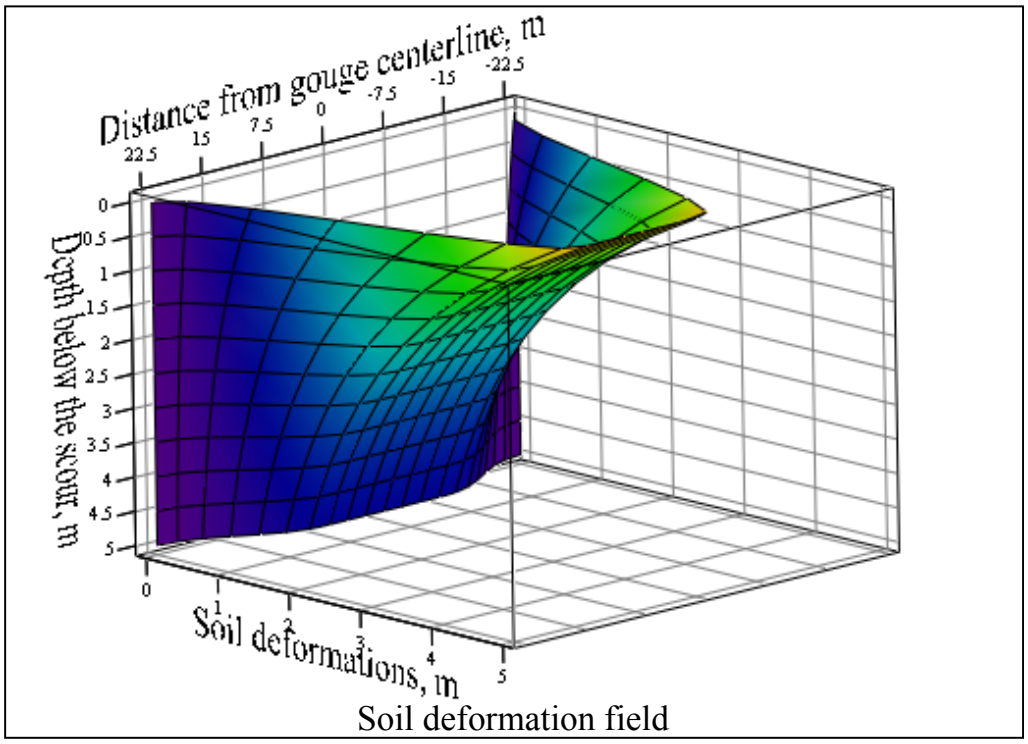

u

Figure 5.1. Subscour horizontal sand deformation field according to equation (5.2; 5.3)

The deformations in clay, which were studied in the context of gouge depth analysis, are shown in figure 5.2 in comparison with sand. It might be seen, that for given conditions the clay at the gouge base exceed sand movements by 25%, whereas below the scour the clay deformations die off less rapidly, such that at 5 m depth clay displacements are twice greater than in sands. Though this phenomenon could be considered as error, since it is known, that despite the initial deformations in weaker soil are higher, their decay with depth is observed to be more rapid [15,16].

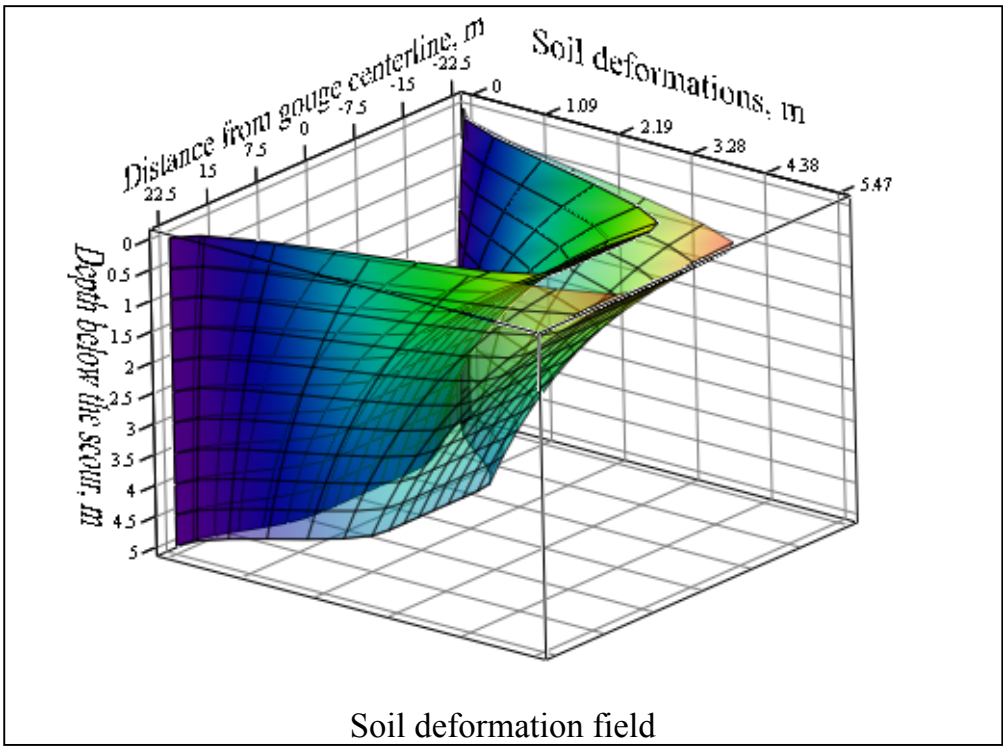

u, u2

Figure 5.2. Subscour horizontal deformation fields comparison: sand – entirely shaded; clay – semitransparent; according to equation (5.2; 5.3)

Except horizontal soil displacements, there occur less prominent vertical ones. They are not of big concern in upper layers, though they fall off much more slowly downwards than the horizontal movements, hence at greater depth the pipeline is rather pressed down than dragged along. Palmer [13] suggested the following correlation for the vertical soil displacements:

$$v_s(z) = de^{\left(-\frac{z}{3d}\right)} \tag{5.4}$$

Results for given conditions are shown in figure 5.3. The value of *1,73* m *(2,77* m in clay*)* at *z=0* reflects the soil particles movement from the position at the initial seabed down to the scour. The soil properties are also merely accounted in the gouge depth value.

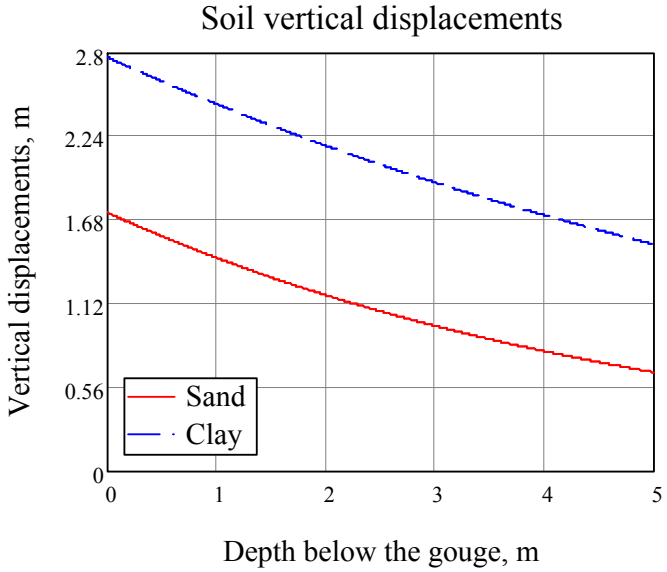

Figure 5.3. Vertical subgouge soil deformations, according to equation (5.4)

5.3.2. Soil properties' behavior subscour

For the purpose of the accurate assessment of soil implications on the pipeline, some soil mechanical properties' behavior below the gouge is analyzed below. In general case it is expected, that the effect, caused by the soil reaction on the pipeline, attempting to resist soil motions, is a function of the shear strength. However the shear strength itself is set differently for cohesive or granular soils.

Three soils with properties given in table 2.14 are analyzed in this section in terms of the best backfill material selection:

- the original sand, relevant for in-situ conditions of the Sakhalin shelf;
- clay with smaller angle of internal friction;
- softer clay with zero angle of internal friction.

The Mohr-Coulomb failure criterion is used in the research, being considered as the best shear strength estimator in condition of vertical stresses increase with depth. Accordingly the failure envelope is described by the general relation:

$$s_u = \sigma \tan \varphi + c \tag{5.5}$$

Where c is the cohesion, σ - normal stress applied, φ - angle of internal friction. For granular soils (sand) the cohesion is almost zero and equation (5.5) goes into:

$$s_u = \sigma \tan \varphi \tag{5.5a}$$

For cohesive soils, such as clay, the internal friction angle is normally much less, but falls within the range from 0° to 45° [17]. Hence the shear strength for the first (stiffer) clay is represented by the generalized equation (5.5), where none of the component could be neglected. For the second (softer) clay type the internal friction angle is equal to zero (table 2.13), hence its shear strength is represented by the following equation:

$$s_u = c \tag{5.5b}$$

It is necessary to note, that the shear strength used in subsequent calculations is the undrained shear strength, since the ridge scouring the seabed moves fast enough to limit the deeper soil layers' saturation with water.

Sustainably elevating, the ridge increase the stress on the soil. Since equation (5.5) involves the strength depending on the applied normal stress, the effect of the ridge action is proposed to be accounted in this thesis. All of examined recent researches [13,16,18], performing a study of subgouge soil displacements action on the pipeline, have not considered this effect, which might led to erratic estimates. But in order to estimate the soil impact on the pipeline properly, the soil stresses themselves at the ridge bottom should be found.

Combining both introduced energy and force models for the ridge scouring the seabed phenomena and under assumption that its deceleration value is negligibly low, the system of forces equilibrium in vertical direction is:

$$N - F_c \sin \alpha_k - F_{li} - \Delta W = 0 \tag{5.6}$$

The normal stress in the soil at the scour level is the seabed reaction N per unit area, which could be found, being equalized by the ridge specific weight in terms of elevation ΔW, the level ice reaction F_{li} and the Coulomb vertical friction $F_c \sin \alpha_k$. From the other hand it is obvious that

the vertical stresses in the soil sustainably increase with the depth H. Hence, the normal stress is characterized by the following:

$$\sigma = \sigma_i + \rho_s g H = \frac{N}{B w_b} + \rho_s g H \tag{5.7}$$

And consequently the generalized equation for the shear strength:

$$s_u = \left(\frac{N}{B w_b} + \rho_s g H\right) \tan\varphi + c \tag{5.8}$$

Independently on the soil type analyzed in the research, the seabed reaction remains constant as the alternative of the trench part backfilling (*subjected to the possible scouring*) by the weaker soil is rejected in Chapter 4.

Figure 5.4 expresses the shear strength as a function of depth H for the three anticipated soil conditions listed above.

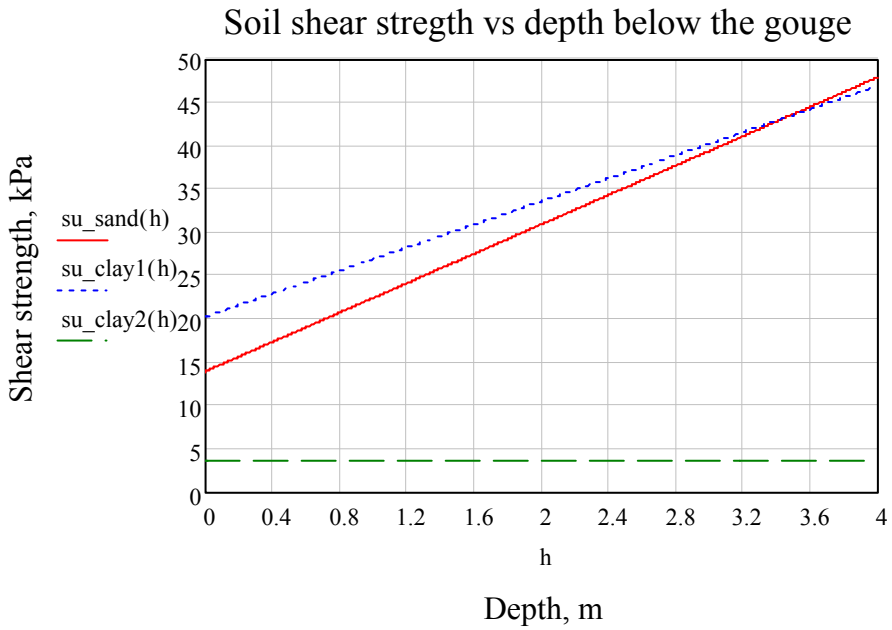

Figure 5.4. Soil shear strength versus depth below the gouge, according to equation (5.8)

The plot brightly reflects the internal friction angle influence on the shear strength. Initially the stiffer clay (clay 1) remains stronger than the sand due to cohesion, but lower friction angle makes it weaker below *3,6* m depth. For softer clay (clay 2) the normal stresses applied do not affect the shear strength, which is constant with depth and equal to cohesion. This outcome implies that for the estimated gouge depth, being ploughed in sand, the deformations below the scour are largest for soft clay, smaller for sand and the least for stiff clay backfills. With that it is clear that for greater shear strength the deformation curve declines less with depth. Hence, the soft clay at the gouge base deforms more than the stiffer clay and sand, which in turn remains substantially displaced, say in 2 m depth, inducing larger forces. This might contradict with the deformations range for different soils analyzed in section 5.3.1 (figure 5.2) as the soil properties were not accounted in latest.

Despite the deformation range is greater for weaker soils it is expected that they will exert less force on the pipeline, flowing around it, unless the relative deformations are very small indeed for stronger soils.

5.4. IMPLICATIONS ON THE PIPELINE

5.4.1. General

As it was mentioned the gouging may cause severe implications on the pipelines rested at the seabed or buried. The current practice is that the pipelines are trenched in zones, where scouring is possible, however the attention paid to this challenge is insufficient and might result in undesirable consequences – for many Arctic pipeline projects the embedment depths are taken from the projects-analogues, while the proper study has to be carried out for each particular case.

Earlier works [13,19] pointed that the pipeline response is different at various burial depths. In this regard three zones can be distinguished (figure 5.5).

- Zone 1: where the soil is carried up in front of the ice into a frontal mound and afterwards sidewise into the berms;
- Zone 2: where soil is deformed plastically;
- Zone 3: the soil deformations are elastic, the stresses, transmitted from zone 2 should be accounted for.

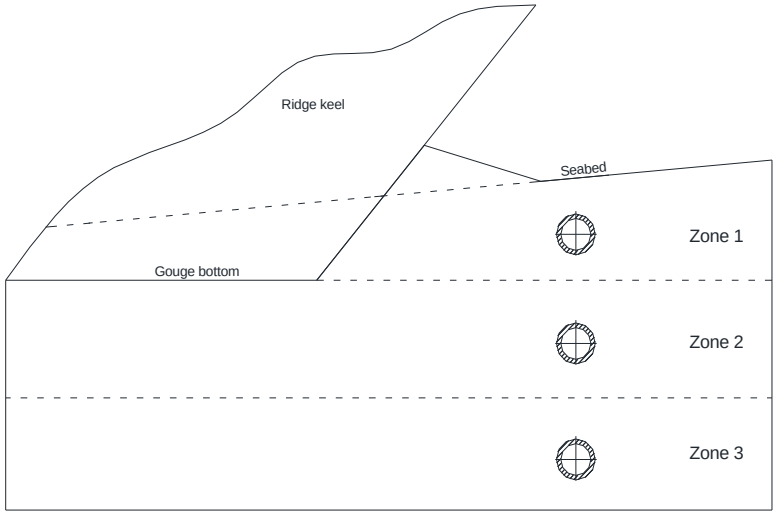

Figure 5.5.Ice-soil-pipeline interaction scenarios

In the upper layer (zone 1), subjected to scouring, the pipe exerts maximum loads directly applied by the ridge. Here the action is expected to be the most hazardous, since all the forces from wind, current, and drifting ice are concentrated on the pipe segment (under the assumption that the ice ridge is strong and rigid enough), without being damped by the soil.

The second zone involves the pipeline embedment below the possible gouge depth. Subgouge soil deformations transmit substantial loading to the buried pipeline, able to stress it beyond the allowable strength. The pipeline, having a significant stiffness, not necessarily moves with the soil (figure 5.6), which causes additional considerations for the soil properties and the pipeline material to be accounted in this work.

The third zone is characterized by relatively low deformation field, such that the safety of the pipeline against dragging, provided in zone 2, is satisfied as well.

Speaking about the pipeline protection in terms of trenching, the question - how deep the pipeline should be trenched – is still open to criticism. The pipeline safety burial level control is essential and appears to be one of the key challenges in present research. In this regard on the basis of mechanical and technical design considerations the attention below is given to the pipeline behavior in each zone in order to provide its safety level for given design conditions.

The sections below establish forces acting on the pipeline segment from the ridge through the soil. Multidirectional stresses appear in the pipeline wall, calling for allowable stressed deformed state analysis. From the other hand the pipeline, being a hollow structure, should be designed against the collapse, though this case is less hazardous.

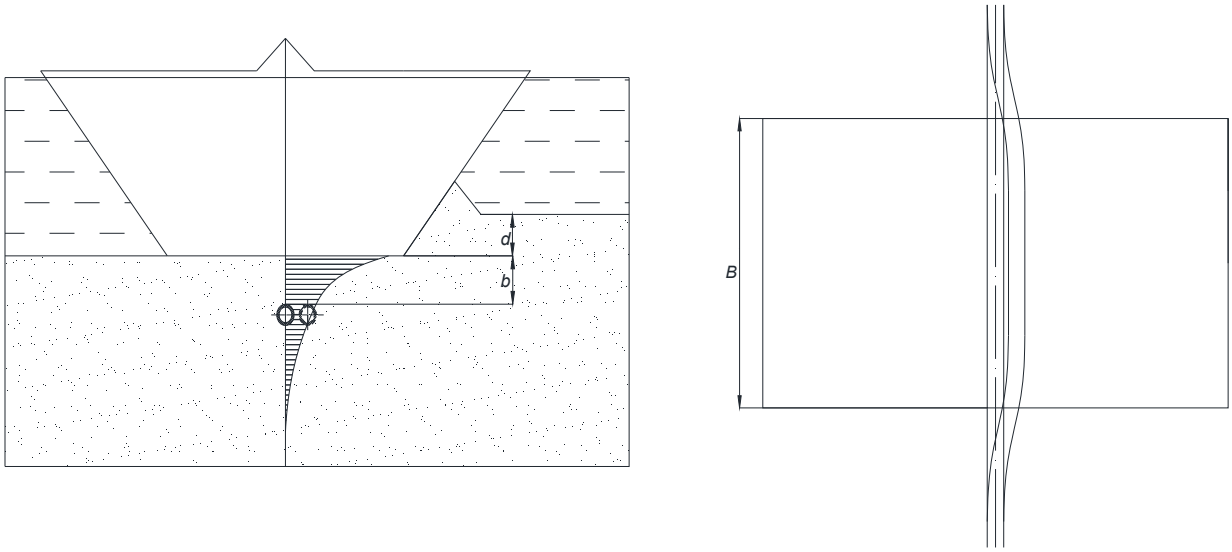

Figure 5.6. Sub gouge soil deformations and pipeline response representation

5.4.2. Ridge contact with the pipeline

Though many times it was said that the pipeline is not able to withstand loads from the anticipated ridge, and the direct contact with the pipeline is not the primary objective in the study, this scenario analysis would show the hazard for the pipeline in conditions, different from those analyzed in this study: interaction with smaller ridge, pipeline with enhanced wall thickness or protective coating, etc.

The improved force model, established in Chapter 4, is proposed in order to evaluate the force, which the pipeline exerts on the ridge (Figure 5.7).

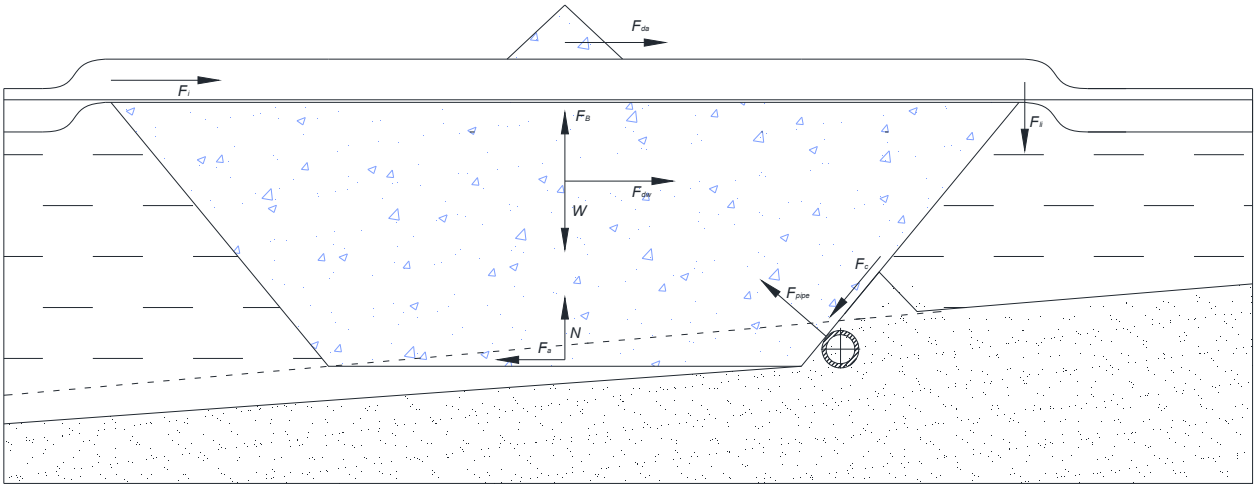

Figure 5.7. Direct contact with pipe model.

All resistant forces are scour depth depended, therefore the values of lateral force on the pipe should be estimated for the gouge depth range from *0 m* to *1,73 m* (corresponding to high keel cohesion).

The force on the pipeline segment is calculated from the following equations:

$$F_i + F_{dw} + F_{da} - F_a - F_c \cos\alpha_k - F_{pipe} \cos\alpha_k = 0 \tag{5.9}$$

$$N + F_{pipe} \sin\alpha_k - F_c \sin\alpha_k - F_{li} - \Delta W = 0 \tag{5.10}$$

$$F_{pipe} = \frac{F_i + F_{dw} + F_{da} - F_c \cos\alpha_k - \mu(F_c \sin\alpha_k + F_{li} + \Delta W)}{\cos\alpha_k - \mu \sin\alpha_k} \tag{5.11}$$

Table 5.1 shows forces on the pipe for different gouge depths: at the moment of initial contact between the ridge and the seabed (*d=0*); under the assumption that the keel strength is limited and the keel fractures before it ploughs maximum depth (*d=1,30*); in condition of substantial keel strength (*d=1,73*). The forces distribution with gouge depth is reflected in figure 5.8 below.

Table 5.1. Forces on the pipeline from the ice ridge for different scour depths

Parameter	***Unit***	***Value***		
Scour depth, *d*	m	0,00	1,30	1,73
Ice force, F_i	MN	16,23		
Wind drag, F_{da}		0,19		
Current drag, F_{dw}		1,32		
Horizontal passive friction, $F_c \cos\alpha_k$		0	4,58	8,74
Vertical passive friction, $F_c \sin\alpha_k$		0	2,01	3,56
Level ice reaction, F_{li}		0	1,26	2,23
Weight due to elevation, ΔW		0	1,25	2,21
Force on the pipe, F_{pipe}		*28,77*	*17,69*	*8,11*

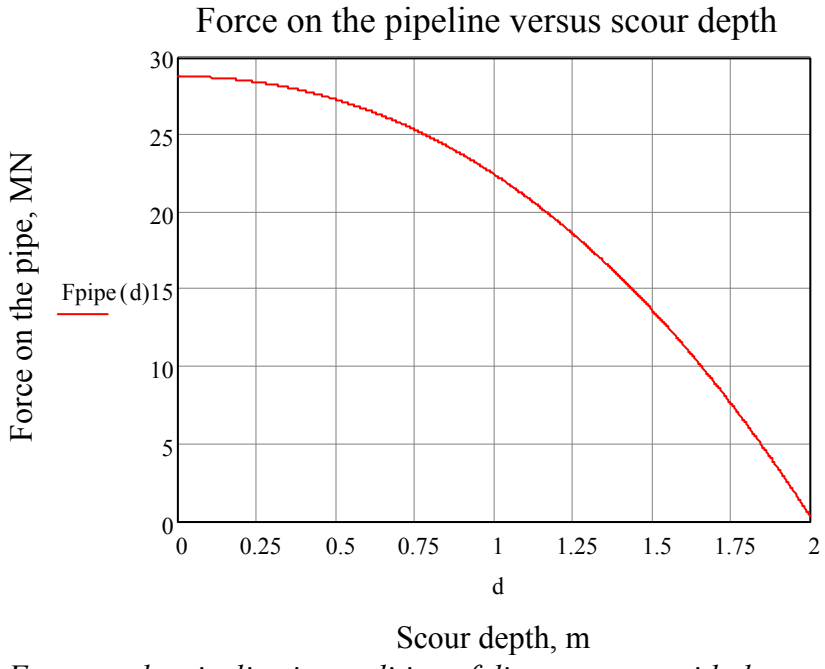

Figure 5.8. Force on the pipeline in condition of direct contact with the considered ridge

According to the energy model, the ice ridge stops at *d=1,73 m*, exerting no action on the pipeline, but since the force model is used for relevant analysis (which is reasonable in the certain conditions), load is significant at the maximum depth level. The forces are huge (1-2 orders of magnitude greater than the anchor forces which are known to cause damage [13]) and easily could rupture the pipeline when the ice ridge approaches. The precise assessment of such forces impact, accounting strength of the pipeline and soil conditions, is shown below in section 5.4.3., where the loaded beam model for pipeline is introduced.

5.4.3. Soil-pipe interaction model

The protection of the pipeline against substantial loads (section 5.4.2) could be achieved by the pipeline embedment into zone 2. This section should be paid with enhanced attention, introducing the safe burial level, which would ensure therefore the pipeline prevention from adverse stresses. The model anticipates the analysis methodology used to assess the pipeline response to Permanent Ground Deformation Hazards described by Vitali et al. [19].

The pipeline is modeled as a beam on a Winkler foundation [16], as shown in figure 5.9 (AutoCAD drawing). This approach is considered as fundamental in many recent researches [2,16,18], especially when accounting the plastic soil behavior when it flows around the pipe. The three series of springs represent the soil acting on the pipeline. The first set simulates axial forces, caused by both operational thermobaric conditions and displacement of the pipeline in the axial direction due to dragging laterally. The second and the third sets of springs provide transverse horizontal and transverse vertical forces on the pipeline in terms of lateral relative movements between the pipe and the soil.

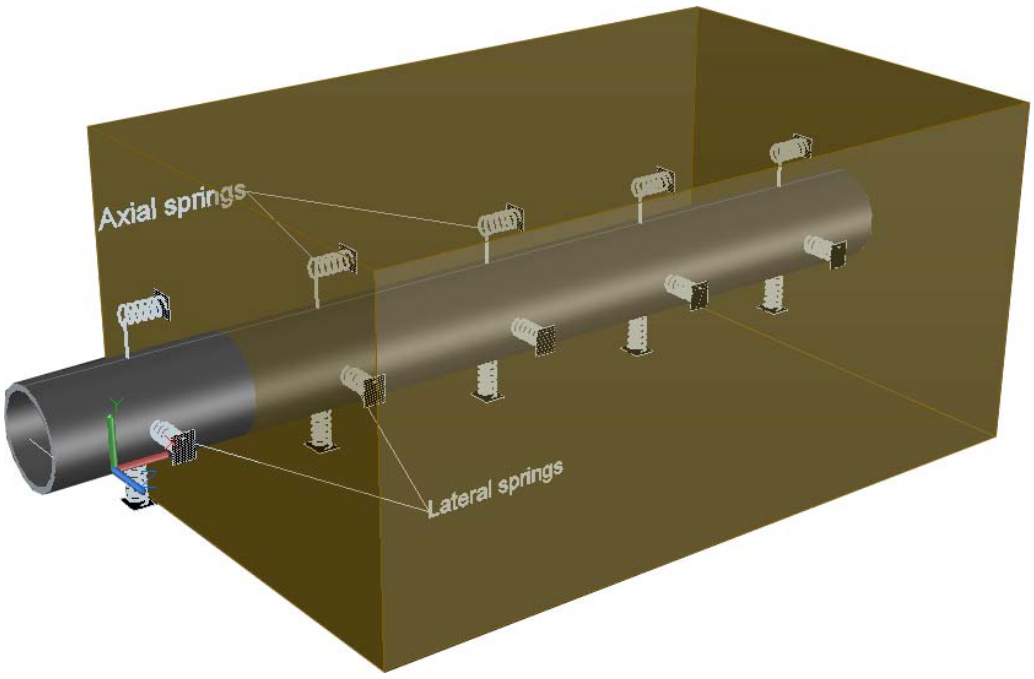

Figure 5.9. Beam on the Winkler foundation model for the pipeline response analysis.

In order to apply the actual forces action on the Winkler springs and develop the relation between them, the mechanical model of loaded beam (pipeline) is introduced in figure 5.10. The model involves an idealization of the subgouge deformations [18], presented above in figure 5.2: the soil moves within the gouge breadth *B,* applying the lateral load *f* on the pipe, and remains

stationary outside it, resisting the pipeline transverse motion. In both cases the soil deformations with respect to the pipeline are represented by the *plastic flow*.

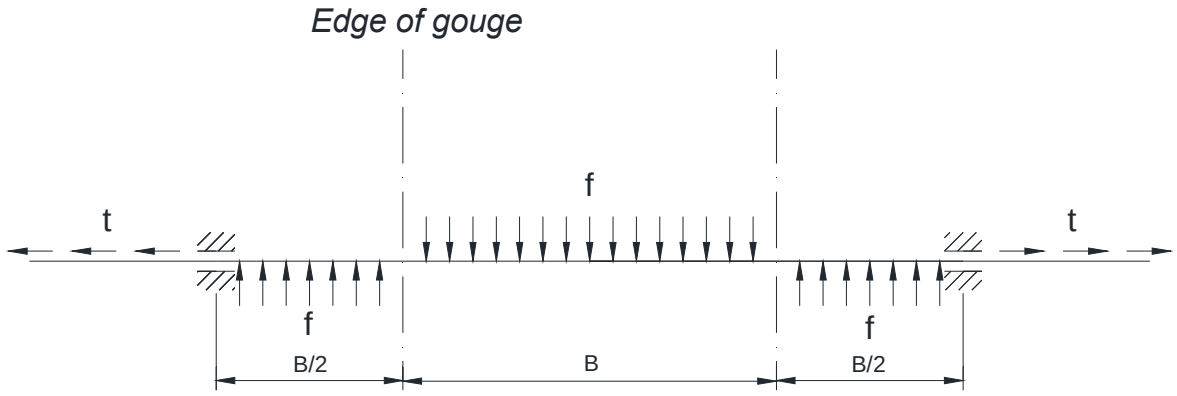

Figure 5.10. Proposed beam model of the soil-pipeline interaction.

In accordance with the model, the pipeline is laterally fixed at a distance of half a ridge breadth from the gouge edge, where neither the pipeline, nor the soil transverse deformations are observed. Both axial resistance of the soil at the pipeline restraints *t*, and residual tension should also be taken into account, while analyzing the structural beam.

Two force components could be distinguished [19]: the lateral force *f* (subdivided into horizontal and vertical forces *p* and *q*), and the axial force *t*. Each component is generally represented by a non-linear function of the relative soil-pipeline displacement as expressed in figure 5.11 [19].

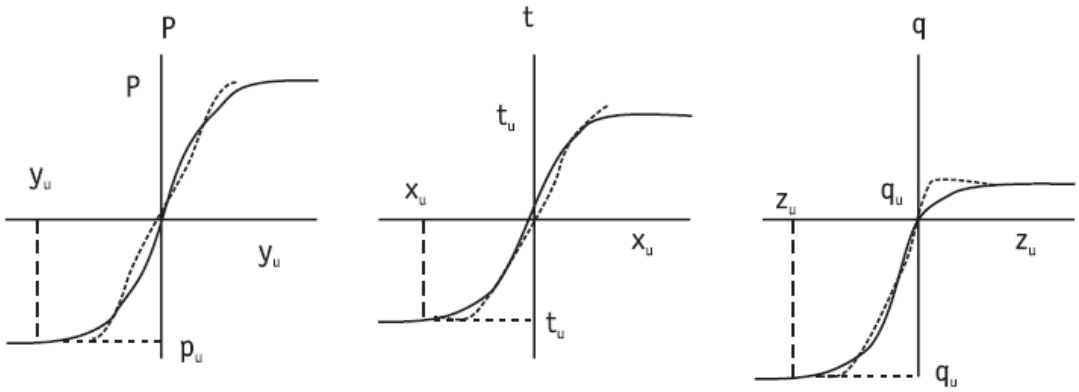

Figure 5.11. Non-linear behavior of the soil- pipeline interaction representation [19]

The deeper the pipeline is trenched, the less are the relative displacements, and the less action the pipeline sustains. If large relative displacements occur, the soil loads reach steady ultimate values p_u, q_u and t_u.

Assume zero cover from the top of the pipeline to the gouged seabed level as the most economically attractive case. Since the soil moves further than *4 m* and the pipeline is much stiffer to exert such motions [1], the relative deformations therefore are likely to exceed their critical values, such that the ultimate forces are used, though this is properly checked below in section 5.4.4. Involving the comparison of the pipeline behavior in the original sand, in stronger clay 1 and in softer clay 2 and accounting the outcome obtained in section 5.3, *the general ultimate axial soil resistance* is given by [19]:

$$t_u = \frac{\pi D}{2}\left(\rho_s H g + \frac{N}{B w_b}\right)(1 + K_0)\tan\varphi + \pi D \alpha c \qquad (5.12)$$

Where α - is the adhesion factor, depending on the undrained shear strength (figure 5.12), H – depth from the surface to the centerline of the pipe, and K_0 is the soil pressure coefficient at rest [20]:

$$K_0 = (1 - \sin\varphi)\frac{1 + 2/3\sin\varphi}{1 + \sin\varphi} \qquad (5.13)$$

Thus for granular cohesionless soils equation (5.12) goes into the first term, while for the cohessive soils with zero angle of internal friction only the second term is relevant.

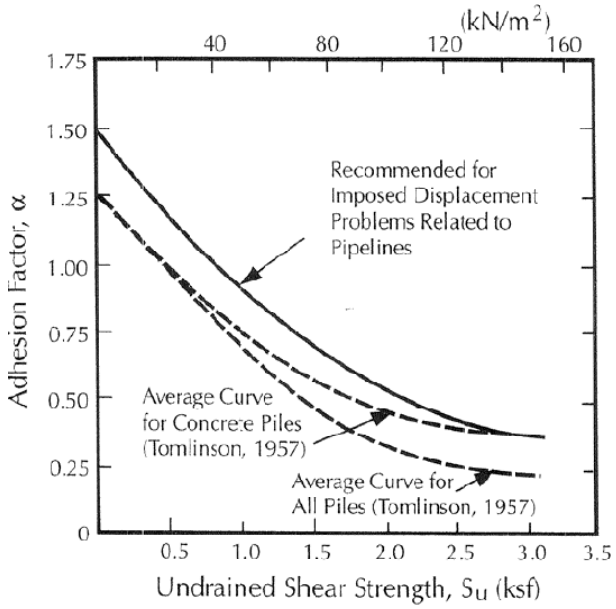

Figure 5.12. Adhesion factors plotted as a function of undrained shear strength [19]

The critical relative displacement between the pipeline and the soil is reported to be very low [19] – in the order of 5 – 10 mm, such that the ultimate resistance value might be used without significant error.

The horizontal transverse ultimate force on the pipeline is given by the pipeline-soil ultimate resistance [19]. Keeping in mind that the ridge presses the soil downwards, the ultimate force is:

$$p_u = s_u N D = \left(\rho_s H g + \frac{N}{B w_b}\right) N_{qh} D + c N_{ch} D \qquad if\ \varphi \neq 0 \qquad (5.14)$$

$$p_u = s_u N D = c N_{ch} D \qquad if\ \varphi = 0 \qquad (5.15)$$

The condition of critical relative deformations should be satisfied by the following equation:

$$y_u = 0{,}03 \cdot H \qquad (5.16)$$

The horizontal bearing capacity factors N_{qh} and N_{ch} are represented in figure 5.13 as a function of H/D, based on the model of Hansen [21]. Since the angle of internal friction is

relevant for original sand and strong clay 1 the bearing capacity factors for both soils are taken as being for *granular soil*. The softer clay 2 involves N_{ch} for analysis.

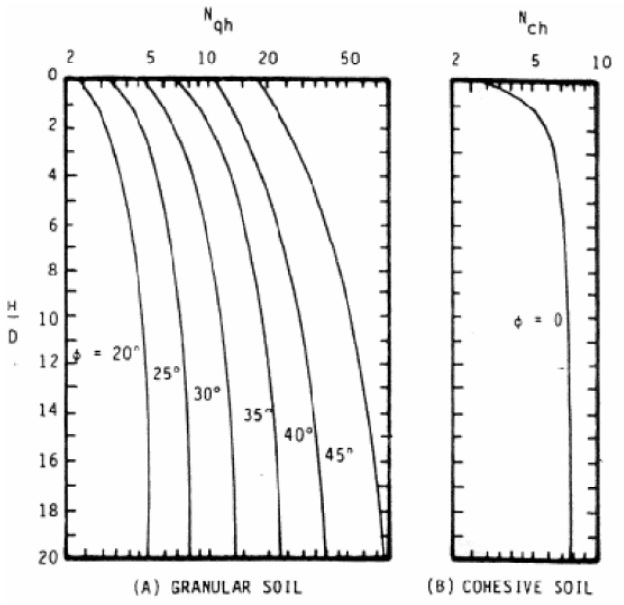

Figure 5.13. Horizontal bearing capacity factors for granular (a) and cohesive (b) soils [21]

The vertical transverse ultimate force has an unsymmetrical response to the direction of the soil motion (figure 5.11): defining deferent relations for upward and downward resistance. Evident that the downward soil drag is much greater than upward one and since the soil vertical displacements are oriented as shown in figure 5.3, thus the upward ultimate soil resistance is relevant in present analysis. Nearly the same relations are used in order to estimate the ultimate vertical soil forces for both sand and clay (equations (5.22, 5.23)). The vertical uplift factors N_{qv} and N_{cv} are shown in figure 5.14 [19].

$$q_u = s_u N D = \left(\rho_s H g + \frac{N}{B w_b}\right) N_{qv} D + c\, N_{cv} D \qquad if\ \varphi \neq 0 \qquad (5.17)$$

$$q_u = s_u N D = c N_{cv} D \qquad if\ \varphi = 0 \qquad (5.18)$$

The critical deformations in vertical direction are:

$$z_u = 0{,}1 \cdot H \qquad (5.19)$$

From the comparison of equations 5.12 and 5.17 one could see that the ultimate forces (both axial and transverse) definitely greater for deeper trenched pipeline. This is mainly associated with the soil failure envelope behavior in accordance with the Mohr-Coulomb theory. From the other hand, the deeper is the pipeline, the greater relative soil-pipeline displacements should take place for the ultimate drag equations applicability, while they consequently die off with depth as shown in figure 5.2, and the actual force per unit length as a sequence decreases.

It is also transparent that the pipe-soil relative displacements, required for steady state ultimate forces, are different for vertical and horizontal components. The simple analysis of equations (5.12) and (5.17) shows that y_u is order of magnitude smaller than z_u, which means that at the certain burial depth the effect of vertical drag could be neglected, while the horizontal one having a significant impact. This implies the change of pipeline moving direction with depth: the

closer to the seabed, the more significant the vertical movements are. Simultaneously, making a comparison of bearing capacity and uplift factors, the values of vertical forces themselves are one order less than horizontal ones.

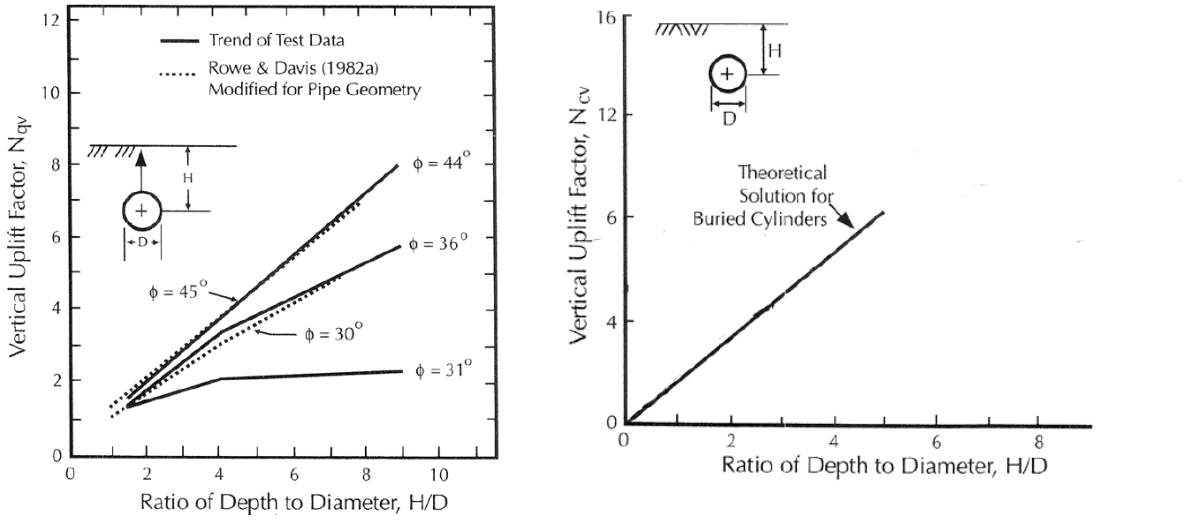

a) b)

Figure 5.14. Vertical uplift factors for sand (a) and clay (b)[19, 22, 23]

Either vertical or horizontal transverse force's components might be united into a single lateral force per unit length *f*, as established in figure 5.10. Its value could be outlined as a superposition of p_u and q_u:

$$f = \sqrt{p_u^2 + q_u^2} \tag{5.20}$$

The angle to the horizontal, determining the direction of the pipeline movement is also the desirable value and could be obtained from:

$$\tan \alpha_p = \frac{q_u}{p_u} \tag{5.21}$$

The values of parameters required for subsequent analysis are shown in table 5.2.

Table 5.2. Parameters of soil impact on the pipeline at the gouge base.

Parameter	***Unit***	***Value***		
		Sand	***Stiff clay ($\varphi \neq 0$)***	***Soft clay ($\varphi = 0$)***
Axial ultimate resistance, t_u	kN/m	14,46	28,11	6,26
Horizontal ultimate drag, p_u		60,77	60,78	5,69
Vertical ultimate drag, q_u		5,52	9,63	1,42
Total lateral force, *f*		61,02	61,53	5,86
Angle of pipeline motion, α_p	deg.	5	9	14

The soil transmits significant forces on the pipeline unless the angle of internal friction becomes zero. In that case the effect of normal stress either from the ridge elevation or from the soil itself is not relevant and the force becomes nearly order of magnitude less (table 5.2). However, in any soil conditions the action on the pipeline is substantially less (100-150 times) than one obtained when the direct contact occurs.

The critical values of the pipeline-soil relative movements in either direction are shown in figure 5.15 below as functions of the pipeline burial depth, while the pipeline deformations to be compared with, are established in section 5.4.5 below.

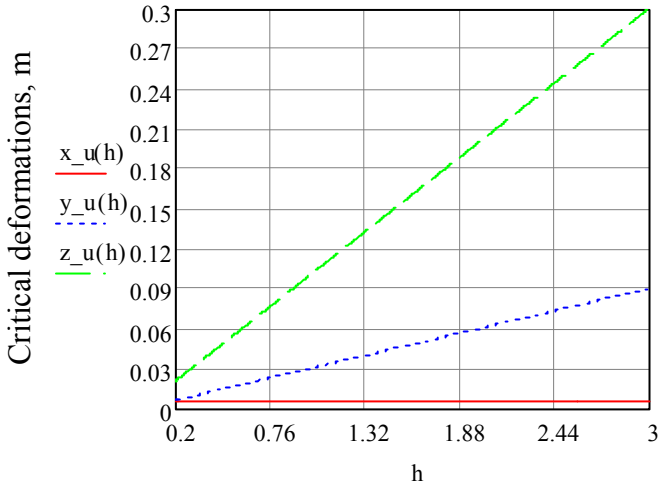

Figure 5.15. Critical pipe-soil relative deformations vs. depth below the gouge.

The model is introduced and ready for analysis; however the embedment level of the pipeline, which minimizes the acceptance criteria for the design of the pipeline being subjected to subgouge soil deformations in the zone 2, should involve the probability of the pipeline damage assessment. Bearing in mind that the pipeline is designed for 30 years and following the practice of limit state design [5] the reliability criterions established below should met:

- *(1) LRFD SLS*: The annual probability of Von Mises stresses occurrence exceeding 90% of yield strength should be equal or less than 10^{-1} [2, 24];
- *(2) LRFD ULS*: The annual probability of excessive compressive/tensile strains should not exceed 10^{-2} [2; 25];
- *(3) LRFD ULS*: Plastic collapse annual probability should not be greater than 10^{-2}.
- *(4) Contact condition*: The annual probability [24] for direct ridge keel accidental contact with the pipe should not exceed 10^{-4}.

Since the pipeline is designed against the combination of multidirectional lateral, axial and circumferential loads (figure 5.10), the attention below is mainly given to the Von Mises equivalent stress estimation and its influence on criteria set above.

The SLS stress criterion (1) is fulfilled on the basis of equivalent stress comparison with the specified minimum yield strength of the steel and by the load controlled condition (section 3.6.3).

The ULS strain criterion (2) is provided by the maximum strain, caused by the equivalent stress in the pipeline, and necessary to be compared with the limiting values of tensile/compressive strains.

The collapse criterion (3) is also accounted as described in below, while the contact probability (4) is governed by the probability of ridge intersecting the pipeline, embedded below the estimated gouge, which is specified in Chapter 4.

5.4.3.1. SLS stress

The DNV [8] governs the following expression for the equivalent stress calculus:

$$\sigma_{eq} = \sqrt{{\sigma_h}^2 + {\sigma_l}^2 - \sigma_h \sigma_l} \tag{5.22}$$

Where the hoop stress is given as a function of internal operating pressure p_i, obtained in Chapter 3 (figure 3.5):

$$\sigma_h = \frac{p_i(D-t)}{2t} \tag{5.23}$$

The longitudinal stress is influenced by the axial force and the moment due to the pipeline bending:

$$\sigma_l = \frac{T'}{A} \pm \frac{M}{W_s} \tag{5.24}$$

Here *T'* is an axial force, *A* – cross-sectional area of the pipe; *M* – bending moment, W_s – sectional modulus. The sign "±" is explained by the compression and tension in upper and lower sections of the pipe.

For pipeline with thin wall:

$$A = \pi d t \tag{5.25}$$

$$W_s = \frac{I}{y} = \frac{\pi(D^4 - d^4)\cdot 2}{64 \cdot D} = \frac{\pi(D^4 - d^4)}{32D} \tag{5.26}$$

The determination of the bending moment and the axial force demands more detailed analysis

Bending moment:

Longitudinal stress proportionally depends on the bending moment which appears to be various along the considered section of the pipe. Since the pipeline has fixed restrains, the system established in figure 5.10 is statically undetermined, as the end restrained moments are unknown.

Let the pipeline section having a length *L*, equal to the double gouge breadth *B*. Assume an infinitely small part *dx* distance *x* apart from the left end of the pipe being under a concentrated load *fdx* [26]. The fixed right and left end moments could be calculated from the integral below.

For the right end:

$$M_R = \int_0^{L/4} \frac{-x^2(L-x)f\cdot dx}{L^2} + \int_{L/4}^{3L/4} \frac{x^2(L-x)f\cdot dx}{L^2} + \int_{3L/4}^{L} \frac{-x^2(L-x)f\cdot dx}{L^2} = \frac{fL^2}{32} \tag{5.27}$$

For the left end the moment is:

$$M_L = -\int_0^{L/4} \frac{-x^2(L-x)f\cdot dx}{L^2} - \int_{L/4}^{3L/4} \frac{x^2(L-x)f\cdot dx}{L^2} - \int_{3L/4}^{L} \frac{-x^2(L-x)f\cdot dx}{L^2} = -\frac{fL^2}{32} \tag{5.28}$$

Thus, the undetermined restrains on the pipeline section ends are replaced by the moments, such that the plot of the bending force and moment areas reflected in resultant diagram below (figure 5.16) are obtained. The three points could be identified where the maximum bending

moments occur: both restraints and the middle of the loaded section. The moments in either point are similar and proportional to the transverse force *f* and squared scour width *B*.

This implies the significant importance of the representative keel breadth, taken for calculations, since its influence is visible on both gouge depth itself and the stresses as a consequence of subgouge deformations.

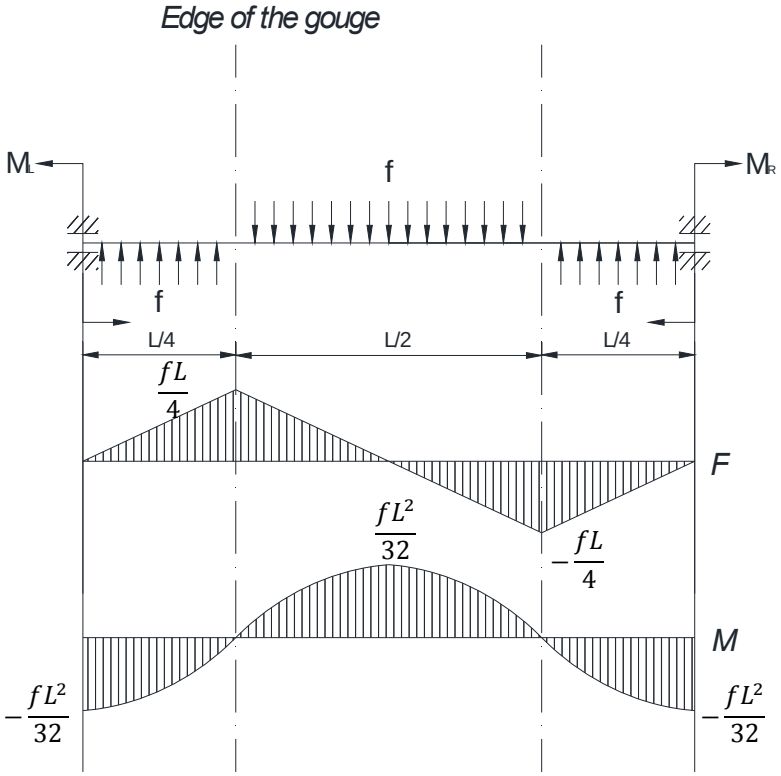

Figure 5.16. Pipeline bending force and moment areas

Axial force.

The axial force, acting on the pipeline is proposed to be represented by the function of several components. The pipeline is put into operation and goes to the stressed state due to increased temperature and pressure:

$$T = -\frac{\pi d^2}{4} p_i (1 - 2\vartheta) - \pi dt E \alpha (T_i - T_e) \tag{5.29}$$

The first term is pipeline expansion due to pressure increase, which is explained by the end cap and Poisson's effects. Here ϑ - Poisson's ratio. The second term is an expansion due to the temperature. Here t – characteristic wall thickness of the pipe, E – the elasticity modulus; α - thermal expansion coefficient and $(T_i - T_e)$ - temperature difference between the surrounding water and the pipeline. In steel pipelines the temperature term dominates, therefore the force is always compressive and negative.

However, after gouging the pipeline is dragged and the axial force becomes tensile *T'* [18]. The changing of the tension induces the additional axial strain. Under the assumption that the pipeline displacements are small compared to scour width *B*, and the behavior of the pipeline is dominated by the interaction between the effective axial force and the lateral force, Palmer proposed the following equation [18], which easily could be solved for *T'*:

$$\frac{f^2B^3}{24(T')^2} = \frac{(T'-T)B}{S} + \frac{(T'-T)^2}{2t_uS} \quad (5.30)$$

Where S is the elastic axial rigidity, which is given by:

$$S = \pi dtE \quad (5.31)$$

Substituting axial force and bending moment in equation (5.24) the longitudinal stress and then the Von Mises equivalent stress could be found. Consider the pipeline section allocated in 22 m water depth area, corresponding to the maximum water depth, where the most hazardous gouging occurs. The obtained maximum stresses for different soil conditions are shown in table 5.3. The stresses occur in case of direct contact with the ice ridge (section 5.4.2) are reflected in the right column.

Table 5.3. Stresses in the pipeline in terms of scouring

Parameter		***Unit***	***Value***			
			Sand	***Clay***	***Soft clay***	***Direct contact***
Pipeline SMYS		MPa	448,0			
Hoop stress			133,7			
Longitudinal stress	Tensile		3471,9	3539,7	340,2	11631,6
	Compressive		-3145,6	-3144,3	-299,5	-10928,8
Maximum Von Mises equivalent stress			3407,0	3474,8	384,3	11565,3

Table results discussion

Although the pipeline embedment below the maximum scour depth reduces the ridge action, stronger soils apply the forces able to cause stresses far beyond the steel yield strength (table 2.5), unless the soil is very weak indeed. Granular soils independently on their cohesion values transmit huge loadings, since their shear strength could be huge in terms of normal stress from the ridge. Cohesive soils (clays) with zero internal friction flow around the pipeline without significant impact.

Thus *the soft clay* with low cohesion is proposed as a best backfilling material for the trench part, where gouging is not relevant. Elsewhere in subsequent criterion analysis only the *soft clay condition* is used. From the top of the pipeline to the seabed level – the original sand should be used in order to minimize the ridge penetration into the soil. Such a "sandwich" trenching scheme was used in many experiments [15, 25] and showed promising results yielding that the pipeline bending strain and, consequently, stresses are substantially less. The effect is even better if the layer of plastic sheeting (geotextile) covers the top of the pipeline, such that the soil is displaced less, transmitting fewer forces.

Hence, if the soil force on the pipeline has a limit, determined by the soil strength, than the magnitude of the subgouge displacements is no longer a key factor in the determination of a safe burial depth for the pipeline.

However several parameters' influence on the pipeline response should be investigated in terms of stresses arising in the pipeline. In this regard the major interest is appealed by the soil shear strength and the scour width B, established in relation with the equivalent Von Mises stress in the pipeline in figure 5.17. In order to fulfill the serviceability limit state requirement the equivalent stress intersection with the 90% of X65 steel yield strength is shown. This sets the upper limit for the backfilling clay shear strength (cohesion) value of ≈3,8 kPa for the given

scour width (30 m), corresponding to very soft clay. Less scour width implies the possibility of backfilling with stronger soils; however the pipeline damage probability then apparently increases.

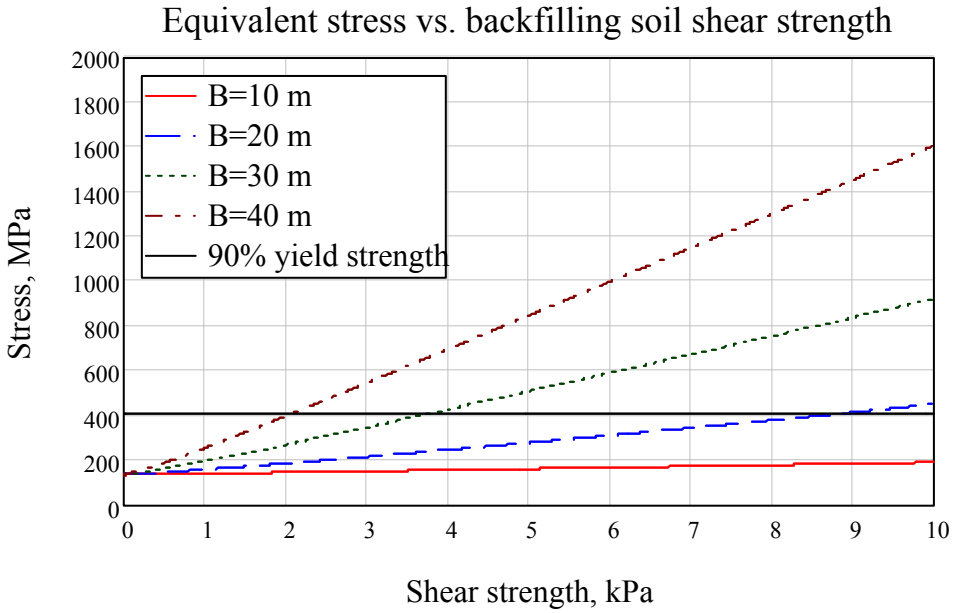

Figure 5.17. Pipeline equivalent stress versus soil shear strength and scour width.

5.4.3.2. ULS strain

Stresses in the pipeline segment subjected to subgouge soil action induce longitudinal compressive and tensile strains. DNV [8] requires the satisfaction of the following limiting compressive strain value:

$$\varepsilon_{lc} = \frac{\varepsilon_c}{\gamma_e \gamma_F} \tag{5.32}$$

Where γ_e, γ_F- design factors, indicated in table 2.7

$$\varepsilon_c = 0{,}78\left(\frac{t}{D} - 0{,}01\right)\left(1 + 5\frac{\sigma_h}{f_y}\right)\alpha_h^{-1{,}5}\alpha_{gw} \tag{5.33}$$

$\alpha_{gw} = 1{,}0$ from Sec. 13 E1000 of DNV [8];

$\alpha_h = 0{,}93$ from table 7-5 [8];

f_y is given by equation (3.23) in Chapter 3

The constant tensile strain limit of 2,5% is used as a limiting value of longitudinal steel deformations.

The actual strain in the pipeline is obtained from the Ramberg-Osgood relation [27], accounting yielding at the certain point:

$$\varepsilon_p = \frac{\sigma_l}{E}\left[1 + A\left(\frac{\sigma_l}{\sigma_y}\right)^{n-1}\right] \tag{5.34}$$

Where

$$A = 0{,}005\left(\frac{E}{\sigma_y}\right) - 1$$

$$n = \frac{\log\left[\frac{\left(\varepsilon_t - \frac{\sigma_t}{E}\right)}{\left(0{,}005 - \frac{\sigma_y}{E}\right)}\right]}{\log\left(\frac{\sigma_t}{\sigma_y}\right)}$$

Here σ_l - stress in the pipeline (longitudinal), σ_y - SMYS; σ_t – SMTS (table 2.6); ε_t – ultimate tensile strain, corresponding to SMTS (table 2.6).

Since the strains in the pipeline apparently depended on the longitudinal stress and they are following the stress-strain curve, established in figure 2.3, they might be expressed as functions of backfilling soil shear strength for different scour widths in analogue with the previous section. Figures 5.18 and 5.19 plot compressive and tensile strains compared to their limiting values.

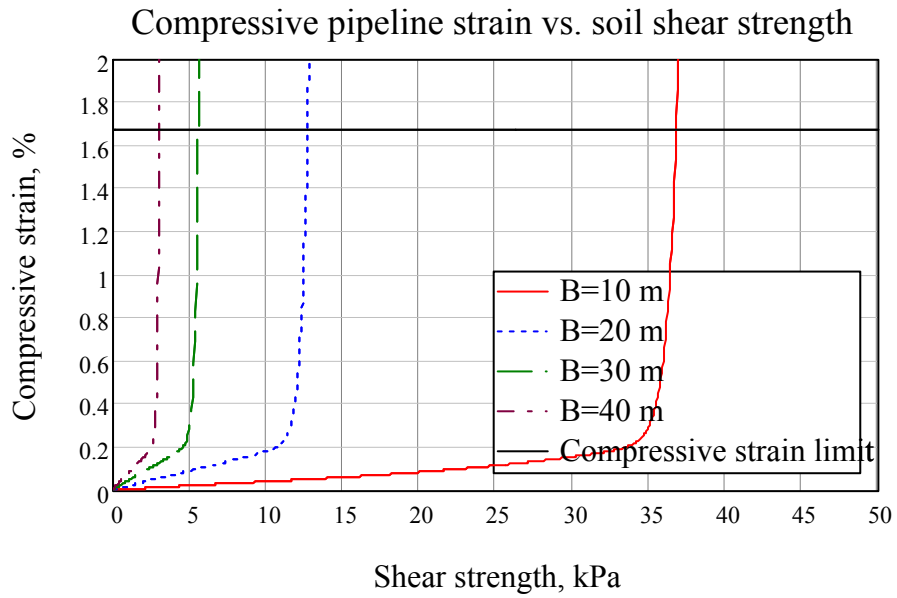

Figure 5.18. Pipeline compressive strain curves for different scour width.

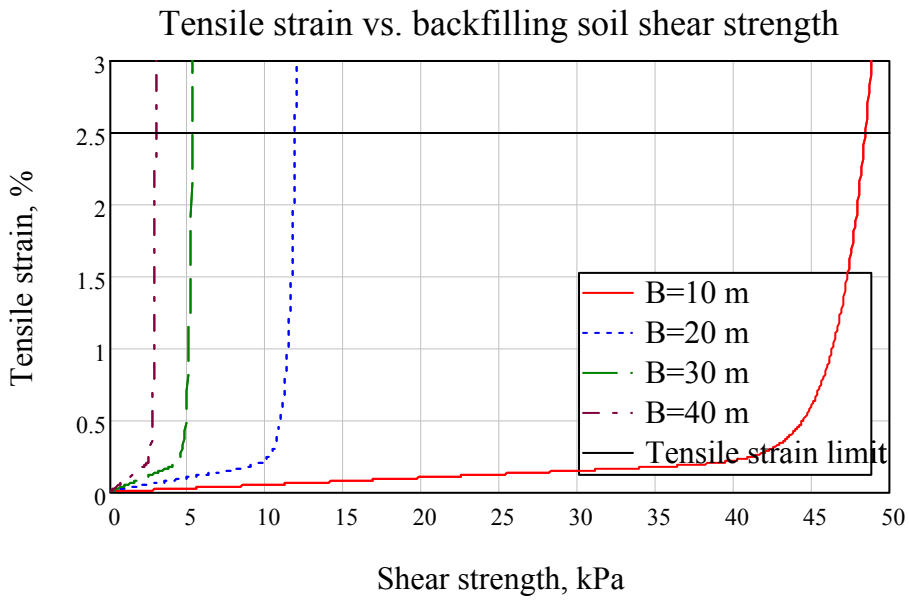

Figure 5.19. Pipeline tensile strain curves for different scour width.

Curves obtained provide nearly identical results and for given gouge breadth of *30 m*, the soil shear strength is recommended to be less than *5,5 kPa*, which is met by the stress controlled requirement (5.4.3.1) for soil shear strength though.

5.4.3.3. ULS collapse

Once the pipeline is embedded into the soil, the collapse criterion might be checked for the external overpressure, caused by vertical and horizontal soil action. It is proposed to refer to DNV code [8] in order to check whether the soil pressure is small enough for the pipeline to withstand the buckling. The stability against collapse is met if the following condition is satisfied:

$$p_s - p_i \leq \frac{p_c}{\gamma_{sc}\gamma_m} \tag{5.35}$$

Where the safety class factor γ_{sc} is set as "high" with value of *1,308* (table 2.7). The collapse pressure p_c could be outlined as a root of the following equation:

$$(p_c - p_{el}) \cdot (p_c^2 - p_p^2) = p_c \cdot p_{el} \cdot p_p \cdot f_0 \frac{D}{t} \tag{5.36}$$

Where p_{el} and p_p are elastic and plastic collapse pressures respectively, f_0 – constructional ovalisation (table 2.3).

$$p_{el} = \frac{2E\left(\frac{t}{D}\right)^3}{1-\vartheta^2}$$

$$p_p = f_y \alpha_{fab} \frac{2t}{D}$$

The calculations shown in Appendix E provided the extreme value of soil pressure $p_s = 42{,}3\ MPa$, which is possible to occur only in the case of direct contact with the ice ridge. The collapse, therefore, is unlikely to occur if the pipeline somewhat buried into the soil.

5.4.4. Pipeline displacement

The investigation of the pipeline lateral deflections is critical in terms of assessment of the relative pipe-soil displacements. This analysis shows the application boundaries of the ultimate soil forces on the pipeline and governs an embedment depth, where the stronger soil might be used.

Since the pipeline apparently is much stiffer than the soil, it is expected that its lateral displacement falls far below the critical soil deformation values below the gouge. The pipeline deflection in any point could be defined by Mohr integral:

$$u_p = \int_0^L \frac{M \cdot \bar{M}}{EI} dx \tag{5.37}$$

Here M - bending moment area as expressed in figure 5.16. The unit moment area $\bar{M}$ is defined from the unit load, applied in the point of desirable deflection to be determined. The calculation of the integral (5.37) with respect to the certain point of pipeline deflection *i* might be carried out using Simpson's relation [28]:

$$u_p = \int_0^L \frac{M \cdot \bar{M}}{EI} dx = \frac{L}{6EI}(M_L \cdot \bar{M}_L + 4M_i \cdot \bar{M}_i + M_R \cdot \bar{M}_R) \tag{5.38}$$

In order to construct the pipeline bending curve, define five points *(A, B, C, D, E)* within the considered section. Two of them *(A, E)* are represented by laterally fixed ends, while the remaining three *(B, C, D)* correspond to the gouge edges and its axis. This implies the construction of moment areas for points *B* and *C* as shown in figure 5.20 (point D is symmetrical to B). The expressions for moments in either point are established in table 5.3.

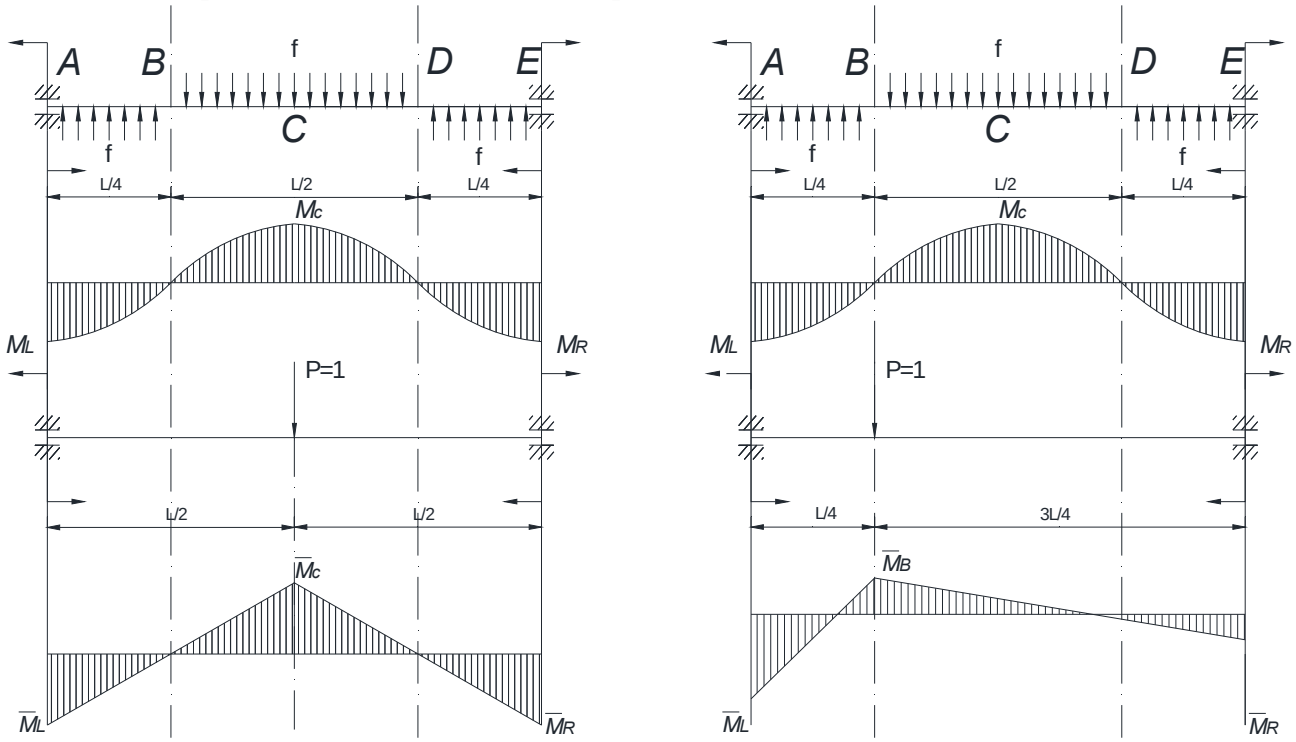

a) *b)*

Figure 5.20. Pipeline bending and unit moment areas in points C (a) and B (b)

Table 5.4.Pipeline bending and unit moments' expressions

Parameter	***Deflection point***	***Point i***				
		A	***B***	***C***	***D***	***E***
Bending moment, M_i	any	$-\frac{fL^2}{32}$	0	$\frac{fL^2}{32}$	0	$-\frac{fL^2}{32}$
Unit moment, $\overline{M_i}$	B	$-\frac{9L}{64}$	$\frac{9L}{128}$	-	-	$-\frac{3L}{64}$
	C	$-\frac{L}{8}$	-	$\frac{L}{8}$	-	$-\frac{L}{8}$
	D	$-\frac{3L}{64}$	-	-	$\frac{9L}{128}$	$-\frac{9L}{64}$

Substituting expressions from table 5.3 into equation 5.37 the displacements are:

$$u_p(B) = \frac{fL^4}{1024 \cdot EI} = \frac{fB^4}{64 \cdot EI}$$
$$u_p(C) = \frac{fL^4}{256 \cdot EI} = \frac{fB^4}{16 \cdot EI} \quad (5.39)$$
$$u_p(D) = \frac{fL^4}{1024 \cdot EI} = \frac{fB^4}{64 \cdot EI}$$

Comparing equations 5.39 and 5.1 one can see that the pipeline displacement depends on B^4, whereas soil deformations are represented by the function of $\sqrt{B}$. This means that for certain value of gouge width B the pipeline deformations might exceed the soil's ones, which of course physically impossible. However, approaching to zero, relative displacements induce less lateral load f, reducing pipe's bending deflections. The figure 5.21 below establishes the sketch of the modeled above scouring process implications on the pipeline, being bent from its original position.

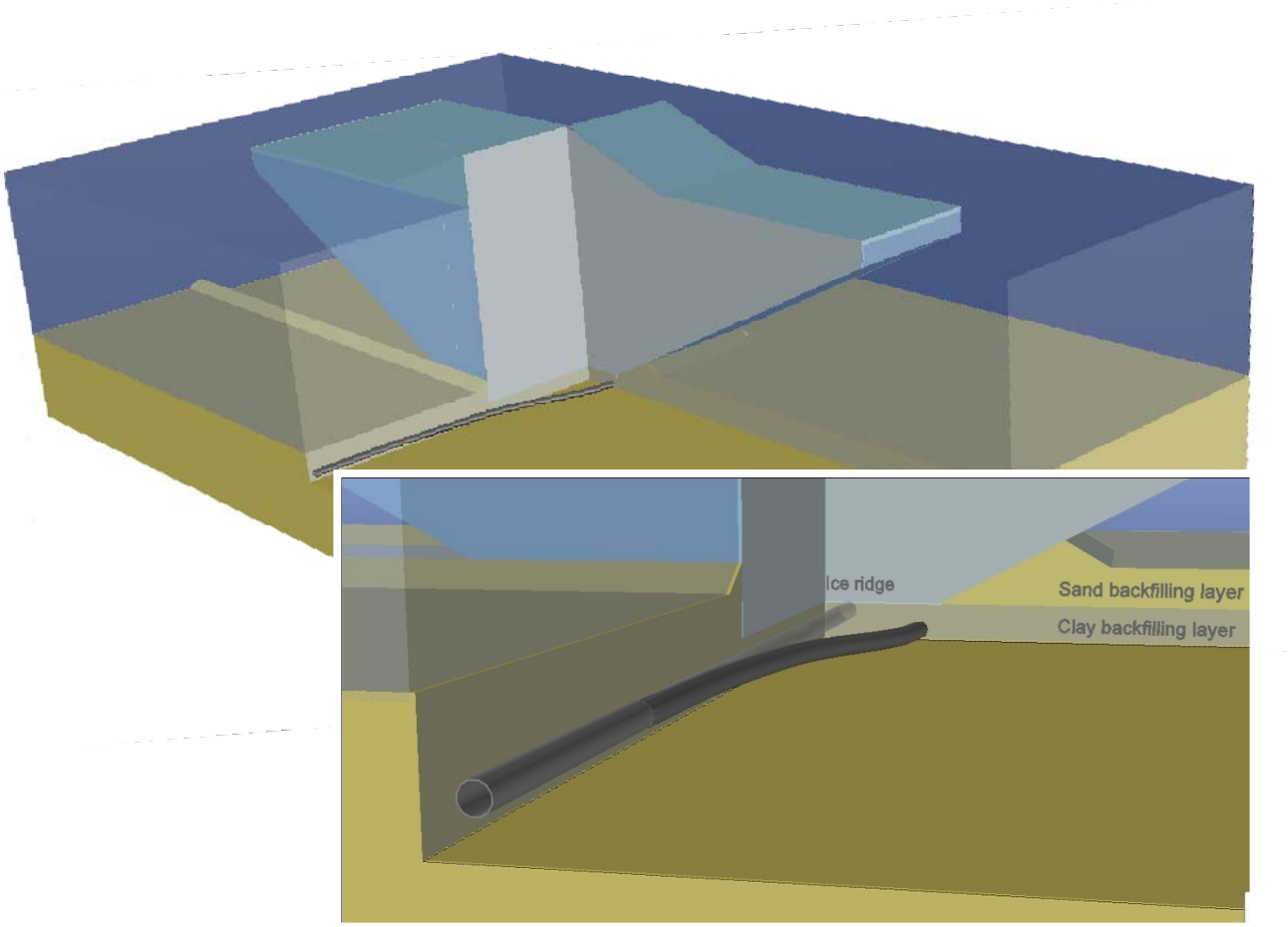

Figure 5.21. 3D sketch of the results from proposed theoretical approach to the modeling of ice ridge scouring and its effect on the embedded pipeline (AutoCAD)

It is visible that the pipeline lateral movement is not purely horizontal: vertical component appears due to the vertical force q, which is substantially less than horizontal one. Consequently, if the soil conditions allow the horizontal displacements decline intensively with depth (very soft soils), the eventual lateral force might be less than the designed one. The calculations (Appendix E) provide the pipeline centerline displacement of *3,4 m* from its initial position, which falls within the capacity of the relative displacements range in order to ultimate forces' values be applicable in this study.

5.4.5. Pipeline trenching

Since the trenching costs are believed to be enormous, the pipeline trench and its parameters are critical from the practical considerations, namely providing what kind of trenching equipment should be used and how the trench should be developed.

The pipeline trenching is possible to carry out using different modes: pre-trenching, simultaneous trenching and post-trenching, defining the time when the trench should be excavated with respect to the pipe lay [25]. From the point of this study the attention is not given to the specific technique, though the advantages of either the simultaneous or the post-trenching are evident in terms of maintaining the accuracy of the introduced trench parameters, which are as follows:

- The trench depth is the sum of the pipeline external diameter (including the anti-corrosion coating) and the design gouge depth;
- The trench is backfilled with the recommended soft clay to the top of the pipeline, then – with the in-situ sand to the original seabed level;
- The trench width should be taken as double value of the designed soil-pipeline relative displacements; otherwise the surrounding sand might exert unacceptable loads, when all clay is flown out of the pipeline position. The relative deformations are relevant for the sand deformations, since beyond the trench bounds the clay is not able to move further than the sand;
- As a sequence the trench walls should be slant.

Accounting for all these positions the trench cross-sectional profile is established in figure (5.22).

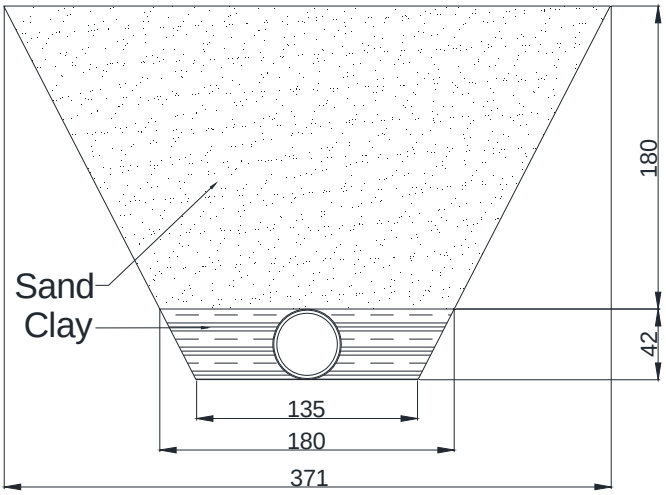

Figure 5.22 Trench parameters for the backfilling with clay layer (in cm)

This gives the technical solutions with respect to the trench, listed below:

- The slope for such a trench amounts to *1:1,88* which is acceptable from the practice of pipeline trench construction for granular soils [29];
- The volume of required clay outbound for considered seabed slope is approximated as *1320* m^3;
- The soil backfill density allows the pipeline stability on the trench bottom, such that it doesn't float up (*1800* kg/m^3 vs. *1300* kg/m^3).

There also proposed an alternative of the backfilling by the original sand, which is required to provide the pipeline integrity in case of soil subscour deformations do not exceed those critical for the pipeline. As arbitrary assessment of sand subgouge displacements showed (section 5.3) the sand is able to shift *3,4 m* laterally (corresponding to the pipeline axis critical bending deformations for given steel and gouge width) on the depth *0,62 m* below the gouge base: the

trench therefore should be *2,6 m* deep (figure 5.23) in order to ensure the pipeline limit states requirements.

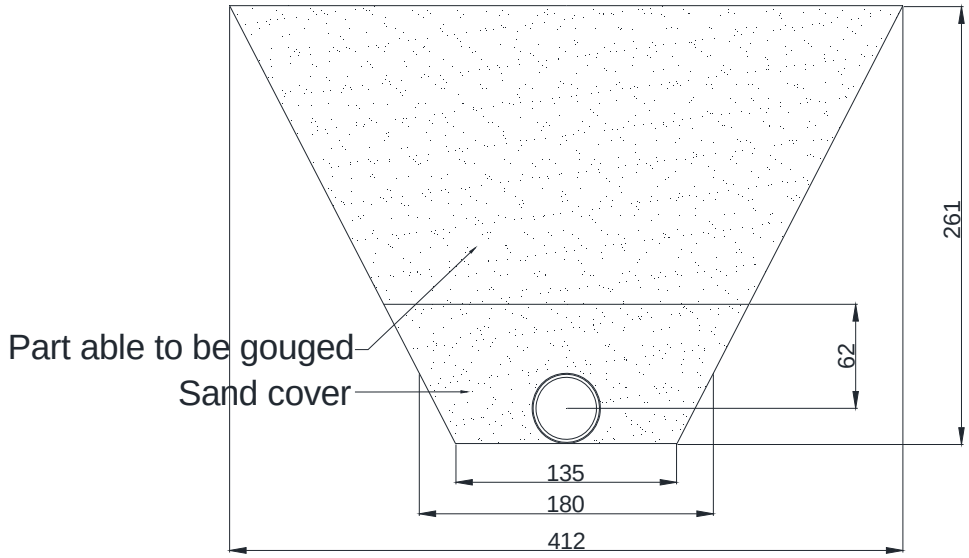

Figure 5.23 Trench parameters for backfilling with sand (in cm)

5.4.6. Discussion

As concluded the gouging process exerts a significant influence on the overall pipeline design logic. The pipe should be properly protected against the direct contact with the ridge: tens MNs of forces easily able to rupture the pipeline. Even being buried the pipeline is susceptible to substantial forces, able to load the pipeline beyond its critical state, unless the certain conditions are met.

Following the limit state criterion with the probability of collapse 10^{-4} it is proposed to bury the pipeline in the trench with the depth of *2,2 m* (*1,8 m* to the top) with the sandwich backfilling: soft clay to the top of the pipeline (with cohesion of *3,8 kPa* and zero internal friction angle), and then – with the in-situ sand – to the original position of the seabed. This arrangement provides prudent results in the following:

- The gouge depth is sufficiently reduced compared to the ridge penetration in softer soil;
- The weak clay backfill flows around the pipe, exerting less forces on it then the sand;
- Being the most severe, the trenching costs are reduced, though additional expenditures are required when backfilling with the outbound clay.

As an alternative the pipeline might be trenched deeper with the original sand on its entire trenching depth, however it demands the proper analysis of the sand deformations below the gouge and their subsequent comparison with the pipeline critical bending displacements, obtained in previous section. Hence in the certain depth the sand displacements might coincide the pipeline's ones, delineating the critical safe embedment for the pipeline. Present research doesn't use the deformations, obtained by the empirical correlations in section 5.3.1 [1] in terms of their inaccuracy and significant deviations from real conditions [2]; hence, it is required to carry out either laboratory experiments or the numerical modeling (or both), following the simulation of in-situ physical properties of the seabed.

The designed trench depth should be maintained on the entire length of the pipeline from the shoreline to the water depth of *22 m* (associated with the design keel draft), while the end point of the pipeline embedment (where the trench depth is equal to zero) corresponds to *27 m* water depth (associated with 10^{-4} probability of the ridge keel occurrence, established in figure 4.12). However the real project should account for many additional factors, influencing the fluctuations of the pipeline burial level [2]. Among them one can distinguish the seabed erosion, the pipeline direction orientation, the seabed topography and the distribution of the ridge densities with the water depth. All this demands comprehensive in-situ research for each specific project.

5.5. SUMMARY

The chapter gives a comprehensive analysis of the ridge implications on the pipeline, trenched in the nearshore area, and its influence on the integral pipeline design concept. Two fateful cases have been analyzed in this thesis part: the direct pipeline-ridge contact and the ridge action on the pipeline through the thickness of soil. The first one is classified as accidental case – the loads' values, which ridge exerts on the pipeline, lays far beyond the pipeline resistance capacities, such that it easily could be ruptured. For this end it was proposed to avoid the contact, reducing its probability below the acceptable likelihood of collapse, which requires the trenching on the design gouge depth (*1,73 m* from Chapter 4).

To protect the pipeline against the adverse subguge soil deformations an analysis of the "ridge-soil-pipeline" interaction scheme has been carried out. Due to theoretical difficulties of undetermined 3-parametric system it was proposed to split it into 2 sub-systems.

The introduced "Ridge-soil" theoretical approach focuses on the soil mechanics subscour. It accounts the determination of the soil shear strength, considered as the main link, connecting the "ridge-soil" and "soil-pipeline" sub-systems. The shear strength, being the function of the soil cohesion, internal friction angle and normal stress applied, has been obtained for sand, stiff and soft clays in terms of depth below the gouge, which allowed to calculate the ultimate loads on the pipeline in different soil conditions.

The "Soil-pipeline" sub-system analysis was based on the introduced model of loaded pipeline, susceptible to multidirectional loadings in terms of both: operational and seabed scouring considerations. When the ridge scours the seabed above the pipeline, it bends horizontally towards the ridge movement direction and vertically downwards. Following the limit state criterions (ULS, SLS, ALS) the conclusion was obtained that the pipeline is safe right below the estimated gouge if the certain mechanical properties of backfilling soil are met, which, of course attractive from the economical reasons. This delineated an effective proposed protection measure for the pipeline against considered phenomenon – its trenching with a subsequent backfilling by different types of soils. The alternative of the trench backfilling by sand on its entire depth is considered to be inaccurate, though it could be improved using numerical modeling in Chapter 6.

5.6. REFERENCES

[1] A. Palmer (1990): *Ice gouging and the safety of marine pipelines*. Offshore Technology Conference, Houston, Texas, 7-10 May 2000, paper number OTC-6371.

[2] S.A. Vershinin, P.A. Truskov, P.A. Liferov (2007): *Ice features action on seabed.* IPK "Russkaya kniga", Moscow, Russia, 196 p. (in Russian).

[3] I. Stava, P. Nystrøm, N. Viske, O.T. Gudmestad, P. Liferov, K. Grønil (2008): *Small scale model tests of ice gouge in soft sandy silt.* Proceedings of the ASME 27th International Conference on Offshore Mechanics and Arctic Engineering, Estroil, Portugal, 15-20 June 2009, paper number OMAE2008-57086.

[4] P. Liferov (2005): *First-year ice ridge scour and some aspects of ice rubble behavior.* Doctoral thesis, Department of Civil and Transport Engineering, NTNU, Trondheim, 162 p.

[5] ISO/FDIS 19906 (2010): *Petroleum and natural gas industries – Arctic offshore structures.* International standard, International Standardization Organization, Geneva.

[6] ISO 13623 (2000): *Petroleum and natural gas industries – Pipeline transportation systems.* International standard, International Standardization Organization, Geneva.

[7] API Recommended practice 2N (1995): *Recommended Practice for Planning, Design and Constructing Structures and Pipelines for Arctic Conditions.* 2d edition, Washington D. C., USA.

[8] DNV (2007): *Submarine pipeline systems*. Offshore Standard DNV-OS-F101, Det Norske Veritas, Høvik.

[9] CAN/CSA S471-92 (1992): *General requirements, design criteria, the environment and loads*. Canadian Standards Association, National Standard of Canada, 87 p.

[10] RMRS 2-020301-001 (2008): *Rules of classification and construction of subsea pipelines*. Russian Maritime Register of Shipping, Saint-Petersburg, Russia.

[11] F. Pooroshasb, J. Clark, C. Woodworth-Lynas (1989): *Small scale modeling of iceberg scouring of the seabed*. Proceedings of the 10th International Conference on Port and Ocean Engineering under Arctic Conditions, Lulea, 1, pp. 133-145.

[12] G. Hodgson, J. Levelr, C. Woodworth-Lynas, C. Lewis (1990): *The dynamics of iceberg grounding and scouring (DIGS) experiment and repetitive mapping of the Eastern Canadian continental shelf*. Environmental Studies Research Fund, Report № 094, Ottawa, 318 p.

[13] A. Palmer, C. Woodworth-Lynas, D. Nixon, R. Phillips (1996): *Subgouge deformations and the security of Arctic marine pipelines*. Offshore Technology Conference, Houston, Texas, 6-9 May 1996, paper number OTC-8222.

[14] R. Sancio, K. Been, J. Lopez (2011): *Large scale indenter test program to measure sub gouge displacements*. Proceedings of the 21st International Conference on Port and Ocean Engineering under Arctic Conditions, Montreal.

[15] M. Chua, A. Palmer, H. Tjiawi (2011): *Protecting Arctic marine pipelines against subgouge deformation.* Journal of Pipeline Engineering, Vol.10, No.2, June, 2011 Pp. 81-85.

[16] K. Been, A. Fredj, G. Comfort (2011): *Pipeline strains in soft clay backfill subject to ice gouging* . Journal of Pipeline Engineering, Vol.10, No.2, June, 2011 Pp. 87-98.

[17] S. Piyankov, Z. Azizov (2008): *Soil mechanics (in Russian).* Uliyanovsk State University, Uliyanovsk, 103 p.

[18] A. Palmer (2000): *Are we ready to construct submarine pipelines in the Arctic*. Offshore Technology Conference, Houston, Texas, 1-4 May 2000, paper number OTC-12183.

[19] L. Vitali, R. Bruschi (2004): *Pipeline seismic design.* Method statement, Snamprogetti, Fano, Italy.

[20] J. Jaky (1948): *Pressure in soils.* Proceedings of the 2d International Conference on Soil Mechanics and Foundation Engineering, Rotterdam, The Netherland, pp. 103-107.

[21] J. Hansen (1961): *The Ultimate Resistance of Rigid Piles Against Transversal Forces.* Bulletin 12, Danish Geotechnical Institute, Copenhagen, Denmark.

[22] R. Rowe, E. Davis (1982): *The Behaviour of Anchor Plates in Sand.* Geotechnique, vol. 32, no. 1, pp. 25-41.

[23] A. Vesic (1971): *Breakout Resistance of Objects Embedded in Ocean Bottom*. ASCE Ocean Engineering Conference, Miami Beach.

[24] T. Walle (2004): *Ice gouging offshore Sakhalin Island*. Master thesis, Department of Material Science and Technology, Stavanger University College, Stavanger, 105 p.

[25] F. Adwele (2011): *Protection of Arctic Pipelines against Ice Gouging from Moving Ice Ridges*. Master thesis, Department of Material Science and Technology, University of Stavanger, Stavanger, 101 p.

[26] http://en.wikipedia.org/wiki/Fixed_end_moment.

[27] W. Cimbali, F. Marchesani, D. Zenobi (2002): *Structural Reliability Analysis to Strain Beased Design of Offshore Pipelines.* Proceedings of the 12th International Offshore and Polar Engineering Conference, Kitakyushu, Japan, May 26-31, 2002.

[28] http://edu.dvgups.ru/METDOC/ITS/STRMEH/COPROMAT/METOD/UP_TEST/frame/6_1.htm (in Russian)

[29] From personal communication with Feodor Chumichev – pipeline construction engineer in JSC «MRTS»

[30] S.V. Duplenskiy (2011): *First year ice ridges interaction with marine pipelines*. Arctic Offshore Engineering course project report. UNIS, Longyerbyen.

CHAPTER 6. FINITE ELEMENT ANALYSIS OF THE RIDGE-SOIL-PIPELINE INTERACTION

6.1. GENERAL

The above performed mathematical modeling of the processes, related to the ridge scouring, educes the necessity of more accurate assessment of subscour soil deformations and their effect on the pipeline design in the context of overall system interaction. In this chapter it is proposed to carry out the finite-element analysis, focused on the soil response, such that the results obtained in Chapter 5 are adjusted for the practical reason.

The analysis model is introduced in ANSYS 13.0 Workbench, implying the numerical modeling in accordance with the theoretical part of the thesis organization. The simulation studies the scouring process itself, without the ridge movement trajectory crossing the pipeline section, for the purpose of subscour in-situ sand displacements' assessment and correction of the trench parameters, established in figure 5.23.

The organization and description of the model establishment follows the flow chart (figure 6.1), built in ANSYS software, which requires the development of the following positions:

- *Analysis system selection* – decide upon the suitable analysis system, able to solve the desirable model;
- *Engineering data* – setting up the data base of used materials in order to specify the properties of either body, involved in the model. The challenge here is to choose the sufficient amount of physical parameters, such that the program could distinguish soil, ice and the pipeline steel;
- *Geometry* – the construction of 3D bodies, representing the ridge, the soil and the pipeline;
- *Model* – the most challenging part of FEA, which requires the materials assignment for the geometry; body interactions mechanisms description; mesh formation and alignment; loads, inertial environment and constrains application; solution and evaluation of results.

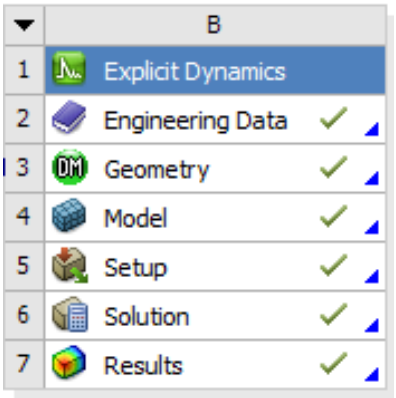

Figure 6.1. Flow chart of the FEA process

Thus before the outcome is ready for analysis, each step should be exercised and optimized in accordance with the desirable accuracy of calculations and computational capacities of the

hardware, which is discussed in subsequent sections below. The theoretical background is eliminated somewhat, as it is anticipated that previous chapters gave substantial data and study material, needed for finite-element analysis.

6.2. ANALYSIS SYSTEM SELECTION

An «Explicit Dynamics» analysis system has been selected for the model realization, which allows the performance of more accurate and efficient dynamic simulations [1] involving large deformations and strains, able to originate in soil and in the pipeline, and accounting for the non-linear material behavior and complex contact between anticipated bodies. Normally this system is used for short-time processes when immediate response is analyzed, which implies the energy error control necessity, when applying the system to the considered phenomenon simulation.

The basic equations solved by an Explicit Dynamics analysis express the conservation of mass, momentum and energy in Lagrange coordinates [1]. These together with a material model and a set of initial and boundary conditions, define the complete solution to the problem.

For Lagrange formulations the mesh moves and distorts with the material it models, such that the conservation of mass is automatically satisfied. The density at any time can be determined from the current volume of zone and its initial mass:

$$\frac{\rho_0 V_0}{V} = \frac{m}{V} \tag{6.1}$$

The partial differential equations which express the conservation of momentum relate the acceleration to the stress tensor σ_{ij} [1]:

$$\rho\ddot{x} = b_x + \frac{\partial\sigma_{xx}}{\partial x} + \frac{\partial\sigma_{xy}}{\partial y} + \frac{\partial\sigma_{xz}}{\partial z} \tag{6.1a}$$

$$\rho\ddot{y} = b_y + \frac{\partial\sigma_{yx}}{\partial x} + \frac{\partial\sigma_{yy}}{\partial y} + \frac{\partial\sigma_{yz}}{\partial z} \tag{6.1b}$$

$$\rho\ddot{z} = b_z + \frac{\partial\sigma_{zx}}{\partial x} + \frac{\partial\sigma_{zy}}{\partial y} + \frac{\partial\sigma_{zz}}{\partial z} \tag{6.1c}$$

Conservation of the energy is expressed via [1]:

$$\dot{e} = \frac{1}{\rho}\left(\sigma_{xx}\dot{\varepsilon}_{xx} + \sigma_{yy}\dot{\varepsilon}_{yy} + \sigma_{zz}\dot{\varepsilon}_{zz} + 2\sigma_{xy}\dot{\varepsilon}_{xy} + 2\sigma_{yz}\dot{\varepsilon}_{yz} + 2\sigma_{xz}\dot{\varepsilon}_{xz}\right) \tag{6.1}$$

For each time step these equations are solved explicitly (directly) for each element in the model, based on input values at the end of the previous time step. However only mass and momentum are strictly constrained by the program, while energy conservation is constantly monitored, showing the quality of the final solution.

The explicit dynamics solver computes the forces from inertial stress, contact or boundary conditions at the elements' nodes and estimates subsequently the nodal accelerations $\ddot{x}_i$ by dividing force F_i by mass of the node m_i:

$$\ddot{x}_i = \frac{F_i}{m_i} + b_i \tag{6.1}$$

b_i is the component of body acceleration. With the accelerations at time *n-1/2* determined, the velocities at time *n+1/2* are found from:

$$\dot{x}_i^{n+1/2} = \dot{x}_i^{n-1/2} + \ddot{x}_i^n \Delta t^n \tag{6.1}$$

Finally the positions are updated to time *n+1* by integrating the velocities:

$$x_i^{n+1} = x_i^n + \dot{x}_i^{n+1/2} \Delta t^{n+1/2} \tag{6.1}$$

The disadvantage of such a model behavior is that all elements have Lagrange formulations and follow the deformation of the body, not able to be displaced out of its boundaries, which complicates the simulation realization in terms of the large energy error accumulation possibility and difficulties in its control. Nevertheless «Explicit Dynamics» analysis system is able to give reasonable results falling within the acceptable energy error range [1].

6.3. ENGINEERING DATA SET-UP

Materials used in the model should follow the design basis, when defining their properties in finite-element modeling software. It is proposed to describe the model by the following set of materials: sand, clay, ice, pipeline steel (figure 6.2). Due to complexity of liquids behavior simulation in the analysis system selected, water is not anticipated in the model setting.

Outline of Schematic D2: Engineering Data

	A	B	C	D
1	Contents of Engineering Data			Description
2	Material			
3	Ice			Chapter 2, table 2.15; Chapter 4
4	Sand			Chapter 2, table 2.14
5	Soft clay			Chapter 2, table 2.14
6	Steel X65			According to API 5L - Specification for line pipe
*	Click here to add a new material			

Figure 6.2. Engineering data of materials set-up

The “Ice” material is applied to the ice ridge and simulates mainly the rubble ice inside the keel with properties given in table 2.15 of the design basis. For a large extent its behavior is described similarly to soil by the set of parameters listed below:

- Ridge ice blocks density;
- Isotropic elasticity, which is determined by:
  - Young’s modulus;
  - Poisson’s ratio;

  These two values are indicated in tables 2.14 and 2.15;
  - Bulk modulus;
  - Shear modulus;

  Bulk and shear modulus are calculated automatically as functions of the first two parameters.

- Drucker-Prager strength linear – coincides to the Mohr-Coulomb theory in a given context and includes:
  - Yield stress (at zero pressure) – corresponds to cohesion;
  - Slope (degrees) – equals to internal friction angle;

Soil properties are described with some distinctions from those proposed in design basis, but reflecting the same effect:

- Density of the solid part;
- "MO Granular" – an extension of Ducker-Prager model, which takes into account effects, associated with granular materials, such as soil and sand [1]. The advantage of this model is that it uses variable shear modulus as a function of pressure applied, which is essential, when estimating subscour soil deformations;
- Shear modulus at zero pressure;
- Tensile failure pressure;
- "Compaction EOS Linear" – defines plastic compaction path as a function of pressure versus density

The steel is determined by density, isotropic elasticity and stress-strain data, obtained in accordance with Ramberg-Osgood relationship (section 2.4.1).

6.4. SEABED SCOURING SIMULATION

6.4.1. Geometry

Initially it was proposed to use full-scale simulation for seabed scouring analysis, starting it from the initiation of gouging process, when the ridge contacts the seabed. Although the pipeline was suppressed in this model, the geometry implied its position to be perpendicular to the ridge motion direction, such that the pipe laid *143,4 m* from the point of the ridge-soil contact, corresponding to maximum gouge depth condition; the trench parameters were maintained in accordance with section 5.4.5 calculus. The seabed box was given with inclination angle of *1°*.

Then it was realized that such a model demands substantial numerical capacities of the data-machine, since the subscour soil deformations are of several meters, while the scouring length is *143,4 m*, which requires fine mesh applied to the bodies. In terms of the slow ice ridge movement, the time of model realization was increased unacceptably. Moreover, the Lagrange mesh did not allow high deformations, limiting the simulation of the ridge penetration into the soil [3]. Therefore it was proposed to compact the model longitudinally (figure 6.3), such that the ice ridge starts scouring, being *22,4 m* from the pipeline axis, which corresponds to *5°* seabed slope for the energy model (chapter 4) condition feasibility.

The body, representing the soil, has been split into 6 parts in order to construct fine-meshed area of sub-scour deformations, while the rest of the soil box's mesh is anticipated to be coarse. The ridge is constructed according to the design ridge geometry, established in Chapter 4 from the rigid elements, not able to be deformed during the contact with the seabed. The main parameter in the ridge geometry to control is the attack angle, which substantially determines the soil response [2]

The pipeline has not been involved in the scouring simulation, since its dimensions (mainly wall thickness) substantially diminish the mesh size and increase the time of calculations up to several hundred hours.

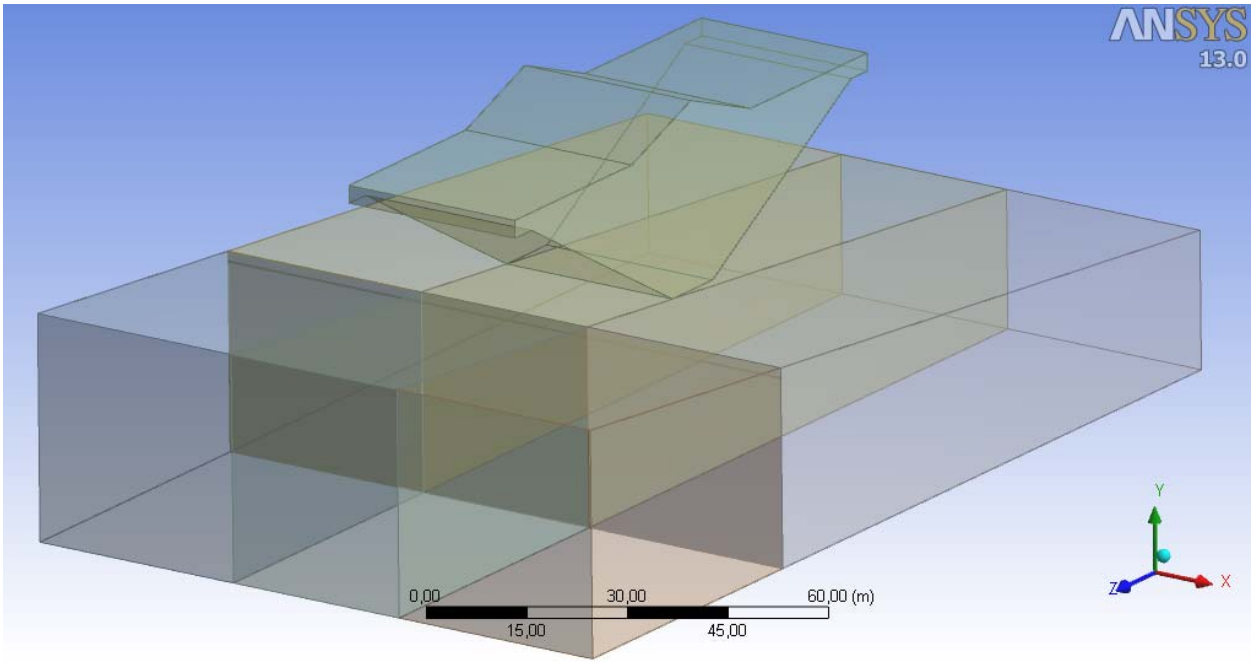

Figure 6.3. Geometry of the seabed scouring simulation model

6.4.2. Mesh

As mentioned the Langrage mesh is applied to either body, when simulating the scouring process. In order to provide high speed of the model realization the fine mesh has been constructed only for the ridge-soil contact region, whereas sidewise and downwards elements have been expanded. (figure 6.4), which allowed the soil mesh elements to be properly decreased without trading the quality of desirable results.

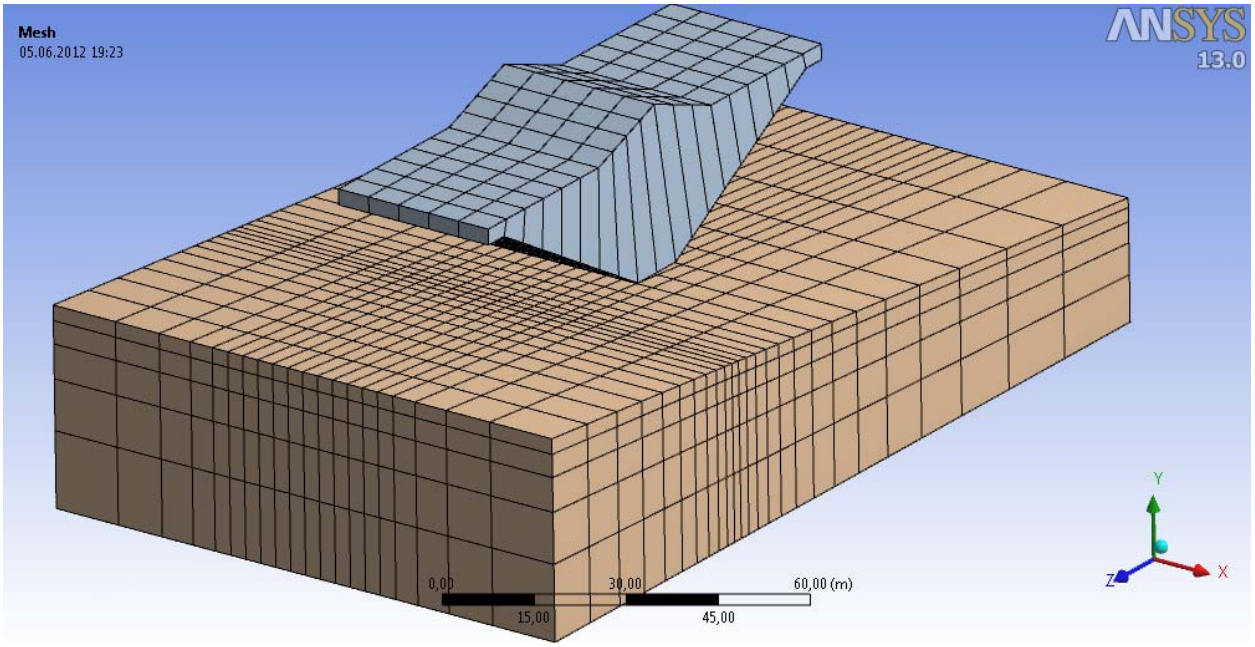

Figure 6.4. Mesh for the seabed scouring simulation model

6.4.3. Loads and boundary conditions

In the scope of this model it is proposed to combine the input data with some results of theoretical approach: all environmental loads from wind, current and ice action have been

replaced with the ridge displacement, fixed in horizontal and vertical directions, such that the scenario of scouring *1,73 m* of the seabed, estimated above in Chapter 4, is adjusted in terms of soil displacements. The ridge uniformly decelerates in time and stops after *26,7 s*, when all the energy is dissipated into the soil resistance work.

The parts, simulating the soil box, have been given with "bonded" connections, which allows the program to consider six different geometrical bodies as the single one without any possibility of sliding. The friction contact between the ridge and the soil has been applied with the friction coefficient as indicated in table 2.14.

The fixed support condition is set to the soil box's bottom and vertical faces, which simulates confinement by surrounding soil, not able to be deformed, being far enough from the scouring ridge (figure 6.5).

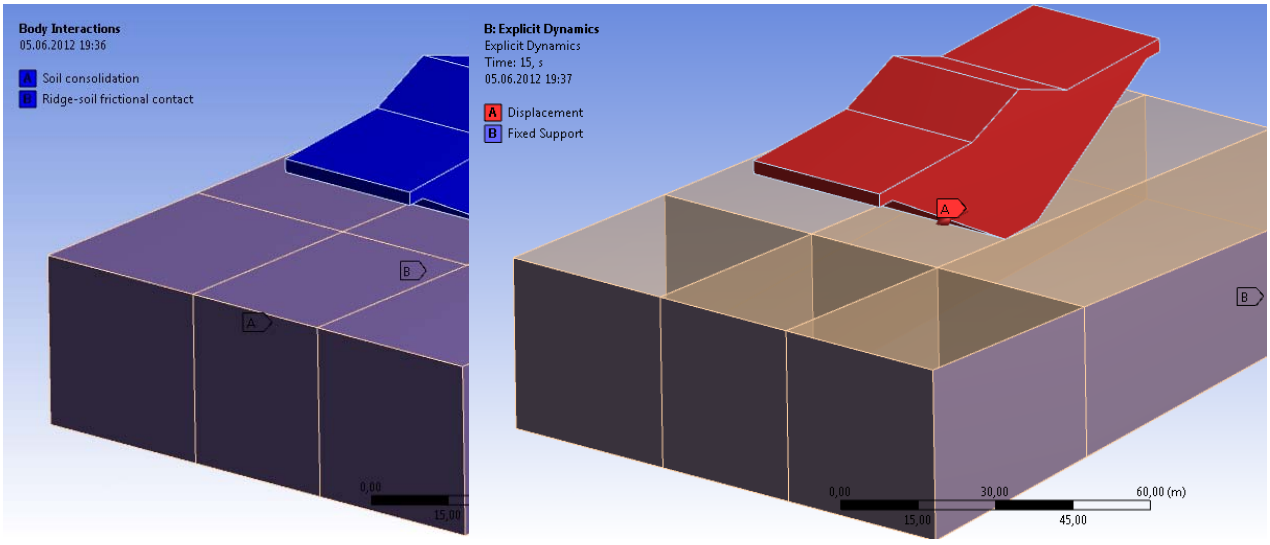

Figure 6.5. Boundary conditions' and contacts' settings

6.4.4. Analysis settings

As the soil deformations are expected to be of their large values, it is necessary to control some analysis settings in order to ensure the simulation process runs to the end.

- Maximum energy error is set to 10%. Energy is critical to control in case of large soil deformations assessment, its omission might result in the accumulated ambiguity disturbs the accuracy of outcomes. Energy error is estimated as follows:

$$Energy\ error = \frac{Current\ energy - Reference\ energy - Work\ done}{Max\ (Current\ energy, Reference\ energy, Work\ done)} \quad (6.1)$$

- Erosion controls. Erosion is a numerical process for the automatic removal of much distorted elements during a simulation [1]. The erosion of elements is set on 150 % *geometric strain limit* of the elements' effective strain. The process continues in a reasonable way due to "Retain inertia of eroded material" function, which allows free nodes of destructed elements to transfer momentum in subsequent impacts. Elements erosion in the scope of given model is useful especially in simulation of the frontal soil wedge movement, since the deformations there are large indeed.

6.4.5. Results evaluation

The model mainly focuses on the sub-scour deformations, which are shown in figures 6.6 and 6.7 for the scouring in original sand. Obviously the results follow those, studied above and almost repeat the distribution, shown in figure 5.1. However, several new findings might be observed. The most important one is that the sub-scour horizontal displacements are somewhat higher than it was initially estimated in section 5.3. Figure 6.6 shows that the maximum deformations right below the gouge base are almost twice greater (*7 m* versus *4,3 m*). This outcome implies that the pipeline is *not safe*, when embedded *2,6 m* deep as shown in figure 5.23, since the unacceptable ultimate forces are still taking place. The hazardous potential loads fall off only at the depth of *≈4 m* subscour, which demands enormous trenching costs and excludes the possibility for the pipeline to be backfilled by the in-situ sand.

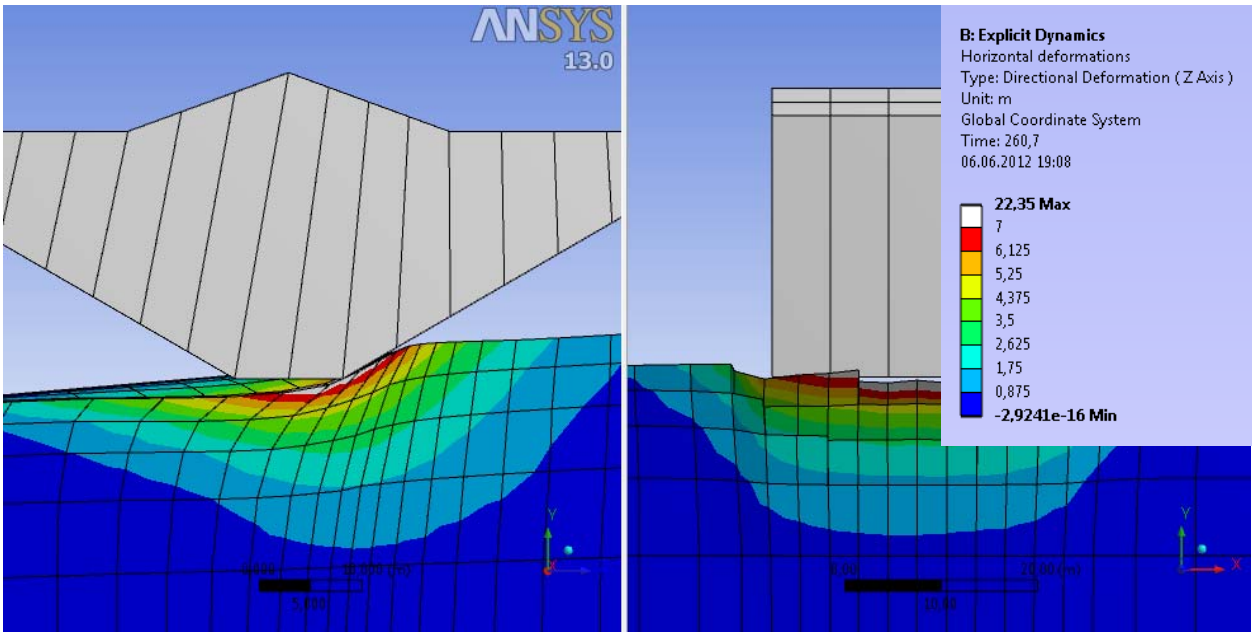

Figure 6.6. Horizontal sand deformations

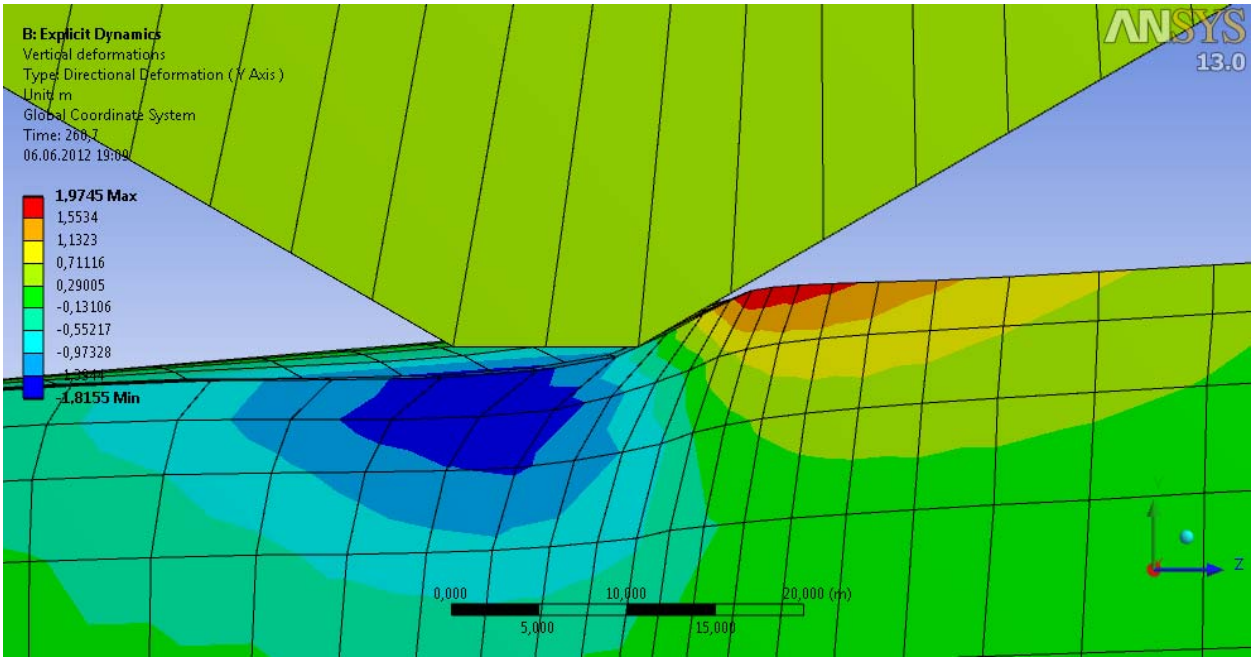

Figure 6.7. Vertical sand deformations

Vertical deformations (figure 6.7) analysis shows the displacements, almost corresponding ones, obtained in figure 5.3, however their action on the pipeline should be neglected, since it is visible, that the maximums of horizontal and vertical soil movements occur in different places with respect to the ice ridge position: near-bottom frontal soil wedge displaces horizontally for a large extent, though its vertical motions are almost absent. This is shown better in figure 6.8, where the mesh nodes' velocities vectors are established (at the moment of the ridge stoppage). Moreover *1,8 m* independent downward soil motion will not yield the pipeline limit state, which occurs if the pipeline bends *3,42 m* laterally.

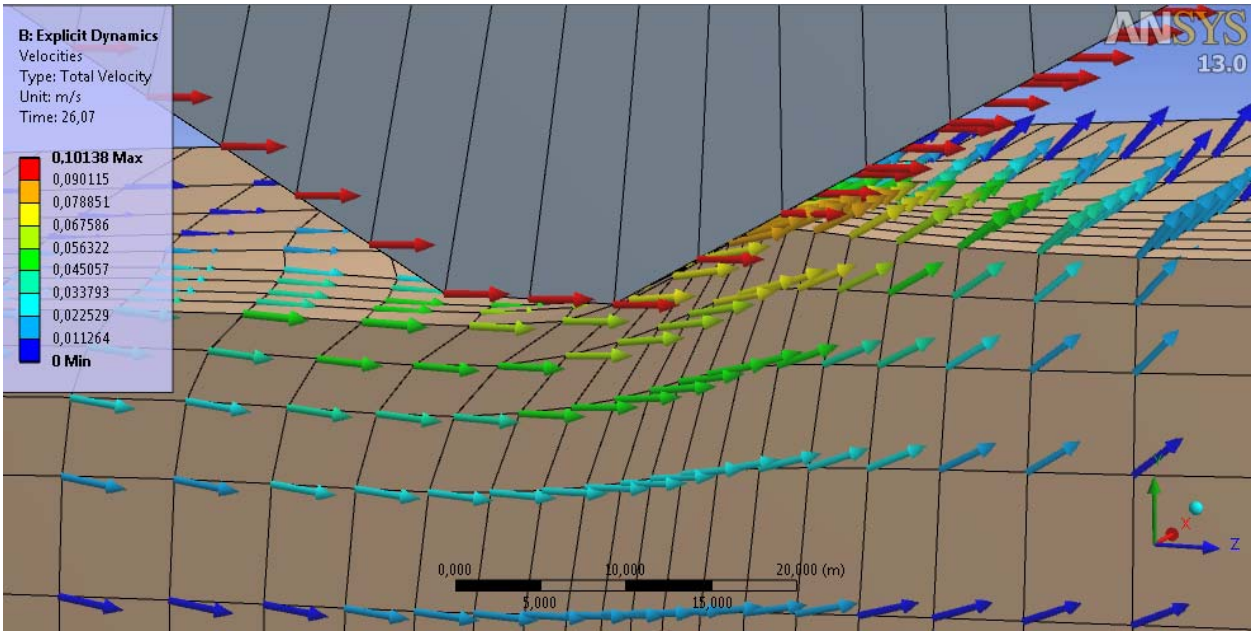

Figure 6.8. Velocity field of the soil movement

The velocities are distributed in such a way that the part of it in front of the ridge rebounds upwards, forming the wedge-out prism; below the gouge the smaller part uplifts as well, though the main soil direction subscour is horizontal, which totally follows the outcomes of other researches [2, 3, 4]

6.5. SUMMARY

Concentrating on the subscour soil deformations' studies the finite-element model's results repeat the main observations of theoretical approach, proposed in Chapters 4 and 5. However, the results' implications on the pipeline are substantially more severe, than it was anticipated above, as the soil deformation field below the gouge base extends twice further, than the theoretical model [5] showed. The product of the present numerical model therefore are considered to be unreliable as they did not found proof in other numerical and physical models [2,3], which might be associated with the Lagrange mesh type used, not able to simulate large soil deformations indeed. Anyway, the possibility of trenching the pipeline against seabed scouring by the design ridge in original sand is rejected in terms huge uncertainties involved, such that the most effective and robust proposed way to maintain the pipeline's integrity is to backfill it to the top of the pipeline by the weak clay.

6.6. REFERENCES

[1] ANSYS 13.0 User's Guide.

[2] S.A. Vershinin, P.A. Truskov, P.A. Liferov (2007): *Ice features action on seabed.* IPK "Russkaya kniga", Moscow, Russia, 196 p. (in Russian).

[3] I. Konuk, R. Gracie (2004): *A 3-dimensional Eulerian finite element model for ice scour.* Proceedings of IPC 2004, Calgary, AB. Paper IPC04-0075.

[4] P.A. Liferov, S.M., Kapustyansky, A.G., Gilenkov, L. and Vitali (2006): *Subgouge soil deformations: free field vs. pipeline included.* Submitted to J. Cold Regions Science and Technology.

[5] A. Palmer (1990): *Ice gouging and the safety of marine pipelines*. Offshore Technology Conference, Houston, Texas, 7-10 May 2000, paper number OTC-6371.

[6] N. Serre (2011): *Numerical modeling of ice ridge keel action on subsea structures*. Cold Regions Science and Technology 67 (2011), pp. 107–119.

CHAPTER 7. CONCLUSIONS AND FURTHER STUDIES

7.1. CONCLUSIONS

The present research appears to be one of a few comprehensive theoretical studies of the ridge scouring influence on the pipeline design. It accounts for the specificity of either object involved into the analysis, whether they are pipeline, seabed soil or an ice ridge and address the results obtained to the following conclusions:

- The pipeline has been designed for the specific gas field offshore Sakhalin. Its outer diameter of *406,4 mm* provided robustness in the pipeline gas hydraulics and the flexibility of wall thickness selection, such that the additional 50% strength capacity (to internal overpressure) has been given by enhanced *18,2* mm pipeline wall in order to ensure the pipeline integrity against the adverse stresses, able to originate when ridge scours the seabed, as also from actions, not anticipated in the scope of this thesis (trawl action, free-span, pipelay). No insulation coating has been applied, since the temperature distribution in the line doesn't allow either the hydrates to be formatted, or the hydrocarbons liquefaction inside the pipeline. The pipeline on-bottom stability is proposed to maintain differently in three areas 1) Near shore area (*0 – 25 m*) the pipeline is trenched; 2) Shallow water area (*25 – 66 m*) the pipeline is covered by heavy mattresses; 3) Area *66 -85 m* water depths – the pipeline is stable uncoated;
- Two theoretical models, based on the force equilibrium and energy dissipation, have been introduced in terms of the design ridge scouring assessment. Involving the scouring dynamics, soil and environmental conditions, the energy model has been considered as the best scour depth estimator, providing prudent results, similar to those, observed and estimated in other researches.
- The phenomenon of the seabed scouring has addressed substantial implications on the pipeline design. Under the reasonable assumption of high ridge blocks adfreezing the design scour depth in sand, relevant of offshore Sakhalin, has been assessed as *1,73 m*, corresponding to 10000 year pipeline collapse probability if coupled with statistical parameters of the average number of pipeline route intersections by ridges, which is acceptable from the considerations of standards' requirements. The gouge depth sensitivity to soil conditions has shown its incensement, when replacing in-situ sand by weaker clay;
- An accidental case of direct ridge-pipeline contact has been analyzed. As a sequence it was concluded, that the ridge able to exert formidable forces on the pipeline, loading it far beyond its ultimate tensile strength, such that it is proposed to avoid the contact by the pipeline embedment into the soil;
- Subscour soil deformations' study induced the analysis of soil-pipeline interaction below the gouge. The pipeline model, susceptible to stresses from operational loads and soil displacements below the scour, has been introduced and analyzed. Following the limit state approach and economical considerations it was proposed to trench the pipeline right below the possible gouge with its subsequent backfilling by very soft clay with shear strength *3,8 kPa* to the top of the pipeline, and then with in-situ sand to the original seabed level. Such a "sandwich" trench assembly implies the minimization

of the scour depth as also allows clay to flow around the pipe without exerting substantial resistance;

- The trench parameters have been estimated and discussed. Length of ≈*1250 m*, width – *3,7 m* and height *2,2 m*, set a requirement to the amount of *1320* m^3 outbound soft clay to be placed on the trench bottom.
- The finite element analysis has been performed in ANSYS 13.0 adjusted somewhat the theoretical results. It educed sub-scour deformations to be larger those, initially anticipated, such that the alternative of the pipeline protection by the means of deeper embedment into the original sand is rejected in terms of uncertainties involved from one hand and high trenching expenditures expected from another.

7.2. FURTHER STUDIES

It would be wrong stating that the mechanism of "ice-soil-pipeline" interaction is well understood and the problem concerning uncertainties involved in present research, associated with the lack of knowledge, is solved entirely: there are still opportunities for study the relevant issue even deeper, diversifying the approaches and combine them, which would result in overall and universal solution, able to be reflected in design codes. In this regard it is proposed to focus on the following works, necessary to be carried out:

- Numerical simulation improvement in terms of the broad-based analysis of the three-componential system, which is possible to achieve using coupled Lagrange-Euler mesh for the soil in order to simulate its displacement, the formation of the frontal mound and soil dumping sidewise. It is also recommended to make an adjustment on the keel representation by the rubble material, such that the modeling of its destruction is attainable;
- Physical modeling establishment in large-scale conditions. The challenge here is to achieve the full-scale to model-scale properties similitude, especially critical for the first-year ice ridge simulation;
- Transfer the results, obtained in present study to the analysis of ice ridge interaction with subsea facilities, which would probably require protection measures for subsea templates, X-mas trees and manifolds;
- The proper probabilistic approach to the considered phenomenon should be applied, using the long period statistics of updated data basis.

APPENDIX A. FLUID PROPERTIES

Table A.1. Fluid components' properties

Gas component		*Molar fraction, x_i %*	*Molar mass, M_i g/mol*	*Critical temperature, T_{ci} K*	*Critical pressure, P_{ci} MPA*
Methane	CH_4	88,43	16,04	190,56	4,6
Ethane	C_2H_6	3,74	30,07	305,83	4,88
Propane	C_3H_8	1,7	44,1	369,82	4,25
i-Butane	C_4H_{10}	1,1	58,12	408,13	3,65
n- Butane	C_4H_{10}	1,5	58,12	425,14	3,78
i-Pentane	C_5H_{12}	0,71	72,15	460,39	3,38
n- Pentane	C_5H_{12}	0,65	72,15	469,69	3,36
Hexanes	C_6H_{14}	0,5	86,18	506,4	3,03
Heptanes	C_7H_{16}	0,47	100,2	539,2	2,74
Carbon dioxide	CO_2	0,23	44,01	304,2	7,39
Nitrogen + others	N_2 +	0,4	28,01	126,2	3,39
Water	H_2O	0,57	18,02	-	-

Gas molar mass	$\bar{M} = \sum_{i=1}^{n} M_i x_i$	*19,77*	*g/mol*
Gas density	$\rho_0 = 10^3 \cdot \frac{\bar{M} P_0}{R_\mu T_0 Z_0}$	*0,82*	*kg/m³*
Gas specific gravity	$\Delta = \frac{\rho_0}{\rho_a} = \frac{M}{29}$	*0,69*	-
Pceudo-critical temperature	$T_{pc} = \sum_{i=1}^{n} x_i T_{ci}$	*209,70*	*K*
Pceudo-critical pressure	$P_{pc} = \sum_{i=1}^{n} x_i P_{ci}$	*4,52*	*MPa*

The calculations on gas properties, established in section 3.2.1, are performed in MathCAD for the given initial conditions and adjusted in Appendix B according the diameter, which changes actual values of parameters.

Calculation input

Pressure at the pipelin beginning (MPa) $p_1 := 16.7$

Minimum delivery pressure (MPa) $p_2 := 8$

Initial temperature (K) $T_1 := 343$

Enivronmental temperature (K) $T_e := 271.2$

Pceudo-critical pressure (MPa) $p_{pc} := 4.52$

Pceudo-critical temperature (K) $T_{pc} := 209.7$

Gas molar mass (g/mol) $M := 19.77$

Calculation

Average pressure $p_a := \frac{2}{3}\cdot\left(p_1 + \frac{p_2^2}{p_1 + p_2}\right)$ $p_a = 12.861$ MPa

Average temperature $T_a := \frac{T_1 - T_e}{\ln\left(\frac{T_1}{T_e}\right)}$ $T_a = 305.696$ K

Reduced pressure $p_r := \frac{p_a}{p_{pc}}$ $p_r = 2.845$ MPa

Reduced temperature $T_r := \frac{T_a}{T_{pc}}$ $T_r = 1.458$ K

Gas compressability factor

$$A_1 := -0.39 + \frac{2.03}{T_r} - \frac{3.16}{T_r^2} + \frac{1.09}{T_r^3}$$

$$A_2 := 0.0423 - \frac{0.1812}{T_r} + \frac{0.2124}{T_r^2}$$

$$Z := 1 + A_1\cdot p_r + A_2\cdot p_r^2 \qquad Z = 0.768$$

Gas dynamic viscosity

$$B_1 := -0.67 + \frac{2.36}{T_r} - \frac{1.93}{T_r^2}$$

$$B_2 := 0.8 - \frac{2.89}{T_r} + \frac{2.65}{T_r^2}$$

$$B_3 := -0.1 + \frac{0.354}{T_r} - \frac{0.314}{T_r^2}$$

$$\mu_0 := \left(1.81 + 5.95\cdot T_r\right)\cdot 10^{-6}$$

$$\mu := \mu_0\cdot\left(1 + B_1\cdot p_r + B_2\cdot p_r^2 + B_3\cdot p_r^3\right) \qquad \mu = 1.599\times 10^{-5} \text{ Pa·s}$$

Joule-Thompson coefficient

$$H_0 := 24.96 - 20.3 \cdot T_r + 4.57 \cdot T_r^{\,2}$$

$$H_1 := 5.66 - \frac{19.92}{T_r} + \frac{16.89}{T_r^{\,2}}$$

$$H_2 := -4.11 + \frac{14.68}{T_r} - \frac{13.39}{T_r^{\,2}}$$

$$H_3 := 0.568 - \frac{2.0}{T_r} + \frac{1.79}{T_r^{\,2}}$$

$$D_i := H_0 + H_1 \cdot p_r + H_2 \cdot p_r^{\,2} + H_3 \cdot p_r^{\,3}$$

$$D_i = 3.042 \quad \frac{K}{MPa}$$

Isobaric heat capacity

$$E_0 := 4.437 - 1.015 \cdot T_r + 0.591 \cdot T_r^{\,2}$$

$$E_1 := 3.29 - \frac{11.37}{T_r} + \frac{10.9}{T_r^{\,2}}$$

$$E_2 := 3.23 - \frac{16.27}{T_r} + \frac{25.48}{T_r^{\,2}} - \frac{11.81}{T_r^{\,3}}$$

$$E_3 := -0.214 + \frac{0.908}{T_r} - \frac{0.967}{T_r^{\,2}}$$

$$C_p := \frac{8.31}{M} \cdot \left(E_0 + E_1 \cdot p_r + E_2 \cdot p_r^{\,2} + E_3 \cdot p_r^{\,3} \right)$$

$$C_p = 2.905 \quad \frac{J}{K}$$

APPENDIX B. PIPELINE SIZING CALCULATIONS

Calculation input

Hydraulics data

Flow rate (MMscm/day)	$q := 11.6$
Initially assumed hydraulic friction	$\lambda := 0.02$
Gas specific gravity	$\Delta := 0.69$
Pipeline length (km)	$L := 28$
Roughness (mm)	$K := 0.03$
Thermoconductivity for steel (W/mK)	$\lambda_t := 47$
Current speed at the seabed level (m/s)	$u_r := 0.55$
Water dynamic viscosity (Pa s)	$\mu_w := 1.87 \cdot 10^{-3}$
Water isobaric heat capacity (J/K)	$C_{pw} := 4200$
Water density (kg/m3)	$\rho_w := 1030$
Water thermoconductivity (W/mK)	$\lambda_w := 0.6$
Thermoconductivity for asphalt enamel (W/mK)	$\lambda_c := 0.16$
Thickness of anti-corrosion coating (mm)	$t_c := 6$

Pipeline wall data

Steel quality	X65
Corrosion allowance (mm)	$t_{cor} := 3$
Fabrication tolerance (mm)	$t_{fab} := 1$
Material resistance factor	$\gamma_m := 1.15$
Safety class factor	$\gamma_{sc} := 1.138$
Material strength factor	$\alpha_u := 0.96$
SMYS (MPa)	$\sigma_y := 448$
SMTS (MPa)	$\sigma_u := 531$
Temperature de-rating (MPa)	$f_{temp} := 10$
Hoop stress factor (50% reduction)	$\beta := 0.5$
Gravity constant (m/s2)	$g := 9.81$
Water depth (m)	$h_w := 85$

Calculations

Internal diameter calculation

Iteration 1

Minimum required pipeline internal diamter

$$d := \sqrt[5]{q^2 \cdot 9.07 \cdot 10^{10} \cdot \frac{\lambda \cdot \Delta \cdot Z \cdot T_a \cdot L}{p_1^{\,2} - p_2^{\,2}}}$$

$d = 348.659$ mm

Pipeline outside diameter (from API 5L) $D := 406.4$ mm

Wall thickness calculation

Internal pressure $p_i := p_1 \cdot 10^6$ $p_i = 1.67 \times 10^7$ Pa

External pressure $p_e := \rho_w \cdot g \cdot h_w$ $p_e = 8.589 \times 10^5$ Pa

Strength parameter

$$f_y := \left(\sigma_y - f_{temp}\right) \cdot \beta \cdot \alpha_u \cdot 10^6$$

$$f_u := \left(\sigma_u - f_{temp}\right) \cdot \beta \cdot \alpha_u \cdot 10^6$$

$$f_{cb} := \text{if}\left(f_y < \frac{f_u}{1.15}, f_y, f_y\right)$$

$f_{cb} = 2.102 \times 10^8$ Pa

Wall thickness (bursting criteria)

$$t_b := \frac{D \cdot \left(p_i - p_e\right) \cdot \gamma_m \cdot \gamma_{sc}}{4 \cdot \frac{f_{cb}}{\sqrt{3}} + \left(p_i - p_e\right) \cdot \gamma_m \cdot \gamma_{sc}}$$

$t_b = 16.642$ mm

Nominal wall thickness $t_{nom} := t_b + t_{cor} + t_{fab}$

$t_{nom} = 20.642$ mm

Standard wall thickness $t_s := 22.2$ mm

Characteristic wall thickness $t := t_s - t_{cor} - t_{fab}$

$t = 18.2$ mm

Hydraulics adjustment

Iteration 2

Pipeline internal diamter $d := D - 2t$ $d = 370$ mm

Outlet pressure $p_2 := \sqrt{p_1^2 - \frac{q^2 \cdot \Delta \cdot \lambda \cdot Z \cdot T_a \cdot L}{\left(3.32 \cdot 10^{-6}\right)^2 \cdot d^5}}$ $p_2 = 10.917$ mm

Average pressure $p_a := \frac{2}{3} \cdot \left(p_1 + \frac{p_2^2}{p_1 + p_2} \right)$ $p_a = 14.01$

Prandtl number for water $Pr_w := \frac{\mu_w \cdot C_{pw}}{\lambda_w}$ $Pr_w = 13.09$

Heat trensfer to water $\alpha_w := 0.26 \left(\frac{u_r \cdot D \cdot 10^{-3} \cdot \rho_w}{\mu_w} \right)^{0.6} \cdot Pr_w^{0.37} \cdot \frac{\lambda_w}{D \cdot 10^{-3}}$

$\alpha_w = 1.126 \times 10^3$

Average heat trensfer coefficient $k_a := \frac{1}{\frac{t}{\lambda_t} + \frac{t_c}{\lambda_c} + \frac{1}{\alpha_w}}$ $k_a = 0.026$ $\frac{W}{m^2 K}$

Average temperature $a := 225.5 \frac{k_a \cdot D}{q \cdot \Delta \cdot C_p \cdot 10^6}$

$$T_a := T_e + \frac{T_1 - T_e}{a \cdot L} \cdot (1 - \exp(-a \cdot L)) - D_i \cdot \frac{p_1^2 - p_2^2}{2a \cdot L \cdot p_a} \cdot \left[1 - \frac{1}{a \cdot L} \cdot (1 - \exp(-a \cdot L)) \right]$$

$T_a = 334.234$ K

Reduced pressure $p_r := \frac{p_a}{p_{pc}}$ $p_r = 3.1$

Reduced temperature $T_r := \frac{T_a}{T_{pc}}$ $T_r = 1.594$

Gas compressability factor $Z = 0.835$

Gas dynamic viscosity $\mu = 1.582 \times 10^{-5}$ Pa·s

Joule-Thompson coefficient $D_i = 2.519$ $\frac{K}{MPa}$

Isobaric heat capacity $C_p = 2.632$ $\frac{J}{K}$

Reynolds number $Re := 17.75 \cdot 10^3 \cdot \frac{q \cdot \Delta}{\mu \cdot d}$ $Re = 2.427 \times 10^7$

Hydraulic friction coefficient $\lambda := 0.067 \cdot \left(\frac{158}{Re} + \frac{2K}{d} \right)^{0.2}$ $C_p = 2.637 \ \frac{J}{K}$

Minimum required pipeline internal diamter $d := \sqrt[5]{q^2 \cdot 9.07 \cdot 10^{10} \cdot \frac{\lambda \cdot \Delta \cdot Z \cdot T_a \cdot L}{p_1^{\,2} - p_2^{\,2}}}$

$d = 344.589$ mm

Pipeline outside diameter (from API 5L) $D := 406.4$ mm

Iteration 3

Pipeline internal diamter $d := D - 2t$ $d = 370$ mm

Outlet pressure $p_2 := \sqrt{p_1^{\,2} - \frac{q^2 \cdot \Delta \cdot \lambda \cdot Z \cdot T_a \cdot L}{\left(3.32 \cdot 10^{-6}\right)^2 \cdot d^5}}$ $p_2 = 12.921$ mm

Average pressure $p_a := \frac{2}{3} \cdot \left(p_1 + \frac{p_2^{\,2}}{p_1 + p_2} \right)$ $p_a = 14.891$ MPa

Average temperature $a := 225.5 \frac{k_a \cdot D}{q \cdot \Delta \cdot C_p \cdot 10^6}$

$$T_a := T_e + \frac{T_1 - T_e}{a \cdot L} \cdot (1 - \exp(-a \cdot L)) - D_i \cdot \frac{p_1^{\,2} - p_2^{\,2}}{2a \cdot L \cdot p_a} \cdot \left[1 - \frac{1}{a \cdot L} \cdot (1 - \exp(-a \cdot L)) \right]$$

$T_a = 338.156$ K

Reduced pressure $p_r := \frac{p_a}{p_{pc}}$ $p_r = 3.294$

Reduced temperature $T_r := \frac{T_a}{T_{pc}}$ $T_r = 1.613$

Gas compressability factor $Z = 0.841$

Gas dynamic viscosity $\mu = 1.616 \times 10^{-5}$ Pa·s

Joule-Thompson coefficient $D_i = 2.342 \ \frac{J}{K}$

Isobaric heat capacity $C_p = 2.637 \ \frac{K}{MPa}$

Reynolds number $Re := 17.75 \cdot 10^3 \cdot \frac{q \cdot \Delta}{\mu \cdot d}$ $Re = 2.376 \times 10^7$

Hydraulic friction coefficient $\lambda := 0.067 \cdot \left(\frac{158}{Re} + \frac{2K}{d} \right)^{0.2}$

Minimum required pipeline internal diamter $d := \sqrt[5]{q^2 \cdot 9.07 \cdot 10^{10} \cdot \frac{\lambda \cdot \Delta \cdot Z \cdot T_a \cdot L}{p_1^2 - p_2^2}}$

$d = 371.407$ mm

Pipeline outside diameter (from API 5L) $D := 406.4$ mm

Iteration 4

Pipeline internal diamter $d := D - 2t$ $d = 370$ mm

Outlet pressure $p_2 := \sqrt{p_1^2 - \frac{q^2 \cdot \Delta \cdot \lambda \cdot Z \cdot T_a \cdot L}{\left(3.32 \cdot 10^{-6}\right)^2 \cdot d^5}}$ $p_2 = 12.837$ mm

Average pressure $p_a := \frac{2}{3} \cdot \left(p_1 + \frac{p_2^2}{p_1 + p_2} \right)$ $p_a = 14.853$ MPa

Average temperature $a := 225.5 \cdot \frac{k_a \cdot D}{q \cdot \Delta \cdot C_p \cdot 10^6}$

$$T_a := T_e + \frac{T_1 - T_e}{a \cdot L} \cdot (1 - \exp(-a \cdot L)) - D_i \cdot \frac{p_1^2 - p_2^2}{2a \cdot L \cdot p_a} \cdot \left[1 - \frac{1}{a \cdot L} \cdot (1 - \exp(-a \cdot L)) \right]$$

$T_a = 338.391$ K

Reduced pressure $p_r := \frac{p_a}{p_{pc}}$ $p_r = 3.286$

Reduced temperature $T_r := \frac{T_a}{T_{pc}}$ $T_r = 1.614$

Gas compressability factor $Z = 0.841$

Gas dynamic viscosity $\mu = 1.616 \times 10^{-5}$ Pa·s

Joule-Thompson coefficient $D_i = 2.342 \ \frac{K}{MPa}$

Isobaric heat capacity $C_p = 2.637 \ \frac{J}{K}$

Reynolds number $Re := 17.75 \cdot 10^{3} \cdot \frac{q \cdot \Delta}{\mu \cdot d}$ $Re = 2.376 \times 10^{7}$

Hydraulic friction coefficient $\lambda := 0.067 \cdot \left(\frac{158}{Re} + \frac{2K}{d} \right)^{0.2}$

Minimum required pipeline internal diamter $d := \sqrt[5]{q^{2} \cdot 9.07 \cdot 10^{10} \cdot \frac{\lambda \cdot \Delta \cdot Z \cdot T_a \cdot L}{p_1^{2} - p_2^{2}}}$

$d = 370.084$

Pipeline outside diameter (from API 5L) $D := 406.4 \ mm$

APPENDIX C. PIPELINE ON-BOTTOM-STABILITY CALCULATIONS

Calculation input

Material data

Steel density (kg/m^3)	$\rho_s := 7850$
Pipeline outer diameter (m)	$D := 0.4064$
Pipeline wall thickness (m)	$t := 0.0182$
Corrosion coating density (kg/m^3)	$\rho_c := 1400$
Corrosion coating thickness (m)	$t_c := 0.006$

Environmental data

Water density (kg/m^3)	$\rho_w := 1030$
Gravity constant (m/s^2)	$g := 9.81$
Lift coefficient	$C_L := 0.9$
Drag coefficient	$C_D := 0.7$
Mass coefficient	$C_M := 3.29$
Current speed above the seabed (m/s)	$u_r := 0.46$
Reference height (m)	$z_r := 3$
Current attack angle (rad)	$\theta_c := 0.87$
Significant wave height (m)	$H_s := 9.8$
Peak wave period (s)	$T_p := 14.6$
Peakedness	$\gamma := 3.3$
Gravity constant (m/s^2)	$g := 9.81$
Wave attack angle (rad)	$\theta_w := 0.96$
Water depth (m)	$d_w := 25$
Bottom roughness (m)	$z_0 := 0.0000208$
Pipeline-seabed friction coefficient	$\mu_p := 0.7$

Calculations

Wave and current parameters calculations

Significant wave velocity amplitude at the seabed level perpendicular to the pipe

$$T_n := \sqrt{\frac{d_w}{g}} \qquad T_n = 1.596 \quad s$$

$$\frac{T_n}{T_p} = 0.109$$

$$u_s := 0.36 \cdot \frac{H_s}{T_n} \cdot \sin(\theta_w) \qquad u_s = 1.81 \quad \frac{m}{s}$$

Mean zero up-crossing wave period at the seabed level

$$T_u := 0.87 \cdot T_p \qquad T_u = 12.702 \quad s$$

Water particles acceleration

$$A_s := 2\pi \cdot \frac{u_s}{T_u} \qquad A_s = 0.896 \quad \frac{m}{s^2}$$

Keulegan-Carpenter number

$$KC := \frac{u_s \cdot T_u}{D} \qquad KC = 56.584$$

Current velocity over pipeline diameter

$$u_d := \frac{u_r \cdot \sin(\theta_c)}{\ln\left(\frac{z_r}{z_0} + 1\right)} \cdot \left[\left(1 + \frac{z_0}{D + 2t_c}\right) \cdot \ln\left(\frac{D + 2t_c}{z_0} + 1\right) - 1\right]$$

$$u_d = 0.264$$

Validity check

$$A_0 := \frac{u_s \cdot T_p}{2\pi} \qquad K_b := 30 z_0$$

$$\frac{A_0}{K_b} = 6.742 \times 10^3 \qquad \frac{A_0}{K_b} > 30 \qquad \text{OK}$$

$$0.2A_0 \cdot \left(\frac{A_0}{K_b}\right)^{-0.25} = 0.093 \qquad z_r > 0.2A_0 \cdot \left(\frac{A_0}{K_b}\right)^{-0.25} \qquad \text{OK}$$

$$\frac{u_s}{u_r} = 3.936 \qquad \frac{u_s}{u_r} > 1 \qquad \text{OK}$$

Calibration factor

$$M := \frac{u_d}{u_s} \qquad M = 0.146$$

$$F_w := 1.4$$

Pipeline submerged weight

$$w_s := \rho_s \cdot \pi \cdot D \cdot t \cdot g + \rho_c \cdot \pi \cdot D \cdot t_c \cdot g - \rho_w \cdot \frac{\pi \cdot \left(D + 2 \cdot t_c\right)^2}{4} \cdot g$$

$$w_s = 505.387$$

Lift force

$$F_L(\theta) := \frac{1}{2} \rho_w \cdot D \cdot C_L \cdot \left(u_s \cdot \cos\left(\frac{\theta \cdot \pi}{180} \right) + u_d \right)^2$$

Drag force

$$F_D(\theta) := \frac{1}{2} \cdot \rho_w \cdot D \cdot C_D \cdot \left| u_s \cdot \cos\left(\frac{\theta \cdot \pi}{180} \right) + u_d \right| \cdot \left(u_s \cdot \cos\left(\frac{\theta \cdot \pi}{180} \right) + u_d \right)$$

Mass force

$$F_I(\theta) := \frac{\pi \cdot \left(D + 2t_c\right)^2}{4} \cdot \rho_w \cdot C_M \cdot A_s \cdot \sin\left(\frac{\theta \cdot \pi}{180} \right)$$

Required weight

$$W(\theta) := \left[\frac{\left(F_D(\theta) + F_I(\theta)\right) + \mu_p \cdot F_L(\theta)}{\mu_p} \right] \cdot F_w$$

$$W(13) = 2.477 \times 10^3$$

APPENDIX D. SCOUR DEPTH CALCULATIONS

Calculation input

Ice data

Level ice thickness (m)	$h_i := 1.2$
Ridge sail height (m)	$h_s := 6$
Consolidated layer thickness (m)	$h := 2.8$
Keel angle (rad)	$\alpha_k := 0.523$
Sail angle (rad)	$\alpha_s := 0.349$
Keel breadth (m)	$B := 30$
Ridge block size (m)	$T_b := 0.4$
Ice density (kg/m^3)	$\rho_i := 916$
Ice speed (m/s)	$v_i := 1.1$
Elasticity modulus (MPa)	$E_i := 8000$
Poisson ratio	$\nu_i := 0.34$
Ice rubble internal friction angle (rad)	$\phi_i := 0.349$
Keel rubble cohesion (kPa)	$c_i := 15$
Ridge sail porosity	$\eta_s := 0.07$

Soil data (sand)

Wall friction angle (rad)	$\phi_w := 0.443$
Internal friction angle (rad)	$\phi := 0.523$
Friction between ice and soil	$\mu := 0.5$
Soil density (kg/m^3)	$\rho_s := 1500$
Seabed slope (rad)	$\beta := 0.017533$

Environmental data

Water density (kg/m^3)	$\rho_w := 1030$
Current speed (m/s)	$u_c := 2$
Current drag coefficient	$C_{dw} := 0.9$
Air density (kg/m^3)	$\rho_a := 1.3$

Wind speed (m/s) $u_a := 42$

Wind drag coefficient $C_{da} := 0.9$

Wind scin friction coefficient $C_{sa} := 0.001$

Gravity constant (m/s^2) $g := 9.81$

Calculations

Ice ridge parameters

Ridge macro porosity $\eta := 0.11 \cdot \ln(T_b) + 0.37$ $\eta = 0.269$

Ridge density in water $\rho_{iw} := \eta \cdot \rho_w + (1 - \eta) \cdot \rho_i$ $\rho_{iw} = 946.69 \ \frac{kg}{m^3}$

Ridge density in air $\rho_{ia} := \eta_s \cdot \rho_a + (1 - \eta_s) \cdot \rho_i$ $\rho_{ia} = 851.971 \ \frac{kg}{m^3}$

Keel draught $h_k := 3.95 \cdot h_s$ $h_k = 23.7$ m

Keel width at the water line $w_k := 3.91 \cdot h_k$ $w_k = 92.667$

Keel width at the bottom $w_b := w_k - 2 \cdot h_k \cdot \cot(\alpha_k)$ $w_b = 10.454$

Current projection area $A_w := \left(h_k - \frac{\rho_i}{\rho_w} \cdot h_i\right) \cdot B$ $A_w = 678.984$ m

Wind projection areas $A_{a1} := \left(h_s - \frac{\rho_w - \rho_i}{\rho_w} \cdot h_i\right) \cdot B$ $A_{a1} = 176.016$ m^2

$A_{a2} := w_k \cdot B$ $A_{a2} = 2.78 \times 10^3$ m^2

Force model calculations

Wind drag force $F_{da} := \frac{1}{2} \cdot \rho_a \cdot C_{da} \cdot A_{a1} \cdot u_a^2 + C_{sa} \cdot \rho_a \cdot A_{a2} \cdot u_a^2$

$F_{da} = 1.88 \times 10^5$ N

Current drag force $F_{dw} := \frac{1}{2} \cdot C_{dw} \cdot \rho_w \cdot A_w \cdot u_c^2$

$F_{dw} = 1.259 \times 10^6$ N

Ridge weight

$$W := 1.0 \cdot \rho_{iw} \cdot B \cdot g \cdot \left[\frac{\rho_{ia}}{\rho_{iw}} \cdot \left(h_s - \frac{\rho_w - \rho_i}{\rho_w} \cdot h\right)^2 \cdot \cot(\alpha_s) + \frac{\rho_i}{\rho_{iw}} \cdot h \cdot w_k + \frac{1}{2} \cdot (w_k + w_b) \cdot \left(h_k - \frac{\rho_i}{\rho_w} \cdot h\right)\right]$$

$W = 3.969 \times 10^8$ N

Buoyancy

$$F_b := \rho_w \cdot g \cdot B \cdot \left[\frac{1}{2} \cdot \left(w_k + w_b \right) \cdot \left(h_k - \frac{\rho_i}{\rho_w} \cdot h \right) + \frac{\rho_i}{\rho_w} \cdot h \cdot w_k \right]$$

$F_b = 4.014 \times 10^8$ N

Ice force $F_i := 0.43 \cdot 4.059 \cdot B^{0.622} \cdot h_i^{0.628}$ $F_i = 16.232$ MN

Passive friction force (sand)

- Passive earth pressure coefficient

$$K_p := \frac{\cos(\phi)^2}{\cos(\phi_w) \cdot \left(1 - \sqrt{\frac{\sin(\phi + \phi_w) \cdot \sin(\phi)}{\cos(\phi_w)}} \right)^2} \qquad K_p = 7.835$$

- Front resistance $P_f(d) := \frac{1}{2} K_p \cdot \rho_s \cdot g \cdot (d + 0.635 \cdot d)^2 \cdot B$

- Side resistance $P_s(d) := \frac{1}{6} \cdot K_p \cdot \rho_s \cdot g \cdot d^2 \cdot w_b \cdot \left(w_b + \frac{d \cdot \cot(\alpha_k)}{2} \right)$

- Horizontal passive friction $F_{cx}(d) := \mu \cdot P_f(d) \cdot \cos(\phi_w) \cdot \cos(\alpha_k) + \mu \cdot P_s(d) \cdot \cos(\phi_w)$

- Vertical passive friction $F_{cy}(d) := \mu \cdot P_f(d) \cdot \cos(\phi_w) \cdot \sin(\alpha_k)$

Active friction force (sand)

- Seabed reaction $N(d) := F_{cy}(d)$

$F_a(d) := \mu \cdot N(d)$

Scour depth (sand)

$$F_{da} + F_{dw} + F_i \cdot 10^6 - F_a(d) - F_{cx}(d) = 0 \text{ solve}, d \rightarrow \begin{pmatrix} -41.541987279014337505 \\ -2.3915496473490166615 \\ 2.2613641417904355274 \end{pmatrix}$$

$d := 2.26$ m

Frontal mound height (sand)

$$h_f := \sqrt{\frac{d^2 \cdot \cot(\phi)}{\cot(\phi) + \frac{d}{3B} \cdot \cot(\phi) \cdot \cot(\beta)}} \qquad h_f = 1.436$$

$$\frac{h_f}{d} = 0.635$$

Soil data (clay)

Wall friction angle (rad) $\phi_w := 0.349$

Internal friction angle (rad) $\phi := 0.401$

Friction between ice and soil $\mu := 0.4$

Soil density (kg/m3) $\rho_s := 1600$

Seabed slope (rad) $\beta := 0.01753$

Passive friction force (clay)

- Passive earth pressure coefficient

$$K_p := \frac{\cos(\phi)^2}{\cos(\phi_w)\cdot\left(1-\sqrt{\frac{\sin(\phi+\phi_w)\cdot\sin(\phi)}{\cos(\phi_w)}}\right)^2} \qquad K_p = 4.12$$

- Front resistance $P_f(d) := \frac{1}{2}K_p\cdot\rho_s\cdot g\cdot(d+0.557\cdot d)^2\cdot B$

- Side resistance $P_s(d) := \frac{1}{6}\cdot K_p\cdot\rho_s\cdot g\cdot d^2\cdot w_b\cdot\left(w_b+\frac{d\cdot\cot(\alpha_k)}{2}\right)$

- Horizontal passive friction $F_{ox}(d) := \mu\cdot P_f(d)\cdot\cos(\phi_w)\cdot\cos(\alpha_k)+\mu\cdot P_s(d)\cdot\cos(\phi_w)$

- Vertical passive friction $F_{oy}(d) := \mu\cdot P_f(d)\cdot\cos(\phi_w)\cdot\sin(\alpha_k)$

Active friction force (clay)

- Seabed reaction $N(d) := F_{cy}(d)$

$F_a(d) := \mu\cdot N(d)$

Scour depth (clay)

$$F_{da}+F_{dw}+F_i\cdot 10^6-F_a(d)-F_{cx}(d)=0 \text{ solve},d \rightarrow \begin{pmatrix}-37.366944669394726850\\-3.7654621368271543463\\3.4207532757416371804\end{pmatrix}$$

$d := 3.42 \quad m$

Frontal mound height (clay)

$$h_f := \sqrt{\frac{d^2\cdot\cot(\phi)}{\cot(\phi)+\frac{d}{3B}\cdot\cot(\phi)\cdot\cot(\beta)}} \qquad h_f = 1.901$$

$$\frac{h_f}{d} = 0.556$$

Energy model calculations for sandy seabed

Ridge weight

$$W := 1.0 \cdot \rho_{iw} \cdot B \cdot g \cdot \left[\frac{\rho_{ia}}{\rho_{iw}} \cdot \left(h_s - \frac{\rho_w - \rho_i}{\rho_w} \cdot h \right)^2 \cdot \cot(\alpha_s) + \frac{\rho_i}{\rho_{iw}} \cdot h \cdot w_k + \frac{1}{2} \cdot (w_k + w_b) \cdot \left(h_k - \frac{\rho_i}{\rho_w} \cdot h \right) \right]$$

$$W = 3.969 \times 10^8 \quad N$$

Buoyancy

$$F_b := \rho_w \cdot g \cdot B \cdot \left[\frac{1}{2} \cdot (w_k + w_b) \cdot \left(h_k - \frac{\rho_i}{\rho_w} \cdot h \right) + \frac{\rho_i}{\rho_w} \cdot h \cdot w_k \right]$$

$$F_b = 4.014 \times 10^8 \quad N$$

Ridge kinetic energy

$$E_k := \frac{W \cdot v_i^2}{2g}$$

$$E_k = 2.448 \times 10^7 \quad J$$

Work of current drag

$$W_w(L) := \int_0^L \frac{1}{2} \cdot C_{dw} \cdot \rho_w \cdot A_w \cdot \left(u_c - \frac{L - x}{L} \cdot v_i \right) dx$$

Work of wind drag

$$W_a(L) := \int_0^L \frac{1}{2} \cdot \rho_a \cdot C_{da} \cdot A_{a1} \cdot \left(u_a - \frac{L - x}{L} \cdot v_i \right)^2 + C_{sa} \cdot \rho_a \cdot A_{a2} \cdot \left(u_a - \frac{L - x}{L} \cdot v_i \right)^2 dx$$

Work of ice driving force

$$W_i(L) := \int_0^L \frac{x}{L} \cdot 0.43 \cdot 4.059 \cdot B^{0.622} \cdot h_i^{0.628} \cdot 10^6 \, dx$$

Work of passive friction (sand)

- Passive earth pressure coefficient

$$K_p := \frac{\cos(\phi)^2}{\cos(\phi_w) \cdot \left(1 - \sqrt{\frac{\sin(\phi + \phi_w) \cdot \sin(\phi + \beta)}{\cos(\phi_w) \cdot \cos(\beta)}} \right)^2}$$

$$K_p = 8.348$$

$$C_1 := \frac{\cot(\alpha_k)}{1 - \cot(\alpha_k) \cdot \tan(\beta)}$$

- Ridge elevation

$$y = \frac{\mu}{B^2 \cdot \rho_w} \cdot \frac{1}{2} \cdot K_p \cdot \rho_s \cdot B \cdot \left(1 + C_1 \cdot \tan(\beta) \right)^2 \cdot (1 + 0.691)^2 \cdot (x \cdot \tan(\beta) - y)^2$$

$$x(y) := \frac{1000}{17} \cdot y + \frac{10000}{289} \cdot 10^{\frac{1}{2}} \cdot y^{\frac{1}{2}}$$

$$y(x) := \frac{500}{289} + \frac{17}{1000}\cdot x - \frac{1}{289}\cdot(250000 + 4913\cdot x)^{\frac{1}{2}}$$

- Front face resistance

$$P_{f1}(x) := \frac{1}{2}\cdot K_p\cdot\rho_s\cdot g\cdot\left[\left[1.691\cdot\left(x\cdot\tan(\beta) - y(x)\right)\right]\cdot\left(1 + C_1\cdot\tan(\beta)\right)\right]^2\cdot B$$

$$P_{f2}(y) := \frac{1}{2}\cdot K_p\cdot\rho_s\cdot g\cdot\left[\left[1.691\cdot\left(x(y)\cdot\tan(\beta) - y\right)\right]\cdot\left(1 + C_1\cdot\tan(\beta)\right)\right]^2\cdot B$$

- Side face resistance

$$P_s(x) := \frac{1}{6}\cdot K_p\cdot\rho_s\cdot g\cdot\cot(\beta)\cdot\left(x\cdot\tan(\beta) - y(x)\right)^3$$

- Work of horizontal passive friction

$$W_{prx}(L) := \int_0^L \mu\cdot P_{f1}(x)\cdot\cos\left(\phi_w\right)\cdot\cos\left(\alpha_k\right) + \mu\cdot P_s(x)\cdot\cos\left(\phi_w\right)\,dx$$

- Work of vertical passive friction

$$W_{pry}(L) := \int_0^{y(L)} \mu\cdot P_{f2}(y)\cdot\cos\left(\phi_w\right)\cdot\sin\left(\alpha_k\right)\,dy$$

Ridge potential energy

$$E_p(L) := \frac{\rho_w\cdot g\cdot B\cdot w_k\cdot y(L)^2}{2}$$

Ice field potential energy

$$k_i := \sqrt{\frac{E_i\cdot 10^6\cdot h_i^3\cdot\rho_w\cdot g}{24\cdot\left(1 - \nu_i^2\right)}}$$

$$E_{pi}(L) := \frac{k_i\cdot y(L)^2}{2}$$

Work of active friction

$$W_{ar}(L) := \int_0^L \mu\cdot\left(\rho_w\cdot g\cdot B\cdot w_k\cdot y(x) + k_i\cdot y(x) + \mu\cdot P_{f1}(x)\cdot\cos\left(\phi_w\right)\cdot\sin\left(\alpha_k\right)\right)\,dx$$

Scour length

$$E_k + W_a(L) + W_w(L) + W_i(L) = W_{ar}(L) + W_{prx}(L) + W_{pry}(L) + E_p(L) + E_{pi}(L)\ \text{solve}, L$$

$$L := 143.4\ \text{m}$$

Scour depth

$$d := L\cdot\tan(\beta) - y(L)$$

$$d = 1.727\ \text{m}$$

Ridge elvation $y(L) = 0.787 \quad m$

Frontal mound height $h_f := \sqrt{\frac{d^2 \cdot \cot(\phi)}{\cot(\phi) + \frac{d}{3B} \cdot \cot(\phi) \cdot \cot(\beta)}}$

$h_f = 1.193 \quad m$

$\frac{h_f}{d} = 0.691$

Energy model calculations for clayey seabed

Work of passive friction (clay)

- Passive earth pressure coefficient

$$K_p := \frac{\cos(\phi)^2}{\cos(\phi_w) \cdot \left(1 - \sqrt{\frac{\sin(\phi + \phi_w) \cdot \sin(\phi + \beta)}{\cos(\phi_w) \cdot \cos(\beta)}}\right)^2}$$

$K_p = 4.319$

$$C_1 := \frac{\cot(\alpha_k)}{1 - \cot(\alpha_k) \cdot \tan(\beta)}$$

- Ridge elevation

$$y = \frac{\mu}{B^2 \cdot \rho_w} \cdot \frac{1}{2} \cdot K_p \cdot \rho_s \cdot B \cdot \left(1 + C_1 \cdot \tan(\beta)\right)^2 \cdot (1 + 0.618)^2 \cdot \left(x \cdot \tan(\beta) - y\right)^2$$

$$x(y) := \frac{1000}{17} \cdot y + \frac{2000}{17} \cdot 2^{\frac{1}{2}} \cdot y^{\frac{1}{2}}$$

$$y(x) := 4 + \frac{17}{1000} \cdot x - \frac{1}{25} \cdot (10000 + 85 \cdot x)^{\frac{1}{2}}$$

- Front face resistance

$$P_{f1}(x) := \frac{1}{2} \cdot K_p \cdot \rho_s \cdot g \cdot \left[\left[1.618 \left(x \cdot \tan(\beta) - y(x)\right)\right] \cdot \left(1 + C_1 \cdot \tan(\beta)\right)\right]^2 \cdot B$$

$$P_{f2}(y) := \frac{1}{2} \cdot K_p \cdot \rho_s \cdot g \cdot \left[\left[1.618 \left(x(y) \cdot \tan(\beta) - y\right)\right] \cdot \left(1 + C_1 \cdot \tan(\beta)\right)\right]^2 \cdot B$$

- Side face resistance

$$P_s(x) := \frac{1}{6} \cdot K_p \cdot \rho_s \cdot g \cdot \cot(\beta) \cdot \left(x \cdot \tan(\beta) - y(x)\right)^3$$

- Work of horizontal passive friction

$$W_{prx}(L) := \int_0^L \mu \cdot P_{f1}(x) \cdot \cos\left(\phi_w\right) \cdot \cos\left(\alpha_k\right) + \mu \cdot P_s(x) \cdot \cos\left(\phi_w\right) dx$$

- Work of vertical passive friction

$$W_{pry}(L) := \int_0^{y(L)} \mu \cdot P_{f2}(y) \cdot \cos\left(\phi_w\right) \cdot \sin\left(\alpha_k\right) dy$$

Ridge potential energy

$$E_p(L) := \frac{\rho_w \cdot g \cdot B \cdot w_k \cdot y(L)^2}{2}$$

Ice field potential energy

$$k_i := \sqrt{\frac{E_i \cdot 10^6 \cdot h_i^3 \cdot \rho_w \cdot g}{24 \cdot \left(1 - \nu_i^2\right)}}$$

$$E_{pi}(L) := \frac{k_i \cdot y(L)^2}{2}$$

Work of active friction

$$W_{ar}(L) := \int_0^{L} \mu \cdot \left(\rho_w \cdot g \cdot B \cdot w_k \cdot y(x) + k_i \cdot y(x) + \mu \cdot P_{f1}(x) \cdot \cos\left(\phi_w\right) \cdot \sin\left(\alpha_k\right)\right) dx$$

Scour length in clayey seabed

$$E_k + W_a(L) + W_w(L) + W_i(L) = W_{ar}(L) + W_{prx}(L) + W_{pry}(L) + E_p(L) + E_{pi}(L) \text{ solve}, L$$

$$L := 208.7 \text{ m}$$

Scour depth in clay

$$d := L \cdot \tan(\beta) - y(L)$$

$$d = 2.774 \text{ m}$$

Ridge elvation

$$y(L) = 0.886 \text{ m}$$

Frontal mound height

$$h_f := \sqrt{\frac{d^2 \cdot \cot(\phi)}{\cot(\phi) + \frac{d}{3B} \cdot \cot(\phi) \cdot \cot(\beta)}}$$

$$h_f = 1.67 \text{ m}$$

Keel strength controlled condition (sand)

Limit pressure on the ridge

$$\mu_i(p_n) := \frac{p_n \cdot \mu}{c_i + p_n \cdot \tan\left(\phi_i\right)}$$

$$\beta_i(p_n) := \operatorname{atan}\left(\frac{p_n \cdot \tan\left(0.785 + \frac{\phi_i}{2}\right)}{1 + \sqrt{1 - \mu_i(p_n)^2}}\right)$$

$$c_i \cdot \cot\left(\phi_i\right) \cdot \left[\frac{1 + \sin\left(\phi_i\right)}{1 - \sin\left(\phi_i\right) \cdot \sqrt{1 - \mu_i(p_n)^2}} \cdot \exp\left[\left(\pi - 2 \cdot \beta_i(p_n)\right) \cdot \tan\left(\phi_i\right)\right] - 1\right] - p_n = 0 \text{ solve}, p_n \rightarrow 35.77$$

$$p_n := 35.77 \text{ kPa}$$

Increase coefficient

$$k_a := \frac{\tan\left(\frac{\pi}{4} + \frac{\phi_i}{2}\right)^2 \exp\left[2\cdot\left(\pi - \alpha_k\right)\cdot\tan\left(\phi_i\right)\right] - 1}{\tan\left(\frac{\pi}{4} + \frac{\phi_i}{2}\right)^2 \exp\left(\pi\cdot\tan\left(\phi_i\right)\right) - 1}$$

$$k_a = 2.356$$

Limit scour depth

$$h_f(d_l) := \sqrt{\frac{d_l^2\cdot\cot(\phi)}{\cot(\phi) + \frac{d_l}{3B}\cdot\cot(\phi)\cdot\cot(\beta)}}$$

$$d_l := \frac{4\cdot k_a\cdot p_n\cdot 10^3}{3\cdot 1.69\cdot K_p\cdot \rho_s\cdot g} \qquad d_l = 0.541 \quad \text{m}$$

Cohesion for scouring 1.73 m

$$d_l := 1.73$$

$$c_i := 50 \qquad \text{kPa}$$

$$\mu_i(p_n) := \frac{p_n\cdot\mu}{c_i + p_n\cdot\tan\left(\phi_i\right)}$$

$$\beta_i(p_n) := \operatorname{atan}\left(\frac{p_n\cdot\tan\left(0.785 + \frac{\phi_i}{2}\right)}{1 + \sqrt{1 - \mu_i(p_n)^2}}\right)$$

$$f(p_n) := c_i\cdot\cot\left(\phi_i\right)\cdot\left[\frac{1 + \sin\left(\phi_i\right)}{1 - \sin\left(\phi_i\right)\cdot\sqrt{1 - \mu_i(p_n)^2}}\cdot\exp\left[\left(\pi - 2\cdot\beta_i(p_n)\right)\cdot\tan\left(\phi_i\right)\right] - 1\right] - p_n$$

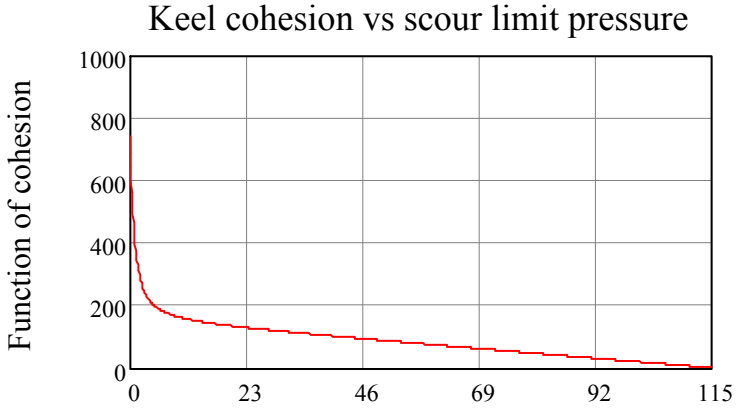

$$p_n := \frac{3\cdot 1.69\cdot d_l\cdot K_p\cdot \rho_s\cdot g}{4\cdot k_a\cdot 10^3}$$

$$p_n = 114.348 \quad \text{kPa}$$

Keel strength controlled condition (clay)

Limit pressure on the ridge

$$\mu_i(p_n) := \frac{p_n \cdot \mu}{c_i + p_n \cdot \tan(\phi_i)}$$

$$\beta_i(p_n) := \operatorname{atan}\left(\frac{p_n \cdot \tan\left(0.785 + \frac{\phi_i}{2}\right)}{1 + \sqrt{1 - \mu_i(p_n)^2}}\right)$$

$$c_i \cdot \cot(\phi_i) \cdot \left[\frac{1 + \sin(\phi_i)}{1 - \sin(\phi_i) \cdot \sqrt{1 - \mu_i(p_n)^2}} \cdot \exp\left[\left(\pi - 2 \cdot \beta_i(p_n)\right) \cdot \tan(\phi_i)\right] - 1\right] - p_n = 0 \text{ solve}, p_n \rightarrow 38.5788$$

$p_n := 38.56$

Increase coefficient

$$k_a := \frac{\tan\left(\frac{\pi}{4} + \frac{\phi_i}{2}\right)^2 \exp\left[2 \cdot \left(\pi - \alpha_k\right) \cdot \tan(\phi_i)\right] - 1}{\tan\left(\frac{\pi}{4} + \frac{\phi_i}{2}\right)^2 \exp\left(\pi \cdot \tan(\phi_i)\right) - 1}$$

$k_a = 2.356$

Limit scour depth

$$h_d(d_l) := \sqrt{\frac{d_l^2 \cdot \cot(\phi)}{\cot(\phi) + \frac{d_l}{3B} \cdot \cot(\phi) \cdot \cot(\beta)}}$$

$$d_l := \frac{4 \cdot k_a \cdot p_n \cdot 10^3}{3 \cdot 1.69 \cdot K_p \cdot \rho_s \cdot g} \qquad d_l = 1.057 \quad \text{m}$$

APPENDIX E. SCOURING IMPACT ON THE PIPELINE CALCULATIONS

Calculation input

Pipeline internal pressure (MPa)	$p_i := 11$
Pipeline temperature (^{0}C)	$T_i := 40$
Pipeline diameter (m)	$D := 0.4064$
Pipeline wall thickness (m)	$t := 0.0182$
Pipeline reference section length (m)	$L := 2B$
Poisson ratio for steel	$\nu := 0.3$
Elastisity modulus for steel (MPa)	$E := 2.07 \cdot 10^5$
Temperature expansion coefficient (1/^{0}C)	$\alpha := 1.17 \cdot 10^{-5}$
External temperature (^{0}C)	$T_e := -1.8$
Steel X65 yield strength (MPa)	$\sigma_y := 448$
Steel X65 tensile ultimate strength (MPa)	$\sigma_t := 530$
Resistance strain factor	$\gamma_e := 3.3$
Environmental load factor	$\gamma_F := 1.3$
Material strength factor	$\alpha_u := 0.96$
Strain factors	$\alpha_h := 0.93$
	$\alpha_{gw} := 1$
Ultimate tensile strain	$\varepsilon_t := 0.2$
Ovality	$f_0 := 0.005$
Safety class resistance factor	$\gamma_{sc} := 1.308$
Material resistance factor	$\gamma_m := 1.15$
Fabrication factor	$\alpha_{fab} := 0.85$

Soil data (sand)

Wall friction angle (rad) $\phi_w := 0.443$

Internal friction angle (rad) $\phi := 0.523$

Soil density (kg/m3) $\rho_s := 1500$

Calculations

Ridge-pipeline direct contact forces

Front soil resistance $P_f(d) := \frac{1}{2} K_p \cdot \rho_s \cdot g \cdot \left[(1.691 \cdot d) \cdot \left(1 + C_1 \cdot \tan(\beta)\right)\right]^2 \cdot B$

Side soil resistance $P_s(d) := \frac{1}{6} \cdot K_p \cdot \rho_s \cdot g \cdot \cot(\beta) \cdot d^3$

Horizontal passive friction $F_{cx}(d) := \mu \cdot P_f(d) \cdot \cos(\phi_w) \cdot \cos(\alpha_k) + \mu \cdot P_s(d) \cdot \cos(\phi_w)$

Vertical passive friction $F_{cy}(d) := \mu \cdot P_f(d) \cdot \cos(\phi_w) \cdot \sin(\alpha_k)$

Elevation $y(d) := \frac{\mu \cdot P_f(d)}{B^2 \cdot \rho_w \cdot g}$

Weight due to elevation $\Delta W(d) := B \cdot w_k \cdot \rho_i \cdot y(d)$

Level ice reaction $F_{li}(d) := k_i \cdot y(d)$

Force on the pipeline

$$F_{pipe}(d) := \frac{F_i + F_{dw} + F_{da} - F_{cx}(d) - \mu \cdot \left(F_{cy}(d) + F_{li}(d) + \Delta W(d)\right)}{\cos(\alpha_k) - \mu \cdot \sin(\alpha_k)}$$

$F_{pipe}(0) = 2.877 \times 10^7$ N

$F_{pipe}(1.30) = 1.769 \times 10^7$ N

$F_{pipe}(1.73) = 8.114 \times 10^6$ N

Forces on the embedded pipeline in sand

Seabed reaction $N := F_{cy} + F_{li} + \Delta W$ $N = 7.589 \times 10^6$

Ultimate axial soil resistance

- pressure coefficient at rest $K_0 := (1 - \sin(\phi)) \cdot \frac{1 + \frac{2}{3} \cdot \sin(\phi)}{1 + \sin(\phi)}$ $K_0 = 0.445$

- parameter H $H := \frac{D}{2}$ $H = 0.203$ m

$t_u := \frac{\pi \cdot D}{2} \cdot \left(\rho_s \cdot H \cdot g + \frac{N}{w_b \cdot B}\right) \cdot \left(1 + K_0\right) \cdot \tan(\phi)$ $t_u = 1.446 \times 10^4$ $\frac{N}{m}$

Horizontal transverse ultimate force

- bearing capacity factor (figure 5.13) $N_{qh} := 5.5$

- critical relative displacement $y_u := 0.03 \cdot (H + 0.5 \cdot D)$ $y_u = 0.012$ m

$$p_u := \left(\rho_s \cdot H \cdot g + \frac{N}{w_b \cdot B} \right) \cdot N_{qh} \cdot D \qquad p_u = 6.077 \times 10^4 \ \frac{N}{m}$$

Vertical transverse ultimate force

- vertical uplift factor (figure 5.14) $N_{qv} := 0.5$

- critical relative displacement $z_u := 0.1H$ $z_u = 0.02$ m

$$q_u := \left(\rho_s \cdot H \cdot g + \frac{N}{w_b \cdot B} \right) \cdot N_{qv} \cdot D \qquad q_u = 5.524 \times 10^3 \ \frac{N}{m}$$

Transverse ultimate force

$$f := \sqrt{p_u^{\,2} + q_u^{\,2}} \qquad f = 6.102 \times 10^4 \ \frac{N}{m}$$

- direction angle

$$\alpha_f := \operatorname{atan}\left(\frac{q_u}{p_u} \right) \qquad \alpha_f = 0.091 \ \text{rad}$$

LSD SLS criterion

Pipeline internal diameter $d := D - 2t$ $d = 0.37$ m

Hoop stress

$$\sigma_h := \frac{p_i \cdot (D - t)}{2t} \qquad \sigma_h = 117.313 \ \text{MPa}$$

Longitudinal stress

- Bending moment

$$M := \frac{f \cdot L^2}{32} \qquad M = 6.865 \times 10^6 \ \text{N} \cdot \text{m}$$

- Axial force

Elastic axial rigidity $S := \pi \cdot d \cdot t \cdot E \cdot 10^6$ $S = 4.379 \times 10^9$ N

Pressure and temperature effect

$$T := \left[-\frac{\pi \cdot d^2}{4} \cdot p_i \cdot (1 - 2\nu) - \pi \cdot d \cdot t \cdot E \cdot \alpha \cdot (T_i - T_e) \right] \cdot 10^6 \qquad T = -2.615 \times 10^6 \ \text{N}$$

$$\frac{f^2 \cdot B^3}{24 \cdot T_1^{\,2}} = \frac{(T_1 - T) \cdot B}{S} + \frac{(T_1 - T)^2}{2 \cdot t_u \cdot S} \ \text{solve}, T_1 \rightarrow \begin{bmatrix} -6577076.6048443021790 \\ (-1518047.7992901929760 - 4542376.1580497507043)i \\ (-1518047.7992901929760 + 4542376.1580497507043)i \\ 3516097.6513205128697 \end{bmatrix}$$

$$T_1 := 3.516 \cdot 10^6 \ \text{N}$$

- Pipeline cross-section area $A := \pi \cdot d \cdot t$ $A = 0.021$ m^2

- Sectional modulus $W_s := \frac{\pi \cdot (D^4 - d^4)}{32 \cdot D}$ $W_s = 0$ m^3

$$\sigma_l := \left(\frac{T_1}{A} + \frac{M}{W_s} \right) \cdot 10^{-6}$$

$\sigma_l = 3.495 \times 10^3$ MPa

Von Mises stress $\sigma_e := \sqrt{\sigma_h^2 + \sigma_l^2 - \sigma_h \cdot \sigma_l}$ $\sigma_e = 3.438 \times 10^3$ MPa

$Safe := if(\sigma_e > 0.9 \cdot \sigma_y, 0, 1)$

$Safe = 0$ NOT SAFE

LSD ULS strain criterion

Limit strain value

$f_y := \sigma_y \cdot \alpha_u$

$$\varepsilon_{lc} := \frac{0.78}{\gamma_e \cdot \gamma_F} \cdot \left(\frac{t}{D} - 0.01 \right) \cdot \left(1 + 5 \cdot \frac{\sigma_h}{f_y} \right) \cdot \alpha_h^{-1.5} \cdot \alpha_{gw}$$ $\varepsilon_{lc} = 0.017$

Actual strain

$$A := 0.005 \left(\frac{E}{\sigma_y} \right) - 1$$

$$n := \frac{\log\left[\frac{\left(\varepsilon_t - \frac{\sigma_t}{E} \right)}{\left(0.005 - \frac{\sigma_y}{E} \right)} \right]}{\log\left(\frac{\sigma_t}{\sigma_y} \right)}$$

$$\varepsilon_p := \frac{\sigma_l}{E} \cdot \left[1 + A \cdot \left(\frac{\sigma_l}{\sigma_y} \right)^{n-1} \right]$$ $\varepsilon_p = 9.437 \times 10^{19}$

$Safe := if(\varepsilon_p > \varepsilon_{lc}, 0, 1)$

$Safe = 0$ NOT SAFE

LSD ULS collapse criterion

Limiting collapse pressure

- elastic collapse pressure $p_{el} := \frac{2E \cdot \left(\frac{t}{D} \right)^3}{1 - \nu^2}$ $p_{el} = 40.861$ MPa

- plastic collapse pressure

$$p_p := f_y \cdot \alpha_{fab} \cdot \frac{2t}{D} \qquad p_p = 32.743 \quad \text{MPa}$$

$$\left(p_c - p_{el}\right)\cdot\left(p_c^{\,2} - p_p^{\,2}\right) = p_c \cdot p_{el} \cdot p_p \cdot f_0 \cdot \frac{D}{t} \ \text{solve}, p_c \rightarrow \begin{pmatrix} -33.75900373690652273 \\ 27.593807190750380072 \\ 47.026481055388546956 \end{pmatrix}$$

$p_c := 47.03 \quad \text{MPa}$

Allowable overpressure

$$p := \frac{p_c}{\gamma_m \cdot \gamma_{sc}} + p_i \qquad p = 42.266 \quad \text{MPa}$$

Forces on the embedded pipeline in stiff clay

Soil data (stiff clay)

Wall friction angle (rad) $\phi_w := 0.443$

Internal friction angle (rad) $\phi := 0.401$

Cohesion (Pa) $c := 10^4$

Soil density (kg/m3) $\rho_s := 1600$

LSD SLS criterion (stiff clay)

Longitudinal stress

- Bending moment

$$M := \frac{f \cdot L^2}{32} \qquad M = 6.923 \times 10^6 \quad \text{N} \cdot \text{m}$$

- Axial force

$$\frac{f^2 \cdot B^3}{24 \cdot T_1^{\,2}} = \frac{\left(T_1 - T\right)\cdot B}{S} + \frac{\left(T_1 - T\right)^2}{2 \cdot t_u \cdot S} \ \text{solve}, T_1 \rightarrow \begin{bmatrix} -7730698.6632771367312 \\ (-1710037.0559589048010 - 5394877.1928780845921\text{i} \\ (-1710037.0559589048010 + 5394877.1928780845921\text{i} \\ 4234861.9682293552496 \end{bmatrix}$$

$T_1 := 4.235 \cdot 10^6 \quad \text{N}$

$$\sigma_l := \left(\frac{T_1}{A} + \frac{M}{W_s}\right)\cdot 10^{-6}$$

$\sigma_l = 3.557 \times 10^3 \quad \text{MPa}$

Von Mises stress $\sigma_e := \sqrt{\sigma_h^{\,2} + \sigma_l^{\,2} - \sigma_h \cdot \sigma_l} \qquad \sigma_e = 3.5 \times 10^3 \quad \text{MPa}$

$\text{Safe} := \text{if}\left(\sigma_e > 0.9 \cdot \sigma_y, 0, 1\right)$

$\text{Safe} = 0$ NOT SAFE

LSD ULS strain criterion (stiff clay)

Actual strain

$$A := 0.005\left(\frac{E}{\sigma_y}\right) - 1$$

$$n := \frac{\log\left(\frac{\varepsilon_t - \frac{\sigma_t}{E}}{0.005 - \frac{\sigma_y}{E}}\right)}{\log\left(\frac{\sigma_t}{\sigma_y}\right)}$$

$$\varepsilon_p := \frac{\sigma_l}{E}\cdot\left[1 + A\cdot\left(\frac{\sigma_l}{\sigma_y}\right)^{n-1}\right] \qquad \varepsilon_p = 1.471\times 10^{20}$$

$$Safe := if\left(\varepsilon_p > \varepsilon_{lc}, 0, 1\right)$$

$Safe = 0$ NOT SAFE

Forces on the embedded pipeline in soft clay

Soil data (soft clay)

Wall friction angle (rad) $\phi_w := 0.443$

Internal friction angle (rad) $\phi := 0$

Cohesion (Pa) $c := 3.5 \cdot 10^3$

Soil density (kg/m3) $\rho_s := 1800$

LSD SLS criterion

Longitudinal stress

- Bending moment

$$M := \frac{f\cdot L^2}{32} \qquad M = 6.598\times 10^5 \quad N\cdot m$$

- Axial force

$$\frac{f^2\cdot B^3}{24\cdot T_l^{\,2}} = \frac{(T_1 - T)\cdot B}{S} + \frac{(T_1 - T)^2}{2\cdot t_u\cdot S} \text{ solve}, T_1 \rightarrow \begin{pmatrix} -3283936.954349668066 \\ -2076588.4927018839143 \\ -693013.2908192568877 \\ 448622.54142610061827 \end{pmatrix}$$

$T_1 := 4.486\,10^5$ N

$$\sigma_l := \left(\frac{T_1}{A} + \frac{M}{W_s} \right) \cdot 10^{-6}$$

$\sigma_l = 341.147$ MPa

Von Mises stress $\sigma_e := \sqrt{\sigma_h^2 + \sigma_l^2 - \sigma_h \cdot \sigma_l}$ $\sigma_e = 300.204$ MPa

$\text{Safe} := \text{if}(\sigma_e > 0.9 \cdot \sigma_y, 0, 1)$

$\text{Safe} = 1$ SAFE

LSD ULS strain criterion

Actual strain

$$A := 0.005 \left(\frac{E}{\sigma_y} \right) - 1$$

$$n := \frac{\log\left(\frac{\varepsilon_t - \frac{\sigma_t}{E}}{0.005 - \frac{\sigma_y}{E}} \right)}{\log\left(\frac{\sigma_t}{\sigma_y} \right)}$$

$$\varepsilon_p := \frac{\sigma_l}{E} \cdot \left[1 + A \cdot \left(\frac{\sigma_l}{\sigma_y} \right)^{n-1} \right] \qquad (\varepsilon_p) = 0$$

$\text{Safe} := \text{if}(\varepsilon_p > \varepsilon_{lc}, 0, 1)$

$\text{Safe} = 1$ SAFE

Pipeline lateral displacement

Moment of inertia $I := \frac{\pi \cdot (D^4 - d^4)}{64}$

Diplacement $u_p := \frac{f \cdot B^4}{16 \cdot E \cdot 10^6 \cdot I}$ $u_p = 3.423$

APPENDIX F. ANSYS FILES

Appendix F contains 2 video files, exported from ANSYS and enclosed to this thesis.